THE NiFeS BATTERY

TECHNOLOGY & PERFORMANCE ANALYSIS

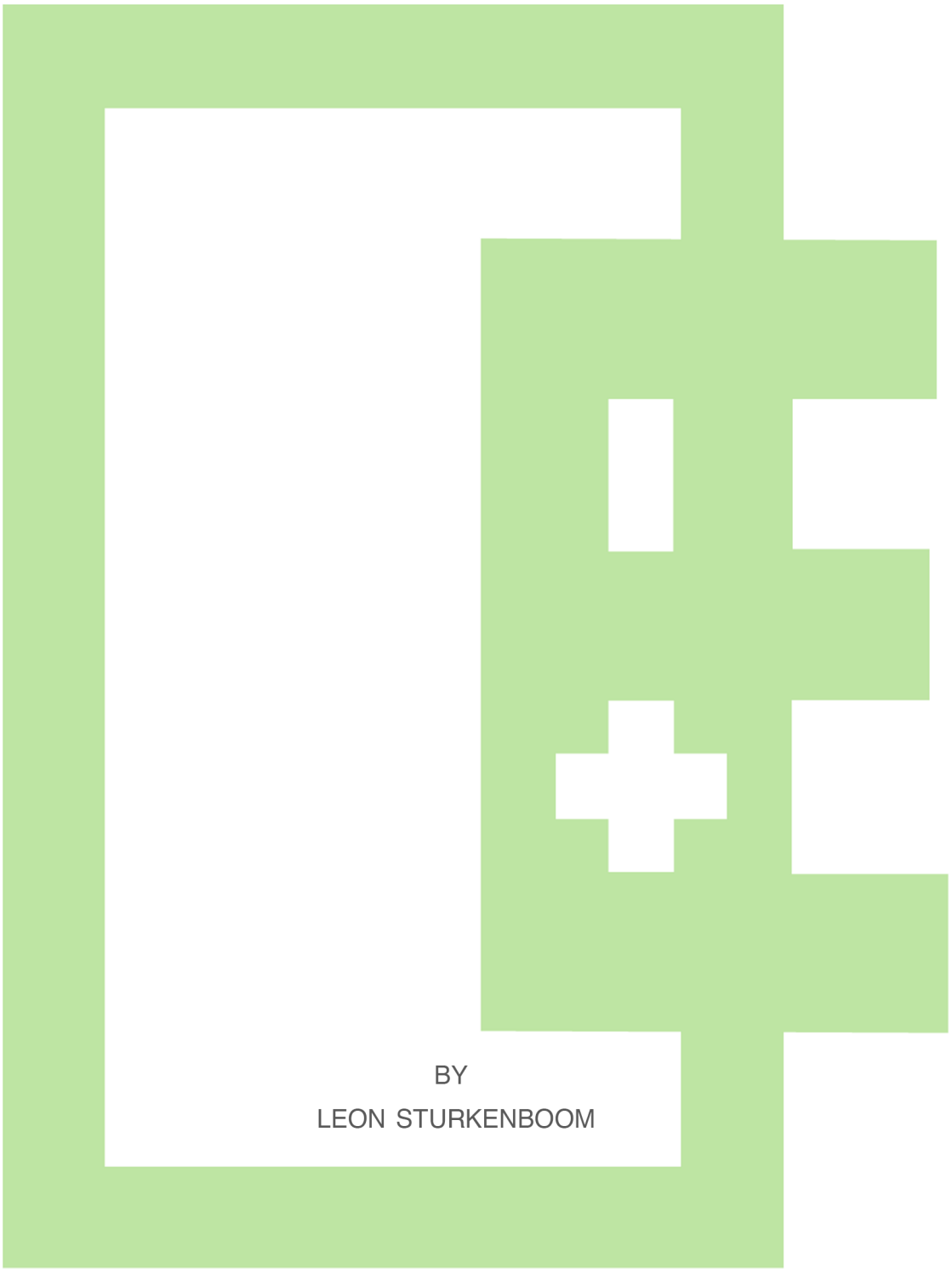

BY

LEON STURKENBOOM

THE_NiFeS_BATTERY

TECHNOLOGY_&_PERFORMANCE_ANALYSIS

Author:
L N Sturkenboom MSc
Rokin 87C 1012KL Amsterdam

Supervisors:
Ir. T van Dijk
A F England PhD
Prof. dr. F Mulder

A thesis submitted in fulfillment of the requirements
for the degree of MSc Energy Science

at the

Faculty of Geosciences

of

UTRECHT UNIVERSITY

in collaboration with

DELFT UNIVERSITY

&

and as supportment for the development

of

E_STONE BATTERIES

April 2016

"Search for the Ideal Storage Battery"

"Between the actual and the ideal there is always room for development. Therefore it seems advisable that the student become familiar with the characteristics of an Ideal Storage Battery. Then, keeping the ideal before him, he will find it intensely interesting to read and observe the different theories advanced and the difficulties that have been overcome in the efforts to reach the ideal.

The ideal Storage Battery is an electrolytic cell in which electrical energy may be stored as chemical energy until ready for use. It must be capable of returning at any time, all or any part, of the electrical energy put into it; and when emptied, the cell must be in its original condition.

To obtain this ideal battery, it is necessary to find a perfectly reversible chemical reaction whose direction and energy relation is perfectly controlled by the electric current. That is, first, no chemical action should take place except that which necessarily accompanies the flow of useful current when on charge or discharge; and, second, the quantity of material whose chemical composition changes should be proportional to the quantity of electrical energy passed through the cell.

To be ideal the cell must be of maximum ***commercial value****. It must be* ***durable****; light in* ***weight****;* ***compact****; sufficiently* ***strong*** *to stand the abuse, carelessness and negligence of a bustling world. It must be* ***dependable****: always ready for work at full rated capacity. Therefore, it must never be laid up for repairs through deterioration or other troubles due to short circuiting, over-charging or too rapid discharging. No* ***expert attention*** *should ever be necessary and, therefore, the* ***general care*** *and* ***instructions for operation*** *should be simple. The* ***life*** *of the ideal battery would of course be practically unlimited, and the* ***cost of maintenance*** *and the* ***repairs*** *negligible."*

The technical staff of the Edison Storage Battery Company (1924): The Edison Alkaline Storage Battery

UTRECHT UNIVERSITY

ABSTRACT

Faculty of Geosciences

MSc Energy Science

THE NiFeS BATTERY

by L N Sturkenboom

CONTENTS

LIST_OF_FIGURES

LIST_OF_TABLES

ABBREVIATIONS

FORMULAE

AgFe	Silver-iron
CV	**C**yclic **V**oltammetry
E_0	Reduction potential
FeO_2	Iron-air
FeOx	Undefined iron **Ox**ide species
HER	**H**ydrogen **E**volution **R**eaction
I	Electric Current
NiCd	**Ni**ckel-**Cd**mium
NiFe	**Ni**ckel-iron
NiFeS	**Ni**ckel-iron **S**ulfide
NiH_2	**Ni**ckel-**H**ydride
NiMH	**Ni**ckel-**M**etal**H**ydride
NiZn	**Ni**ckel-**Zn**c
OER	**O**xygen **E**volution **R**eaction
R_L	Load of **R**esistance
RDS	**R**ate **D**etermining **S**tep
SoC	**S**tate **o**f **C**harge
SEM	**S**canning **E**lectronic **M**icrograph
SESS	**S**tationary **E**nergy **S**torage **S**ystem
U	Electric Potential
U_{OC}	**O**pen **C**ircuit potential
U_{OP}	**O**ver **P**otential

CHEMICAL SYMBOLS

Bi_2O_3	Bismuth trioxide, Bismuth(III) oxide
Bi_2S_3	Bismuth(III) sulfide, dibismuth trisulfide
$Co(OH)_2$	Cobalt(II) hydroxide
CuO_2	Copper(IV) oxide
CuS_2	Copper(IV) sulfide
CuS_2	Copper(II) sulfide
Cu_2S_2	Copper(I) sulfide
Fe	Iron
Fe2+	Ferrous iron
Fe3+	Ferric iron
FeOOH	iron(III) oxide-hydroxide
α-FeOOH	Goethite
β-FeOOH	Akáganeite
γ-FeOOH	Lepidodocrocite
δ-FeOOH	Feroxyhyte
α-Fe_2O_3	Iron(III) oxide, hematite
Fe_3O_4	Iron(II,III) oxide, magnetite
FeO	Iron(II) oxide
Fe(OH)	Iron(I) hydroxide
$Fe(OH)_2$	Iron(II) hydroxide
$Fe(OH)_3$	Iron(III) hydroxide, bernalite
FeS	Iron(II) sulfide, troilite
FeS_2	Iron(II) disulfide, pyrite, marcasite
FeS_3	Iron(III) disulfide
FeSe	Iron(II) selenide
$FeSO_4$	Iron(II) sulfate
FeTe	Iron(II) teluride
H_2S	Hydrogen sulfide
HS^-	Bisulfide anion, sulfanide anion

S^{2-}	Sulfide anion
KOH	Potassium hydroxide
K_2S	Potassium sulfide
LiOH	Lithium hydroxide
NaOH	Sodium hydroxide
Na_2S	Sodium sulfide
Ni	Nickel
Ni2+	Nickel(II) ion
Ni3+	Nickel(III) ion
β-Ni(OH)$_2$	β-Nickel(II) hydroxide
β-NiOOH	β-Nickel(II) oxide-hydroxide
OH^-	Hydroxyl anion
PbS	Lead(II) sulfide

CHAPTER 1

INTRODUCTION

A rechargeable battery gives the possibility to store electrical energy into chemical energy using different valence states of a material, which can be used reversibly through so called redox-reactions. With the revived interest in electronic vehicles and renewable energy production technologies, the need for cheap- and lightweight storage has never been bigger for society today. Batteries are still more expensive and have much lower energy density than fossil fuels but burning coal, gasoline or natural gas generates unwanted greenhouse gas emissions that are a major cause of global warming. A battery in combination with a renewable energy generation technique, as shown in figure 1.1, is a way towards a future with a low carbon footprint, also regarding the product lifecycle [1, 2].

FIGURE 1.1: Envisaged residential application of E-stone batteries in combination with solar panels connected to the grid (Used in approval from E_STONE Batteries).

Whether it is for your smartphone or laptop, the ever increasing performance requirements of electronics are and always have been a challenge for the battery industry. Energy storage is often cited as the limiting factor for the lifetime of a portable product and today it seems to be the same case for renewables [16].

THE ENERGY CRISIS OF MODERN SOCIETY

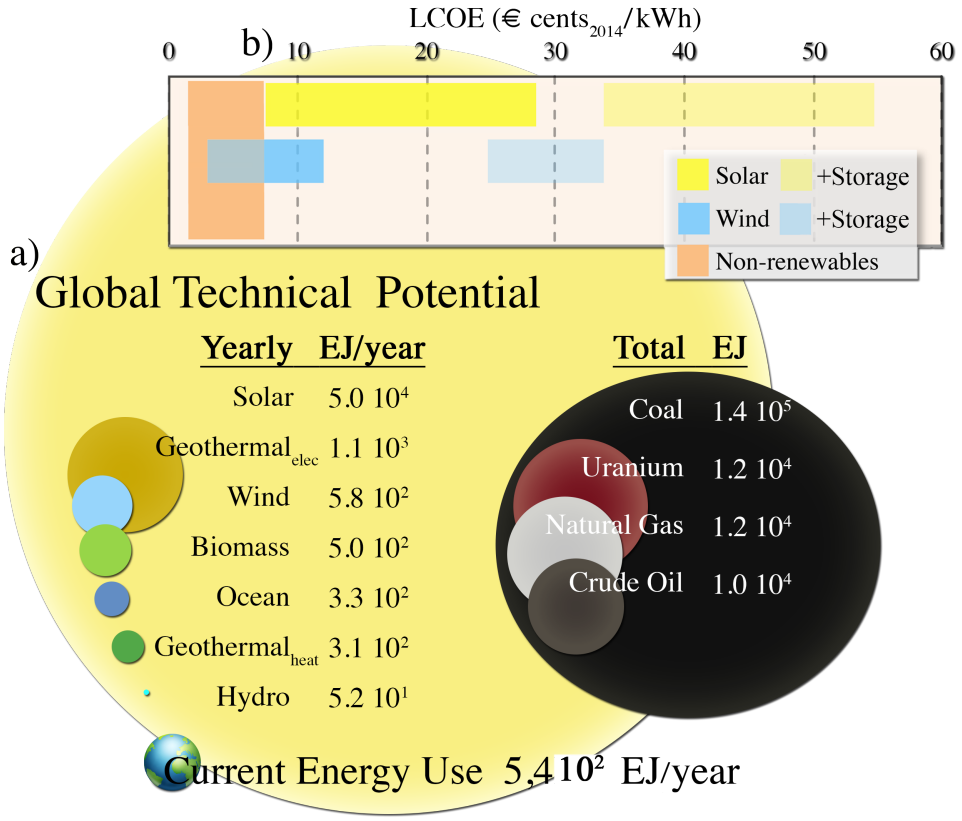

FIGURE 1.2: a) Global technical potential per year of renewables compared to total technical potential of conventional energy sources. b) Levelized Cost Of Electricity of renewables and renewables plus the current cheapest residential storage alternative compared to non-renewables (Based on IPCC calculations [1–3]).

To cope with the increasing global population, our current energy production of 5.4 10^2 EJ_{2014} over the year 2014 must be doubled by 2050 [1, 20]. At the same time we want to decrease greenhouse gas emissions, our dependency on fossil fuels and above all the last mentioned is finite. Renewables are already on the rise due to current implementation strategies worldwide and are expected to continue to increase. In 2014 only 1.3% of the total energy consumption is produced by solar- and wind energy ($\sim$7.0 EJ_{2014}/year) but this could be up to 40% of the current total energy use by 2050 ($\sim$2.0 10^2 EJ/year) following the IPCC Cat. 1 projection [1, 2]. The unlimited source of energy for powering our planet is the sun. Direct solar energy has the largest global technical potential of 1.6 10^3-5.0 10^4 EJ/year, shown in figure 1.2a. Wind energy has a significant smaller share of 85 - 5.8 10^2 EJ/year. However, wind energy production is already on an implementation track worldwide, which has led to a Levelized Cost Of Electricity [1] (LCOE) of €3-12 $cents_{2014}$/kWh, while PV still accounts for a LCOE of

[1] The levelized cost of electricity is an indication of all initial and daily costs of an electricity generating system based on its lifetime. It is calculated as the per-unit price at which electricity must be generated from a specific source over its lifetime to break even. Normally it includes only private costs, excluding the downstream costs. In this case a range of the LCOE is given also excluding interest, taxes, depreciation and amortization, based on IPCC calculations. The range of the LCOE is dependent of various factors: The characteristics of the technology, size, regional variations in cost and performance and differing discount rates. The lower range takes into account most favorable input values, while the upper range is based on a combination of the least favorable input values.

€8-29 cents$_{2014}$/kWh as depicted in figure 1.2b [1, 2, 21]. Having an LCOE of €2-7 cents$_{2005}$/kWh, non-renewables are current still cheaper than renewables but prognoses are that the LCOE of renewables will drop further.

The close cost-competitiveness of renewables looks promising but what often is forgotten is that solar- and wind energy can not be stored beforehand as can be done with fossil fuel generated energy. The wind and the sun, the fuels of renewables, blow and shine capriciously, depending on the weather, which we do not empower. Thus a transition to a renewable energy economy will lead to daily and seasonal intermittent and intrinsically variable generated electricity not directly in accordance with the demand of the consumer. Currently fossil fuelled power plants already need to deal with the variable load generated of renewables by being powered up and down. Thereby renewables decrease the operational utilization of these plants, which can subsequently lead to increased energy production costs. On the long-term when renewables account for a bigger share of the energy production, fossil fuel-powered plants alone can not cope with the renewable peak power production no more.

To deal with the variable generation of electricity by wind- and solar peak energy production techniques an addition of a storage system to sustain reliability is inevitable. With the current Stationary Energy Storage Systems (SESS) available this will significantly affect the cost-competitiveness of renewable energy production techniques, by at least an increase of ∼€23 cents$_{2014}$/kWh [2] mostly not taken in consideration as shown in figure 1.2 and 1.3 [3, 20, 22]. From another perspective low-cost storage systems could also diminish the need for costly fluctuating energy production on the demand side, paving the road to a future based on a low-cost nuclear energy economy [23]. Either way the SESS market is await-

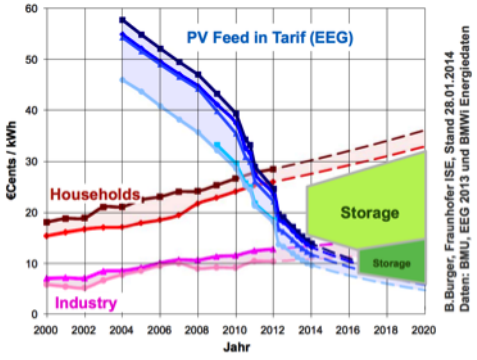

FIGURE 1.3: Decreasing costs of electricity make room for storage costs possibilities (Used from Leuthold, 2014 [4])

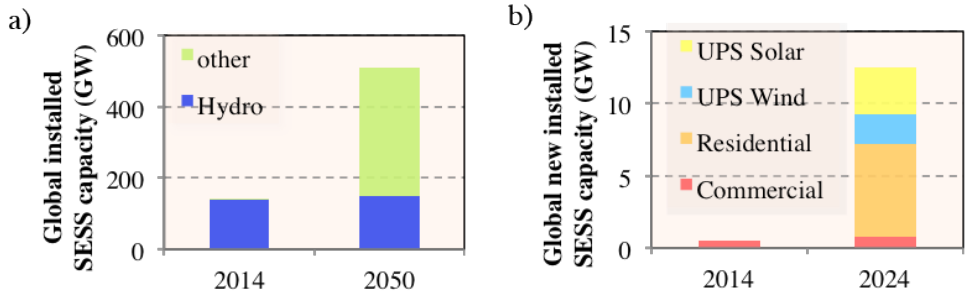

FIGURE 1.4: Global Stationairy Energy Storage System a) installed capacity (Based on prognoses from International Energy Agency [1]) and b) new installed capacity (Based on a Navigant consultancy forecast [5]).

For more information on the input parameters I would like to refer to the special IPCC report on renewable energy sources and climate change mitigation [2].

[2]The increase in costs for renewables by addition of a storage system is based on currently lowest LCOE of a commercial battery storage system by Tesla Motors [3]

ing massive growth and is about to take off. Following calculated outputs of renewable energy production of F. M. Mulder et al. (2014), which is based on IPCC Cat. 1 projections, this can lead to 0.2 EJ necessary daily (short term) storage and 30 EJ seasonal (long term) storage capacity by 2050 [22]. Depicted in figure 1.4a and b are respectively the current and projected global installed energy storage capacity and the installed new storage capacity by respectively the IEA and Navigant Research. In 2014 worldwide installed SESS power capacity was 1.4 10^2 GW (of which 99% is pumped hydro that will not increase significantly due to geographical factors) but is expected to grow to 5.1 10^2 GW by 2050 leading to a quadrupling based on the breakthrough scenario of the IEA [1]. This will lead to an investment need of € 5.6 10^2 billion [1]. On a yearly basis the new installed SESS capacity was only 5.4 10^2 MW in 2014 but is expected to grow to 21 GW in 2024, lead by the residential sector. This will cause a worldwide revenue growth from € 5.1 10^2 million in 2014 to € 16 billion in 2024 [5]. In comparison, the global net coal export revenue in 2014 was € 12 billion [24].

THE SEARCH FOR STATIONARY ENERGY STORAGE SYSTEMS

The last decade intensive effort has been directed to the search of lower-cost and sustainable stationary storage systems for load-levelling applications of electricity, on- and off-grid. Among the potential short term storage alternatives is electrochemical storage in the form of rechargeable batteries. In contrast to other storage alternatives, electrochemical storage does not require an inefficient energy conversion and generates electricity operating benefits for short term storage in turn, such as instantaneous backup [23, 25]. Yet for the greater part, electrochemical storage alternatives in the form of rechargeable batteries separates itself as it can be implemented on small residential scale as well next to large scale grid balancing, which is shown in figures 1.1 & 1.5, respectively. Thereby rechargeable batteries could unlock a market niche. So far, no battery or other energy storage systems have been capable of meeting all SESS requirements, which is mainly about the costs, while the battery industry is heavily competitive and material intensive. Consequently, the implementation of renewable production technologies is still conflicted.

FIGURE 1.5: Envisaged large-scale grid application of E-Stone batteries.

Main prerequisites for a environmental-friendly stationary energy storage system are that the **performance** must go up or the **costs** need to go down significantly, while the materials used need to be **non-toxic**, **environmentally benign** and of excellent **safe operation**. Performance mainly depends on the maturity of the product. For SESS weight is not necessarily an issue. Therefore, in contrast to portable electronics and electric vehicles applications the essential parameter for SESS is not the weight of the system but a prolonged and carefree **lifetime**, more than 15 years to be ideal for renewables with a high round-trip **efficiency**. **Robustness** for temperature and overcharge is a plus. On the other hand, costs mainly depend on the **interest** in-, **availability**- and **abundance** of the materials used and the **production techniques** and **maintenance** required. Regarding the planned scale of implementation of renewables and the necessity of stationary energy storage systems, the abundance of the materials used could be a critical but maybe also a limiting parameter in the sense of sustainability.

BATTERY SYSTEMS FOR STATIONARY ENERGY STORAGE

There are several kinds of elemental combinations having a high enough difference in redox potential, the ability to recharge and thus to be used for a rechargeable battery system. Based on performance and abundance of materials used, the most interesting electrochemical storage options for large scale implementation of SESS are aqueous metal-ion (Li^+, Mg^{2+} & Na^+), aqueous alkali nickel-metal variants (Cd^{2+}, MH^{2+} & Fe^{2+}), lead-acid, redox flow batteries and super capacitors. However, regarding the projected scale of growth and the distinguishable applications and market segments it is expected that several types of stationary energy storage solutions are necessary.

The awakening search for a cheap scalable stationary energy storage system during the last decade has led to revived attention for the NiFe system. This is primarily because weight does not have to be an issue for stationary applications and the NiFe battery is well-known for its robustness. Nevertheless the NiFe battery suffers from severe drawbacks, mostly at the anode, that lead to poor charging rates and low efficiencies. In addition expensive production methods are required for the electrodes. These drawbacks prevent the existing NiFe battery from being a viable commercial alternative.

Increasing the energy efficiency and costs of production could make the NiFe battery a viable alternative again. Although the nickel-based electrode has excellent performance, the environmental effects, toxicity and abundance of nickel are a matter of concern. Iron is non-toxic, the fourth most abundant material in the earth crust, easily obtainable due to the huge existing steel industry worldwide and thereby comparatively low-cost. Either way, enhancing the performance of the iron electrode could create advances for other iron-based batteries, such as the iron-air battery.

Since 2012 E_STONE Batteries, an Amsterdam based start-up, tailors the iron-based electrode chemistry by using iron(II) sulfide (FeS) not as additive but as primary active component of the anode, while exploring cheap upscalable production techniques. Anionic sulfur species are found to have beneficial effects on the performance of the iron electrode [12, 26–45].

CHAPTER 2

PROBLEM STATEMENT & APPROACH

PROBLEM STATEMENT

Concerns remain regarding the stability of FeS as basic starting material of the electrode and if the resulting performance in terms of lifetime and efficiency are sufficient for the NiFeS battery to be an interesting alternative within the current fast changing short term stationary energy storage market. To define the potential of the NiFeS system, an intensive empirical and market study is necessary. The main objectives of this thesis as shown in figure 2.1 are to:

- Identify, combine and enhance current performance parameters of the FeS anode E-Stone Batteries develops, namely the reproducibility-, stability- and maintenance parameters.
- Perform a preliminary cost analysis based on the performance of the NiFeS battery together with an investigation into the material requirements for a complete battery system.
- Compare the NiFeS battery with viable alternatives in the current and future short term SESS market.

RESEARCH QUESTIONS

Therefore the main question of this research will be:

Does the nickel-iron(II)sulfide (NiFeS) battery have sufficient potential to be an interesting competitor as Stationary short-term Energy Storage System (SESS)?

The short term SESS market is defined as $<$ 5C charge rates. the C-rate is a measure for the power rate. Hence, a 5C rate stands for charging a battery in 12 minutes. Critical technical performance parameters of the FeS anode will be investigated, which are depicted in the following sub-questions:

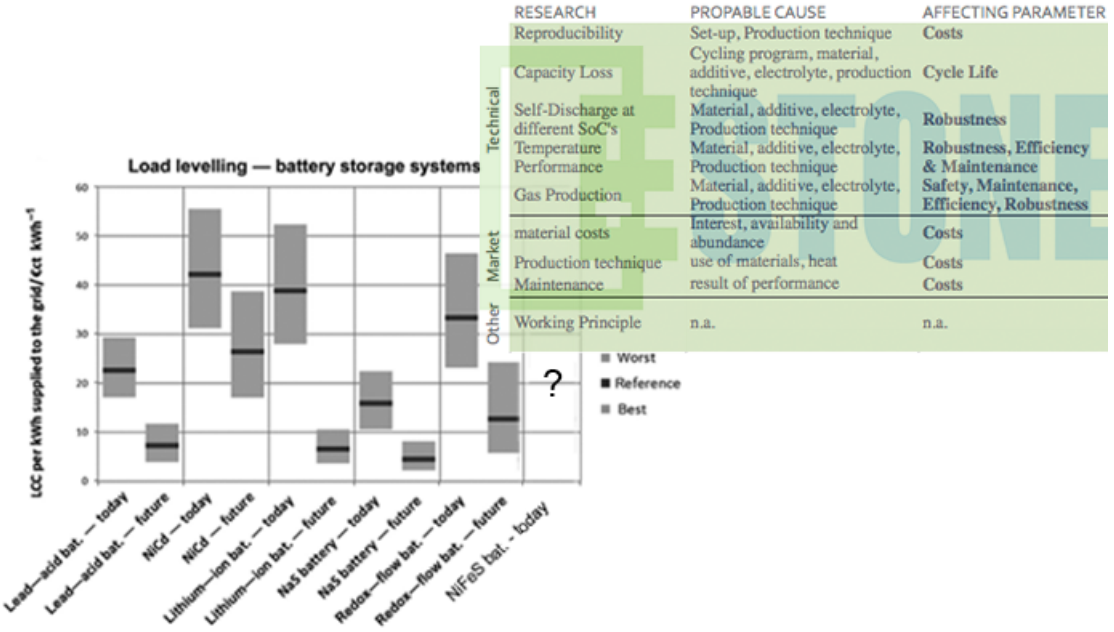

FIGURE 2.1: Representation of the goal of this research. The table shows the research pillars of E-Stone, suggested causes and affected parameters, while the figure indicates current and future estimates of the levelized costs of electricity of stationary energy storage system competitors (Used from Thien et al., 2015 [6]).

What are currently the best obtainable stable capacity, efficiency, cycle life, to what extend is self-discharge a limiting parameter and what are the causes under standard cycling conditions?

To investigate whether bismuth and sulfur containing additives are actual effective additives is validated by the sub-question:

Are bismuth- and sulphur containing species necessary additives to the cell to effectively delimit the Hydrogen Evolution Reaction, passivation of the iron and by doing so, respectively decrease the self-discharge and capacity loss?

To appoint also the possibility to introduce the NiFeS battery for high performance applications is validated by the sub-question:

Has the nickel-Iron(II)sulfide (NiFeS) battery also the potential to be an alternative for high performance applications?

The high performance market is defined as $>$5C charge rates. Based on the identified technical performance parameters the economic potential of the NiFeS battery as short-term SESS will be investigated following the sub-question:

What are the minima of criteria an iron(II)sulfide (FeS) based battery needs to meet to be an interesting alternative?

If the nickeldihydroxide cathode is limiting in costs, or abundance and if there are alternatives is validated by the sub-question:

Is the toxicity, accessibility and abundance of nickel limiting and are there alternatives for the nickeldihydroxide ($Ni(OH)_2$) cathode?

Assuming a large-scale transition to a renewable energy economy in which storage systems are a prerequisite.

CHAPTER 3

TECHNOLOGY

3.1 INTRODUCTION

WORKING PRINCIPLE OF A BATTERY

A battery consists of one or multiple galvanic cells. A galvanic cell is an electrochemical cell in which spontaneous electrochemical redox reactions can occur to generate electrical energy. An electrochemical cell, as shown in figure 3.1, comprises two half-cells. These half-cells have an *electrode* and *electrolyte*. The electrodes in contact with the electrolyte can lose their electrons via a reduction redox reaction. This necessitates a transfer of electrons to the counterelectrode to neutralize charge. Thereby the counterelectrode gains electrons via an oxidation redox reaction. The electrolyte provides ionic conductivity between the electrodes by using (an)ions as charge carriers. The half-cells in a cell can have the same electrolyte depending on the redox reactions. A permeable membrane or *separator* separates the half-cells, while maintaining ionic conduction between the two electrodes. Consequently, during a so called discharge, the electrolyte and separator facilitate electrons to flow via an external closed circuit at a certain **current** I via the *current collector* to apply work on a **load of resistance** $\mathrm{R_L}$. Thereby a difference in charge is established between the half cells. The SI units of current and resistance are Ampere [A] and Ohm [Ω]. The *anode* and the *cathode* are respectively the electrode at which the current enters and leaves the electrochemical cell. For a rechargeable cell the redox reactions are also possible in reverse for which electrons need to be forced into the battery. This results in non-spontaneous reactions leaving the electrodes in a higher energy state. Open circuit leads to an impediment of current flow to neutralize the charge of the electrodes. Thereby energy can be 'stored' in an electrochemical cell. The redox or half reactions occurring between the electrode and electrolyte are equilibrium reactions between different oxidation states of ions. This equilibrium can be quantified by the **redox potential** $\mathrm{E^\circ}$ under standard conditions and determines the tendency of the chemically active specie to acquire electrons to reduce to a more

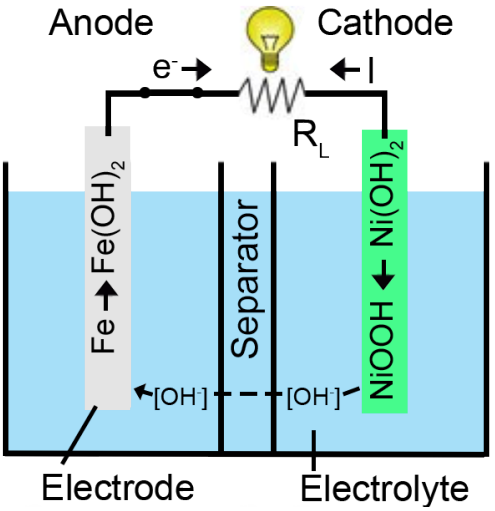

FIGURE 3.1: Illustration of a galvanic cell

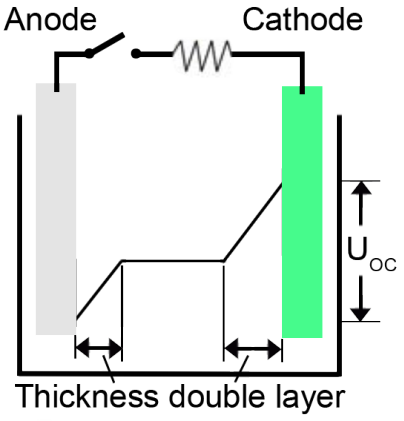

FIGURE 3.2: Internal voltage level distribution in a cell at open circuit.

stable state. When this equilibrium is reached also the maximum potential is attained. The redox potential, of which the SI unit is Volt [V], depends on the materials used for the half cell. The established difference in charge within an electrochemical cell can be measured by the difference in **potential** U. The difference in potential at open circuit is quantified with the **open circuit potential** $\mathrm{U_{OC}}$. Figure 3.2 illustrates the voltage level distribution within a cell at open circuit. The mobile (an)ions of the electrolyte neutralize the electrode charge at the surface of the electrodes. The voltage drop can be observed solely across the double layers within a cell.

BATTERY PERFORMANCE PARAMETERS

The total potential and current that can be drawn from an electrochemical cell determine the **power capacity** output P by:

$$\mathrm{P = UI}$$

The SI unit of power is Watt [W]. The amount of energy that can be stored and generated can be defined by its **current capacity** Q. Multiplying the current by the time t gives the current capacity and is usually stated in Amp-hour [Ah]. The power and current capacity both depend on the amount of the electrode material, the cell chemistry and the temperature. The current capacity is also determined by the current density and the storage period. The Peukert's law relates the current density and cell capacity by:

$$\mathrm{Q = I^k t}$$

k is the Peukert coefficient, which is a value between 0 and 1. The higher the discharge current density the lower the capacity of a cell. Therefore the capacity is often expressed at a certain **C-rate** that describes the discharge current relative to its rated nominal or maximum capacity. A 1C rate means the cell will be discharged fully in one hour. By multiplying the current capacity with the required potential the energy capacity can be determined. The presence of reactions at open-circuit at a certain State of Charge (SoC) or at low current densities that consume charge carriers without producing current lead to **self-discharge** and loss of capacity. These so called side-reactions together with rate determining limitations of the current density within the cell also lead to internal energy losses during charge or discharge and is quantified by the **efficiency** of the cell. The overall energy efficiency η is defined as the energy put into a battery divided by the energy output during discharge by:

$$\eta = \frac{\text{Useful power output}}{\text{Total power input}} = \eta_{\mathrm{coulombic}}\eta_{\mathrm{voltage}} = (\frac{\mathrm{I_{discharge}t_{discharge}}}{\mathrm{I_{charge}t_{charge}}})(\frac{\mathrm{V_{discharge}}}{\mathrm{V_{charge}}})$$

The overall energy efficiency depends on the coulombic- and voltage efficiency. The coulombic efficiency is the energy acquired on discharge divided by the energy put into the battery on charge. Loss of voltage efficiency is caused by overpotential ($\mathrm{U_{OP}}$). The overpotential is the difference between the reaction its thermodynamically determined potential and the actual potential at which the redox reaction is observed. The **lifetime** in terms of **cycle life**, is the number of charge/discharge cycles that can be attained before losing 20% of its capacity. Other important commercial parameters are the **costs** and hazards of the materials used, regarding **safety** and **toxicity**.

DEVELOPMENT OF THE ALKALINE BATTERY

THE DISCOVERY & DEVELOPMENT OF THE ALKALINE NiFe BATTERY

In 1899 Waldemar Jungner from Sweden discovered the first rechargeable battery in which an alkaline electrolyte is used, such as an aqueous solution of potassium hydroxide (KOH) or sodium hydroxide (NaOH). Jungner focused on nickel-cadmium (NiCd) and nickel-iron (NiFe) as the active materials of the system. The american Thomas Edison claimed to invent and subsequently patented the NiFe battery in 1901. Patent litigation led to the collapse of Jungner's company and Jungner then focused on the NiCd system, using a pocket plate electrode design. Edison developed the NiFe system based on a tubular electrode design, which was primarily intended for electric vehicles [8, 16, 46].

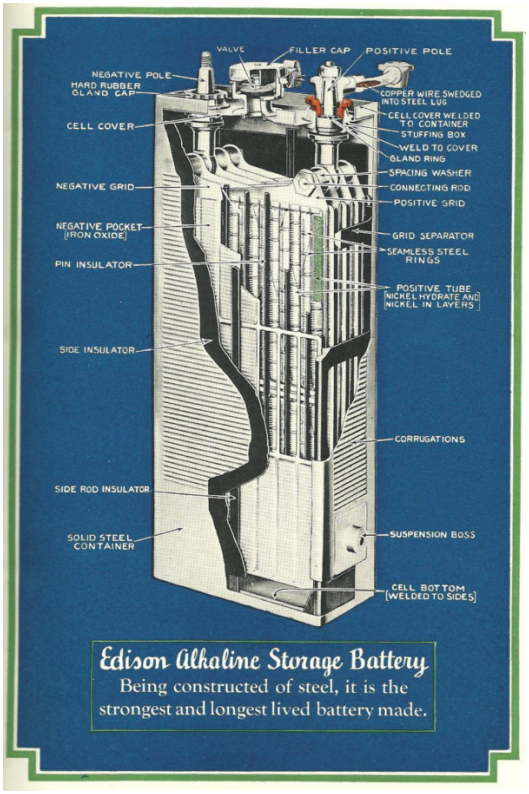

FIGURE 3.3: Advertisement and cross-section of the original Edison battery (Used from Edison et al., 1924) [7]

By 1903 the Edison Storage Battery Company introduced the NiFe battery to the market. From the start the NiFe battery already showed an impressive lifetime of 3000 cycles with an energy efficiency of 65-80% resulting in a cycle life ranging from 20-50 years. This is considered to be due to its well devised robust cell design, shown in figure 3.3. Table D.1 depicts best performance parameters of nickel-based batteries.

TABLE 3.1: Performance characteristics of commercial alkaline Ni batteries [16].

System	Energy & power density						Efficiency	Lifetime		Self-discharge
	Theoretical		Practical							
Ni-	V	Wh/kg	V	Wh/kg	W/kg	Wh/L	%	no.	Year	%/day
Fe	1.37	337	1.2	50	25	55	65-80	∼4000	20-60	0.6-1.0
Cd	1.35	244	1.2	75	300	150	70-90	∼ 2300	10-20	0.2-0.6
MH	∼1.30	240-800 [a]	1.2	120	1000	300	65	∼850	10	?
FeS [b]	1.46	346	1.2	*80*	*330*	?	*80*	*∼200*	?	?

[a] Depends on the composition of the metal hydride.
[b] Based on laboratory experiments [45].

While having a relatively high theoretical energy density possible of 337 Wh/kg the NiFe battery was soon to be replaced by the more efficient NiCd system [8]. Some mention this was due to commercial reasons [45] or the costly production process of the electrodes in combination with the intensive

maintenance of the electrolyte [8] but probably the main reason was the inherent performance limiting characteristics of the NiFe battery that just could not be dealt with that easily. The loss of efficiency results out of the parisitic side-reaction of hydrogen evolution during charge, leading to electrolyte depletion. Therefore the electrolyte needs to be continually topped up. In addition expensive production methods are required for the electrodes. Moreover, the chemistry occurring at the iron-based electrode causes poor performance at high current densities. These drawbacks resulted in staggering poor energy- and power densities of 50 Wh/kg and 25 W/kg in practice, respectively. Ultimately, the NiFe system appeared to be a bit too heavy for electric vehicles since at least double the amount of energy density is necessary for automotive applications. Instead, NiFe batteries have been widely applied for material handling vehicles, underground mining vehicles, miners lamps, railway cars, signalling systems and emergency lighting [16]. Several companies, such as SAFT, Peugeot, VARTA, DAUG, SAB-NIFE and Daihatsu, persisted research of the NiFe system for electric cars [46]. Daihatsu ultimately proved that a NiFe battery system could be reliable for a car over a 100 km range by the year 2000. R&D towards NiFe and FeO_2 batteries for electric cars has effectively ceased [46].

THE DEVELOPMENT OF THE BATTERY MARKET

In the meantime, even better performances were reached for NiCd batteries at a faster paste than its competitors. Main competitor of the NiCd system was the lead-acid system. The achievement of maintenance free sealed cells even led to small portable NiCd batteries. Unfortunately the downfall with cadmium-based batteries is that cadmium is toxic and an environmental hazard. This has eventually resulted in legislative restrictions for the private sector of NiCd batteries in the European Union by 2006 [8]. Philips introduced the NiMH battery at the end of the 1980s, which increased energy capacities attainable to 120 Wh/kg, 30-40% higher than NiCd cells. Notwithstanding Edison's intentions for the NiFe system, this made an alkaline battery design interesting for electric vehicles for the first time. The main drawback of NiMH batteries is that they use rare earth metals such as Lanthanium, which could enhance the price volatility and limit the scalability of this battery type. Currently, NiMH and lithium-ion are the standard choice for electric cars, mainly due to their high energy densities.

Regardless of the market leading positions of the lead-acid and lithium-ion system for respectively, stand by applications and high performance electronics, alkaline nickel-based battery types are still capable of attaining and maintaining a market share for specific applications. This is because of their remarkably long **lifetime**, **robustness** and **simplicity**. The use of the aqueous alkaline electrolyte causes the electrodes not to degrade due to overcharge and in which the electrodes preserve stability.

The oil crisis in the 1970s revived R&D of iron-based systems for the iron-air battery (FeO_2) due to its high theoretical energy density. This was mostly for electric vehicles and military purposes but it abruptly ceased after 1984. Afterwards little R&D existed for the NiFe system with the exception of research in India by Shukla et al. between 1982-1992. Recently, the awakening search for a stationary energy storage system recovered R&D for iron-based electrodes and NiFe batteries are still produced by companies, such as Encell and CHANGHONG.

THE BENEFICIAL EFFECT OF ANIONIC SULPHUR SPECIES FOR THE IRON-BASED ELECTRODE

Since the 1960s, the scientific literature suggests that the anionic sulphur species, sulfides S^{2-} and

bisulfides HS^-, added to the electrolyte or incorporated into the electrodes enhance the electrochemical properties of the iron-based electrode in discharge capacity, efficiency, discharge rate and self-discharge [12, 26–45]. Yet, the working principles of the anionic sulphur species is not yet fully understood. From the discovery of the NiFe battery up to very recently, several attempts have been made to improve the performance by adding sulphur containing species. From 1974-1976 Öjefors studied alkaline aqueous batteries at the department of Chemical Technology, Royal Institute of Technology based in Stockholm, Sweden [47–51]. Öjefors found the prominent beneficial effect of potassium(I) sulfide (K_2S) additives for the discharge capacity and self-discharge for the iron electrode [47]. Research from Shukla et al. from 1982-1992 from the indian institute of Science, Bangalore, India, contributed significantly to understanding the effect of anionic sulfur species on the NiFe cell [33–36, 44, 46, 52–57]. This work has led to incorporating iron(II) sulfide, lead(II) sulfide (PbS), bismuth(III) sulfide (Bi_2S_3) [36] and in a more recent article iron(II) sulphate ($FeSO_4$) [53] into iron-based electrodes. Even more recently, in a series of articles from 2012-2015, Manohar et al. at the University of Southern California, Los Angeles, USA, have tried to introduce different sulfur containing species as additives for the iron-based electrode as viable alternative for a SESS [12, 13, 58–62]. They studied Bi_2S_3 [59] and FeS [58] but also organosulfur additives [60, 61, 63, 64]. Also, Posada and Hall from the Chemical and Biological Engineering institute, University of Sheffield, United Kingdom, investigated K_2S, FeS and Bi_2S_3 added to iron-based electrodes [42, 43, 65, 66]. Recently, an in-depth research by Shangguan et al. (2015), from collaborating universities in China and Canada, introduced the first scientific research concerning FeS as starting material in an anode, showing the strong potential of FeS-based batteries [67]. If current commercially available NiFe batteries already apply anionic sulphur species, is not known. Therefore a patent study can be applied but is not covered by this thesis. Despite all aforementioned efforts the NiFe cell has not yet proved itself to be a viable alternative for SESS.

3.2 FUNDAMENTAL REDOX REACTIONS OF THE NiFeS SYSTEM

In this section possible half reactions at the anode and cathode are given for the aqueous alkaline NiFeS and NiFe cell at a pH of 14. The standard electrode potential of a half reaction can only be empirically determined versus a counter-electrode. In conventional terms the reduction potential is determined versus the Standard Hydrogen Electrode (SHE) as reference electrode. The more positive the standard reduction potential of a redox reaction, the greater the tendency for the reduction to occur. The standard cell potential can then be determined by subtracting the standard anode potential by the standard cathode potential:

$$\Delta \mathrm{E}^{\circ}_{\mathrm{cell}} = \mathrm{E}^{\circ}_{\mathrm{cathode}} - \mathrm{E}^{\circ}_{\mathrm{anode}}$$

For an electrochemical cell with spontaneous redox reactions the Gibbs free energy $\mathrm{G}^{\circ}_{\mathrm{cell}}$, of which the SI unit is Joule, must be negative. Therefore the standard cell potential must be positive as:

$$\Delta \mathrm{G}^{\circ}_{\mathrm{cell}} = -\mathrm{nFE}^{\circ}_{\mathrm{cell}}$$

n is the number of moles and F is the Faraday constant of $\sim$96485 C/mol or 26.801 Ah/mol. The actual voltage also depends on the concentrations or pressure of the reactants involved following the Nernst equation, which relates the reduction potential of a (half-)cell to the standard electrode potential, temperature T, activity and reaction quotient $\mathrm{C_r}$ of the underlying reactions and species used:

$$\mathrm{E} = \mathrm{E}^{\circ} - \frac{\mathrm{RT}}{\mathrm{nF}} \mathrm{ln} \mathrm{C_r}$$

R is the universal gas constant of 8.3145 J/K/mol. Hence, a change in concentration of the reaction species means a change in potential.

The total theoretical current capacity of a half reaction $\mathrm{Q_r}$ is dependent of the mass of the electrode and can be determined at standard conditions by using Faraday's law of electrolysis:

$$\mathrm{Q_r} = \frac{\mathrm{zmF}}{\mathrm{M}}$$

z is the number of electrons transferred, m is the mass and M is the molar mass of the substance of which the SI units are grams. By multiplying the standard cell potential by the theoretical current capacity the theoretical energy capacity can be calculated.

THE NICKEL-BASED ELECTRODE

The underlying reaction at the cathode is based on a redox reaction from Nickel(II) (Ni(II)) to Nickel(III) (Ni(III)). In primary literature, general agreement exists that this happens by a protonation/deprotonation mechanism between nickel dihydroxide (β-Ni(OH)$_2$) and β-nickel oxy hydroxide (β-NiOOH), both in the beta morphology [16, 46, 57]:

$$\beta - \mathrm{Ni(OH)_2} + 2[\mathrm{OH}]^- \underset{charge}{\overset{discharge}{\rightleftharpoons}} \beta - \mathrm{NiOOH} + \mathrm{H_2O} + \mathrm{e}^- \qquad \mathrm{E}^\circ = 0.490\mathrm{V\ vs\ SHE} \qquad (3.1)$$

This is common to all nickel-based alkaline cells. The oxidation of β-Ni(OH)$_2$ by equation 3.1 leads to a theoretical energy density of 577 Ah/kg.

THE IRON-BASED ELECTRODE

The classical aqueous alkaline NiFe system is solely based on the reduction of metallic iron to iron(II) at the anode. General consensus exists that this leads to the formation of iron(II) hydroxide (Fe(OH)$_2$), by the reaction:

$$\mathrm{Fe} + 2[\mathrm{OH}]^- \underset{charge}{\overset{discharge}{\rightleftharpoons}} \mathrm{Fe(OH)_2} + 2\mathrm{e}^- \qquad \mathrm{E}^\circ = -0.880\mathrm{V\ vs\ SHE} \qquad (3.2)$$

On further discharge also iron(III) can be reduced out of Fe(OH)$_2$. Following primary literature this leads to the formation of metastable iron(III) oxide hydroxide in the beta morphology (β-FeOOH) [16, 46, 56, 57, 68]:

$$\mathrm{Fe(OH)_2} + [\mathrm{OH}]^- \underset{charge}{\overset{discharge}{\rightleftharpoons}} \beta - \mathrm{FeOOH} + \mathrm{H_2O} + \mathrm{e}^- \qquad \mathrm{E}^\circ = -0.560\mathrm{V\ vs\ SHE} \qquad (3.3)$$

The theoretical energy densities by oxidation of metallic iron and Fe(OH)$_2$ following equation 3.2 and 3.3 are 959 ah/kg and 298 ah/kg, respectively. By the two electron oxidation process at equation 3.2, the theoretical discharge capacity is triple the amount of equation 3.3, which is a one electron oxidation process. The overall three electron oxidation of metallic iron accounts for 1439 ah kg^{-1}.

THE NiFe SYSTEM

The combined two electron oxidation/reduction reaction for the NiFe system will then be:

$$2\mathrm{NiOOH} + \mathrm{Fe} + 2\mathrm{H_2O} \underset{charge}{\overset{discharge}{\rightleftharpoons}} 2\mathrm{Ni(OH)_2} + \mathrm{Fe(OH)_2} \qquad \mathrm{E_{cell}} = 1.370\mathrm{V\ vs\ SHE} \qquad (3.4)$$

On further discharge, a so called deep discharge, the one electron oxidation process can occur following:

$$\mathrm{NiOOH} + \mathrm{Fe(OH)_2} \underset{charge}{\overset{discharge}{\rightleftharpoons}} \mathrm{Ni(OH)_2} + \beta - \mathrm{FeOOH} \qquad \mathrm{E_{cell}} = 1.050\mathrm{V\ vs\ SHE} \qquad (3.5)$$

The overall reaction shows no variation in concentration of hydroxyl ions [OH]$^-$. Square brackets [ ] refer to concentration of species, so [OH]$^-$ is concentration of the hydroxyl ions. Following equation 3.4, the theoretical specific energy of the oxidation of metallic Fe and Ni(OH)$_2$ is 307 Wh/kg. On further

discharge an overall theoretical specific energy of 337 Wh/kg can be attained. The so-called deep discharge, described by equation 3.5 solely gives 255 Wh/kg for $Fe(OH)_2$ and $Ni(OH)_2$. Table 3.2a illustrates theoretical energy densities of starting materials and table 3.2b summarizes different theoretical specific energies for NiFe and NiFeS systems.

TABLE 3.2: Theoretical energy densities of Iron and iron(II) sulfide (a) electrodes and (b) -systems compared.

a)

Material	**Theoretical energy density**
	(Ah/kg)
Ni(II/III)	456
$Ni(OH)_2$(II/III)	289
Fe(0/II)+Fe(II/III)	1439
Fe(0/II)	959
$Fe(OH)_2$(II/III)	298
FeS(0/II)+FeS(II/III)	914
FeS(0/II)	609
FeS(II/III)	304

b)

System	**Theoretical Energy density**		
Ni-	(Ah/kg)	(V)	(Wh/kg)
Fe(0/II)+Fe(II/III)	242	1,31	337
Fe(0/II)	224	1,37	307
$Fe(OH)_2$(II/III)	243	1,05	255
FeS(0/II)+FeS(II/III)	237	1,46	346
FeS(0/II)	198	1,46	289
FeS(II/III)	100	1,13	113

THE IRON(II) SULFIDE ELECTRODE

As there is little empirical research concerning iron(II) sulfide as starting material of an electrode in an alkaline electrolyte, no exclusive explanation can be given for the basic reaction mechanisms involved. Based on basic redox reaction schemes of Latimer (1939) most plausible redox reaction mechanisms are given in this section [17]. FeS can be reduced to metallic iron via:

$$\mathrm{Fe} + [\mathrm{S}]^{2-} \underset{charge}{\overset{discharge}{\rightleftharpoons}} \mathrm{FeS} + 2\mathrm{e}^- \qquad \mathrm{E}^\circ = -0.970\mathrm{V\ vs\ SHE} \qquad (3.6)$$

On low discharge also Fe(III) species can be reduced out of FeS by reacting with $[S]^{2-}$ or $[OH]^-$ resulting into respectively the formation of iron(III) sulfide (Fe_2S_3) [41] or β-FeOOH following:

$$\mathrm{FeS} + 3[\mathrm{OH}]^- \underset{charge}{\overset{discharge}{\rightleftharpoons}} \beta - \mathrm{FeOOH} + [\mathrm{S}]^{2-} + \mathrm{H_2O} + \mathrm{e}^- \qquad \mathrm{E}^\circ = -0.560\mathrm{V\ vs\ SHE} \qquad (3.7)$$

$$2\mathrm{FeS} + [\mathrm{S}]^{2-} \underset{charge}{\overset{discharge}{\rightleftharpoons}} \mathrm{Fe_2S_3} + 2\mathrm{e}^- \qquad \mathrm{E}^\circ = -0.636\mathrm{V\ vs\ SHE} \qquad (3.8)$$

The standard reduction potential of Fe to FeS by equation 3.6 is lower in comparison to the standard reduction potential of $Fe(OH)_2$ to metallic iron. Hence, from an electrochemical point of view, the Fe/$Fe(OH)_2$ reaction is favored above the Fe/FeS reaction. Shangguan et al. (2015) found that the classical reaction mechanism of the iron-based electrode also accounts for using FeS as starting material. Having FeS as starting material of the electrode a number of different species could be present in solution after initial- and subsequent cycling, including dianionic sulfides at a pH of $>$14. Sulfides are a

strong base. Nickel-based batteries use an aqueous alkaline solution. Having multiple bases involved introduces a possible competitive adsorption mechanism during cycling of the battery, which makes the working principle far more complex. Based on the oxidation of FeS by equation 3.6, equation 3.7 and 3.8 the theoretical energy density is 609 Ah/kg and 304 Ah/kg, respectively. The total oxidation of FeS (out of Fe) accounts for a theoretical energy density of 914 Ah/kg.

THE NiFeS SYSTEM

As the reaction mechanism at the FeS electrode is not known, no overall reaction for the NiFeS system can be given.

FUNDAMENTAL LIMITATIONS

THE AQUEOUS ALKALINE ELECTROLYTE

For every type of battery a limitation in *potential window* applies by the characteristics of the electrolyte within it operates. The alkaline solution can be reduced/oxidized under certain electrochemical conditions. Therefore the nature of the electrolyte determines the voltage window within which the electrodes can operate. More negative potentials than the standard reduction potential of the Hydrogen Evolution Reaction (HER) leads to the decomposition of water into hydrogen and more positive potentials than the standard reduction potential of the Oxygen Evolution Reaction (OER) leads to the decomposition of water into oxygen via:

$$2\mathrm{H_2O} + 2\mathrm{e}^- \rightleftharpoons \mathrm{H_2} + 2\mathrm{OH}^- \qquad \mathrm{E}^\circ = -0.059\ \mathrm{pH\ V\ vs\ SHE} \tag{3.9}$$

$$2\mathrm{H_2O} \rightleftharpoons \mathrm{O_2} + 4\mathrm{H}^+ + 4\mathrm{e}^- \qquad \mathrm{E}^\circ = 1.23 - 0.059\ \mathrm{pH\ V\ vs\ SHE} \tag{3.10}$$

Following the Nernst equation the reduction potential of the HER and the OER depends on the pH. For a pH of 14 the E° of the HER is -0.828 V vs SHE. More negative potentials than the standard reduction potential of hydrogen leads to the irreversible side reaction of splitting water into hydrogen gas. For a pH of 14 the standard reduction potential of the oxygen evolution is 0.404 V vs SHE. More positive potentials than the E° of the oxygen evolution leads to the production of oxygen gas. As the production of gases are irreversible under these conditions it leads to a lowering in efficiency of the cell. Regardless of the pH the theoretical open circuit potential of water is a fixed value of 1.23 V_{OC}. The HER can also occur at open circuit when the standard reduction potential of the HER is more negative than the E° of the Fe(II)/Fe(0) reaction and leads to self-discharge. This also accounts for the oxygen evolution when the E° of the OER is more negative than the E° of the Ni(III)/Ni(II) reaction at the nickel-based electrode. Figure 3.4 shows the thermodynamic voltage window of nickel-based batteries in blue and the voltage window of an aqueous electrolyte at a pH of 14 in red. The production of hydrogen and oxygen gas reduces the volume and changes the alkalinity of the electrolyte. This could affect the solubility of compounds and the potential window of the system and can have negative effects on the performance of the battery. Moreover, the build-up of gases H_2 and O_2 produced can lead to explosion hazards for a sealed system or the necessity to refill the electrolyte. In a different perspective the potential window

of an aqueous electrolyte gives the possibility to apply higher or lower potentials than is necessary for an alkaline system, without attaining unfavorable reactions of the iron electrode. This resistance for so called over(dis)charge) aids to the infamous robustness of aqueous alkaline Ni-based systems.

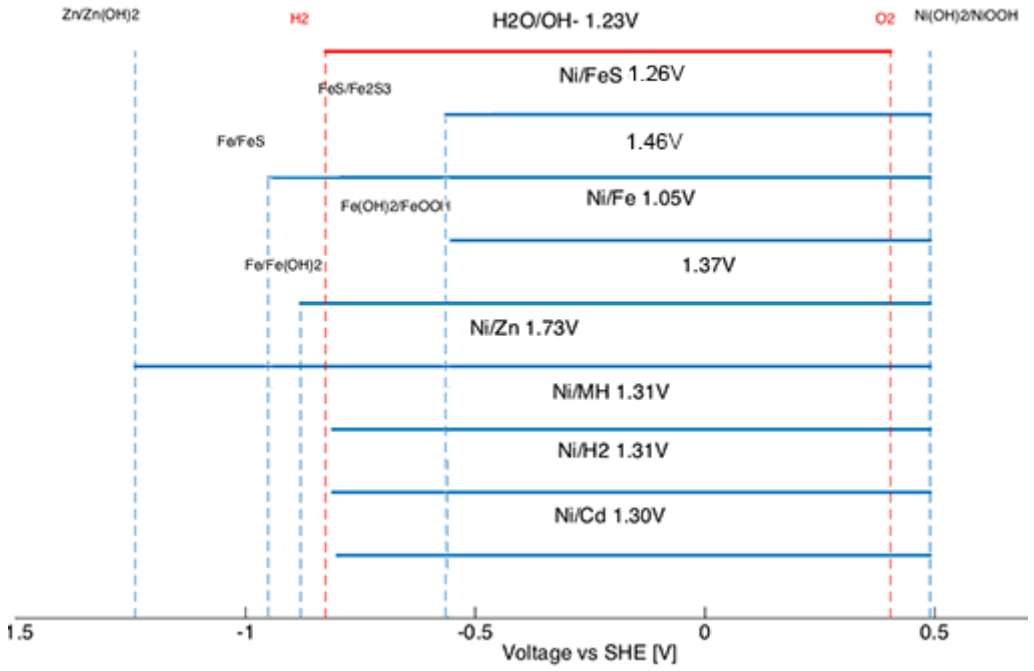

FIGURE 3.4: Thermodynamic voltage window of nickel-based batteries (Modified from Bernardt et al. (2015) [8].

THE OVERPOTENTIAL OF REDOX REACTIONS

In practice the potential at which a half-reaction takes place can differ from the theoretical potential. This leads to the concept overpotential (U_{OP}), which is the difference between the reaction its thermodynamically determined potential and the actual potential at which the redox reaction is observed. The overpotential increases with growing current density and this relation can be explained by the Tafel equation. Overpotential can be related to the activation energy of the electron transfer, activation energy of the chemical reaction prior to the electron transfer, concentrations of the reactants and/or resistance in the cell.

In particular the reaction overpotential can be reduced or eliminated by applying electrocatalysts. There, the dianionic sulfides come into play for the FeS electrode. The actual beneficial effect of sulfur containing species are elaborately discussed in appendix D. The resistance overpotential can be influenced by design parameters of the electrode and cell, further discussed in the design section.

THE OVERPOTENTIAL IN AQUEOUS SOLUTION

The usable potential window of an aqueous electrolyte can also differ significantly, because also an overpotential exist of the HER and the OER, which is dependent of the electrode material content. For instance, for the nickel electrode the OER occurs at +0.56 V vs SHE more positive than the standard reduction potential of the OER, which is 0.49 V vs SHE. Unfortunately, such a relatively high overpotential does not exist for the HER on iron, which is -0.15 V vs SHE more negative than the standard reduction potential of the HER of -0.828V vs SHE.

3.3 ACTUAL REACTION BEHAVIOR OF THE ELECTRODES

Now the redox reactions with their standard reduction potential and the fundamental limitations of the system have been described the actual potentiodynamic electrochemical reactions that occur during charge and discharge of a cell can be investigated and are eloquently illustrated by a Cyclic Voltammogram (CV).

THE NICKEL-BASED ELECTRODE

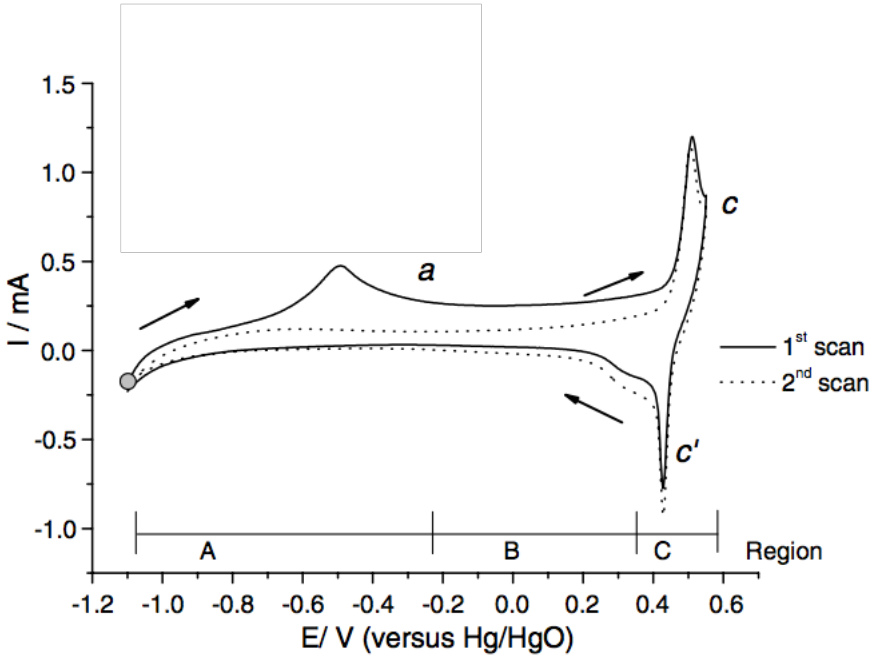

FIGURE 3.5: Cyclic voltammogram of a metallic Ni electrode at 50 mV/s in a solution of 1 M KOH (Used from Medway et al., 2006) [**?**]

Figure 3.5 shows the first two scans of a cyclic voltammetric plot against the potential of a metallic nickel electrode in a solution of 1 M KOH, reported by Medway et al. (2006) [69]. When metallic nickel is submerged in a solution of 1 M KOH, directly nickel(II) hydroxide ($Ni(OH)_2$) is formed on the surface of the electrode. Therefore the plot initiates with $Ni(OH)_2$ as starting material. The potential is measured versus a mercury/mercury(II) oxide (Hg/HgO) reaction based reference electrode in a solution of 1 M KOH. To compare the potentials given of an electrode versus a Hg/HgO reference electrode with potentials given versus the standard hydrogen evolution, the standard reduction potential of the Hg/HgO reaction versus the SHE of 0.140 V in a solution of 1 M KOH must be substracted from the electrode potential given versus Hg/HgO. A scan comprises two potentiodynamic sweeps from more negative to more positive potentials and vice versa. An upwards or downwards peak in current versus potential indicates either a oxidation or reduction, depending on which sweep. The cyclic voltammogram can be splitted into three parts. Part A is the Ni(II) region, which has a negative downward limit indicating hydrogen evolution below $<$1.00 V vs Hg/HgO and with increasing voltage during the first upward sweep a peak *a* can be found at -0.52 V vs Hg/HgO that is ascribed to the formation of $Ni(OH)_2$ in the alpha

structure (α-Ni(OH)$_2$). In the voltage window of B the dehydration of α-Ni(OH)$_2$ to β-Ni(OH)$_2$ is believed to occur, which can be identified by the wide upward peak and is not identified in subsequent upward sweeps. Part C is the oxide hydroxide region in which β-Ni(OH)$_2$ is oxidized to β-NiOOH at *c* at 0.48 V vs Hg/HgO and reduced at *c'* at 0.41 V vs Hg/HgO, which can be identified by the downward peak at the sweep from more positive to negative potentials. Hence it can be said solely the oxidation of β-Ni(OH)$_2$ to β-NiOOH is reversible. The upward positive limit $>$0.6 V vs Hg/HgO indicates the oxygen evolution to occur.

THE IRON-BASED ELECTRODE

Figure 3.6a shows a cyclic voltammetric plot in potential of a metallic iron electrode reported by Hang et al. (2006) [70]. In the upward sweep with increasing voltage two upward peaks can be found at -0.88V and -0.62 V vs Hg/HgO, corresponding with the standard electrode potentials of the Fe/Fe(OH)2 reaction by equation 3.2 and the Fe/FeOx reaction, respectively. In the downward sweep with decreasing voltage, the first downward peak at -1.1 V vs Hg/HgO is ascribed to the FeOx/Fe(OH)$_2$ reduction reaction. The subsequent downward limit at $<$1.1 V vs Hg/HgO is due to the hydrogen evolution. The reaction Fe/Fe(OH)$_2$ by equation 3.2 during charge is said to be overshadowed by the occurrence of the HER and can not be identified in this plot.

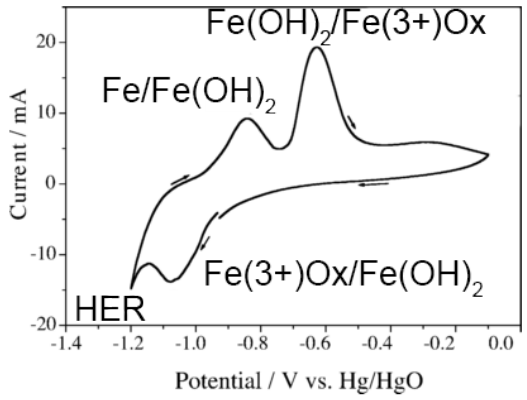

(A) The first scan of an Fe electrode in a mixture of 8M KOH at 0.5 mV/s (Used from Hang et al., 2006 [70]).

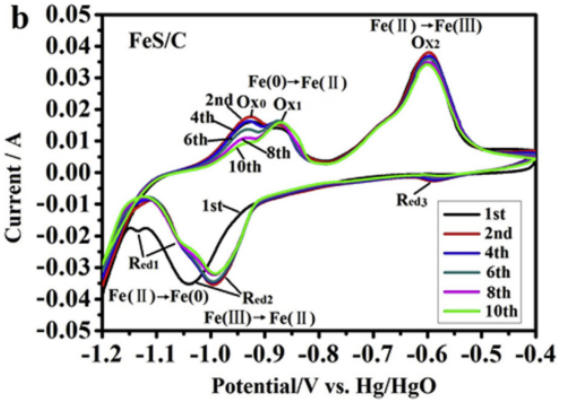

(B) Subsequent scans of a FeS electrode in a mixture of 6M KOH and 0.5M LiOH at 1.0 mV/s (Used from Shangguan et al.,2015 [67])

FIGURE 3.6: Cyclic voltammograms.

Figure 3.6b also shows a cyclic voltammetric plot but then for an iron(II) sulfide electrode reported by Shangguan et al. (2015) [67]. Different to the findings of Hang et al., Shangguan et al. found the Fe/Fe(II) reaction to occur in two subsequent steps over repetitive sweeps (Ox0 and Ox1). The first step is around -0.95 V vs Hg/HgO, which increases over subsequent scans and the second step occurs at -0.9V vs Hg/HgO. The Fe(II)/Fe(III) reaction (Ox2) is found to occur at -0.6 V vs Hg/HgO, which is similar to the iron electrode. During the downward sweep with decreasing voltage an unidentified downward peak (Red3) is observed around -0.58 V vs Hg/HgO but gradually decays after subsequent cycling. Afterwards a downwards peak indicates the reduction of Fe(III)/Fe(II) (Red2), which occurs initially at 1.1 V but shifts to more positive potentials after subsequent sweeps. In contrast to the Fe electrode

reported by Hang et al (2006), for the FeS electrode a downward peak can be found separated from the hydrogen evolution that is ascribed to the Fe(II)/Fe(0) reaction (Red1) at -1.15 V but also shifts to more positive potentials after a series of sweeps. The downwards peaks that illustrate the Fe(III)/Fe(II) and Fe(II)/Fe(0) reactions are more closely together in potential than the Fe(0)/Fe(II) and Fe(II)/Fe(III).

3.4 EMPLOYED MATERIALS FOR THE ELECTRODES

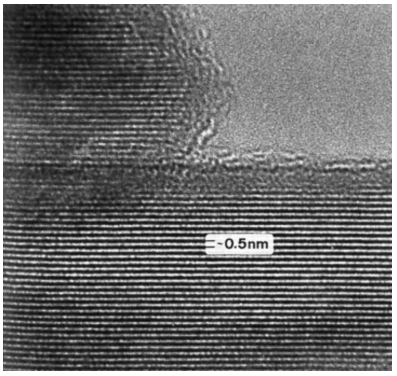

FIGURE 3.7: High resolution electron micrograph of α-FeOOH. The lattice fringes at 0.5 nm indicate the interdistance spacing (Used from R. Cornell et. al,. 2003 [9]).

The properties of the active material determine the operational mechanism of an electrode. The inherent physical and chemical characteristics of the species that form during cycling by the electrochemically forced and chemically spontaneous changes in the species and structure can negatively influence the overpotential by change in (i) reactivity between the active material and the electrolyte, (ii) electric conductivity between the material and current collector and (iii) mechanical strength of the electrodes. Chemical changes could even lead to physical degradation and breakdown. To acquire optimal stability, which means a high reversibility of the redox reactions over the long-term, the redox processes occur under solid state chemistry solely, in which the material properties have minimal change. Therefore an ideal structure of the crystals in the grains have an easy accessible host structure that can inject or reject a proton. The host structure can be described as a packing of solid slabs having a high interdistance in between, as shown in figure 3.7. In this spacing protons can be bonded to the host structure. This section describes the characteristics of the materials, in terms of phase composition, solubility, morphology and crystallinity. What becomes clear is that the Ni cathode structure comes close to the optimal in comparison to the iron anode. General properties of iron and nickel oxides are given in appendix B.

THE WELL STUDIED AND EXEMPLARY NICKEL-BASED ELECTRODE

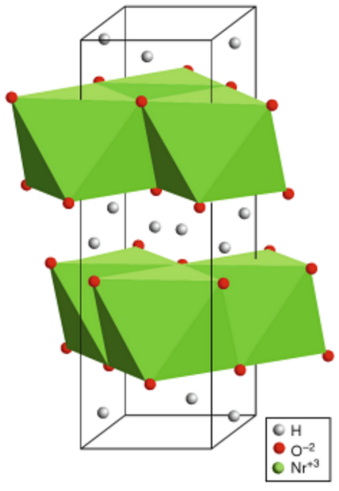

FIGURE 3.8: The $Ni(OH)_2$ layered structure (Used from P. Bernardt et al., 2015 [8]).

The active material of the cathode in alkaline aqueous batteries is nickel hydroxide in the beta morphology (β-$Ni(OH)_2$). Various alkaline aqueous systems are possible with nickel-based species as cathode, such as NiFe, NiCd, NiMH, Nickel-Hydrogen (Ni-H_2) and Nickel-Zinc (NiZn). Their operating potential windows are depicted in figure 3.4. As starting material nickel hydride and nickel oxides are used. Both result in the formation of β-$Ni(OH)_2$ as it is the most favored thermodynamic stable composition of nickel in an alkaline medium and preserves excellent stability due to its low solubility ($K_{SP} \approx 10^{-35}$) [8, 57, 71]. The reaction between β-$Ni(OH)_2$ and β-NiOOH is believed to be of a reversible solid-state-type at which a proton is injected and included in the host structure (intercalation) [8, 46, 57, 71]. Figure 3.8 shows an illustration of the β-$Ni(OH)_2$ structure [8]. The slabs are layered as NiO_6 octahedra having hydrogen atoms located in between bound to the oxygen. The NiO_6 can be seen as the solid host structure with removable H atoms that occupy interstitial sites within the slabs.

β-NiOOH is an electric semiconductor (10^4-10^5 Ω/cm at 25°C). During discharge the electrode attains $Ni(OH)_2$ species which are known to behave as an insulator (10^{10}-10^{12} Ω/cm at 25°C). The formation of electrically insulating species affects the deep discharge capacity or can even lead to a decrease in reactivity by *passivation*, which is the formation of an insulating layer of $Ni(OH)_2$ around β-NiOOH particles that lowers the electric conductivity and active surface area [72]. While the β-NiOOH/β-$Ni(OH)_2$ reaction is seen as a solid state mechanism the species involved are sparingly soluble, leading to dissolved intermediates. The dissolution of the species can act as rate determining at high discharge rates. If both of the species involved in the Ni(II)/Ni(III) reaction would have poor electric conductance no electric conductance to the current collector could be attained leading to a general overall poor performance.

Also the formation of unfavorable species can trouble the performance. Transformation pathways of the nickel-based electrode are eloquently illustrated by the Bode diagram, shown in figure 3.9 [8]. two other possible phases need to be accounted for: γ-$H_xK_yNiO_2.H_2O$ in the charged state, where x and y are often claimed to be 0.33 and 0.66, respectively, and α-NiOOH in the discharged state [8, 46, 57, 71]. By overcharge the γ-$H_xK_yNiO_2.H_2O$ can form and has an enlarged interlayer distance. Thereby it can intercalate species of the electrolyte solution in the structure, by which the electrode can dry-out. During discharge, in addition to the β-form also the γ-$H_xK_yNiO_2.H_2O$ can form α-$Ni(OH)_2$, which in turn spontaneously reforms to β-$Ni(OH)_2$ over time in base conditions. For an electrode comprised of α-$Ni(OH)_2$ rather than β-$Ni(OH)_2$, a higher theoretical capacity is expected, due to the bigger interslab distance [8, 71].

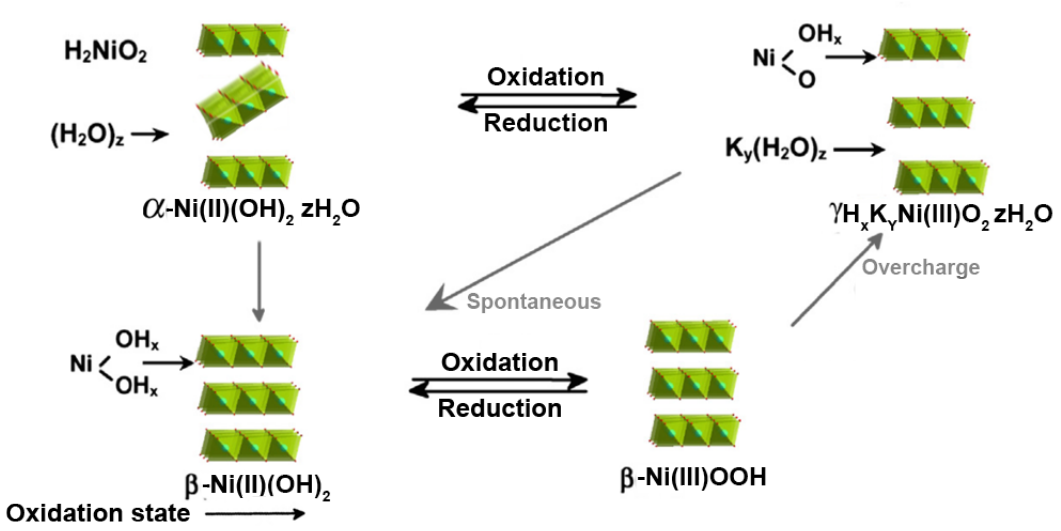

FIGURE 3.9: Bode diagram showing transformations among various phases of the nickelhydroxide electrode (Modified from P. Bernardt et al., 2005 [8]).

Nonetheless, by the application of special preparation methods and the use of substances that improve the performance of the electrode, so-called *additives*, the Ni-based electrode is known in literature for its excellent reversibility and cyclic behavior [8, 46, 57, 71, 72]. The material characteristics of the species has been intensively studied in order to further improve the electrochemical performance. This has recently led to the suggestion that stacking faults, the interruption of the normal stacking sequence in the

crystal structure, cause strong interactions between the nickel ions and protons. 15-20% stacking faults in the crystal structure are suggested to lead to near theoretical energy densities of 289 Ah/kg [8].

PERFORMANCE ENHANCING ADDITIVES FOR NICKEL-BASED ELECTRODES

For the electrode to remain in optimal cycling conditions additives or substances can be added to the electrode material or electrolyte. Additives can influence the overpotential in terms of (i) reactivity, (ii) parasitic side-reactions, (iii) dry-out of the electrolyte, (iv) surface area, (v) solubility (vi) ionic- and/or (vii) electrical conductivity at all state of charges. In general, certain metal complexes within the active mass create stacking faults and prevent the formation of aggregates. In catalyses literature the stacking faults are believed to increase reactivity while the prevention of aggregation is suggested to preserve the homogeneity of the solid mass. Cobalt(II) hydroxide ($Co(OH)_2$), which is isostructural with β-NiOOH and β-$Ni(OH)_2$ is often used as a spacing agent additive [8]. A so called *spacing agent* creates a disordered structure, leading to stacking faults and following preservation of the space between the layers of the crystal and prevention of formation of aggregates. The oxygen evolution is an unfavorable side reaction, of which the standard reduction potential is close to the standard reduction potential of β-NiOOH to β-$Ni(OH)_2$. $Co(OH)_2$ also reduces the potential of the reaction of β-NiOOH to β-$Ni(OH)_2$, leading to the prevention of the OER to occur. Cadmium-, zinc- and magnesium oxide have been found to reduce electrostatic repulsion between the slabs and hence can be employed as additives to prevent the gamma phase formation, which can lead to electrolyte dry-out. Cadmium, magnesium and zinc containing compounds also slightly prevent the OER as $Co(OH)_2$ does [73]. In general, alkaline electrolyte based systems need to deal with oxidized metal species that are less electronically conductive than pure metals. Hence, conductive additives, such as amorphous carbon and graphite can be necessary to sustain conductivity, which also depends on the electrode production technology. Equally, also binder additives can be necessary further elaborated upon in the cell design section.

THE IRON-BASED ELECTRODE

The iron-based electrode is part of the NiFe cell and is also used as counterpart of the Fe-O_2 or silver-iron (AgFe) system. Most commercially applied and studied is the NiFe system. The standard starting material of the Edison battery is ironoxide (FeO) or so called iron rust species [7]. Commercial batteries today use a mixture of synthesized iron(III) oxide (Fe_2O_3) and metallic iron [16]. Impurities such as manganese, magnesium, calcium and phosphorous are believed to facilitate the hydrogen evolution, hence it is suggested to use high purity iron as the active material [52, 58, 59]. A form of such a high purity iron is carbonyl iron, which is prepared from iron(0) pentacarbonyl ($Fe(CO)_5$) and has been found to reduce the HER.

In basic alkaline iron related electrochemistry literature little is mentioned regarding the change in morphology and actual crystal structures formed during the Fe(0/II) and particularly the Fe(II/III) charge/discharge process. Different characterizations of the species involved exist and contradicting theories are suggested concerning the working principle. In this thesis an attempt is done to clarify the involved species and illustrate the working mechanisms of the charge/discharge behavior of the iron electrode via an in-depth literature study. The Fe(0/II) redox reaction mechanism is the standard half reaction used at the iron-based electrode. The Fe(II/III) redox reaction mechanism is only mentioned to occur at

low or so-called deep discharges but is not used as standard solely. The Fe(II/III) is not as well studied as the Fe(0/II) redox reaction mechanism. In 1999, Licht introduced an electrode capable of using the Fe(3+/6+) redox reaction but is kept out of this research [74]. Appendix C shows typical formation and transformation pathways of common iron oxides (FeOx).

WHAT IS KNOWN ABOUT THE IRON(0/II) REDOX PROCESS

The involved species during charge and discharge in strong alkaline solution are consistently reported to be metallic iron in alpha morphology (α-Fe) and iron(II) hydroxide, respectively, which correspond to the Fe(0/II) redox reaction described by equation 3.2. Iron(II,III) oxide (Fe_3O_4) forms at a E_0 of -0.912 V vs SHE close to the E_0 of the Fe/$Fe(OH)_2$ at -0.880 V vs SHE according to the reaction:

$$3\mathrm{Fe} + 8[\mathrm{OH}]^- \underset{charge}{\overset{discharge}{\rightleftharpoons}} \mathrm{Fe_3O_4} + 4\mathrm{H_2O} + 8\mathrm{e}^- \qquad \mathrm{E}^\circ = -0.912\mathrm{V\ vs\ SHE} \qquad (3.11)$$

The formation of metastable $Fe(OH)_2$ is believed to be favored over Fe_3O_4 due to the high kinetic reversibility of reaction 3.2 [75–77]. Only at high overpotentials or deep discharges the formation of Fe_3O_4 is expected to occur as well [12]. Figure 3.10 illustrates the unoxidized α-Fe homogeneous body centered cubic structure. $Fe(OH)_2$ does not exist in nature as mineral due to its intrinsically unstable characteristic and no different polymorphs have yet been found [9]. It has a similar crystal structure as β-$Ni(OH)_2$, as shown in figure 3.8 but then the slabs are layered FeO_6 octahedra. Fe_3O_4 contains both Fe(II) and Fe(III), having an inverse spinel structure as shown in figure 3.12b and has a thermodynamically more stable structure than $Fe(OH)_2$ due to its closer packing. Therefore the hydrogen evolution can give rise to the dehydration of $Fe(OH)_2$ and formation of Fe_3O_4 under anaerobic conditions over time and can be described by the Schikkor reaction [14, 78, 79]:

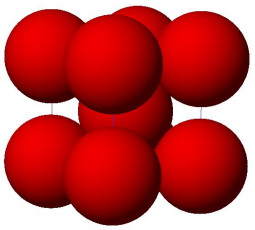

FIGURE 3.10: The homogeneous structure of α-Fe.

$$3\mathrm{Fe(OH)_2} \rightarrow \mathrm{Fe_3O_4} + \mathrm{H_2} + 2\mathrm{H_2O} \qquad (3.12)$$

In 1958, Linnenbom investigated the reaction between metallic iron and water [80]. He found solely $Fe(OH)_2$ formation at room temperature under anaerobic conditions. He stresses the extreme sensitivity to react to Fe_3O_4 by increasing temperature and contaminants, such as tiny amounts of oxygen but also trace amounts of nickel, copper and platinum. An excess of hydroxide ions is found to remarkably inhibit the formation of Fe_3O_4 out of $Fe(OH)_2$. Dissolved oxygen in the electrolyte is also suggested to lead to the formation of Fe_3O_4 from $Fe(OH)_2$ [76, 81]. The hydrogen evolution causes an increased overpotential for the reaction of Fe_3O_4 to metallic iron during charge leading to a higher irreversibility of Fe_3O_4 already in the Fe(0/II) potential window [82]. Hence, the slow formation of Fe_3O_4 by the occurrence of the Schikorr reaction and the parasitic side-reaction by equation 3.11 are suggested to cause long term irreversibility of the iron electrode [12].

In contrast to the predominant solid state reaction of the oxidized species $Ni(OH)_2$ and NiOOH, the oxidation of metallic Fe is believed to contain more soluble intermediates in alkaline environment. A

theoretical study by Schräger (1929) suggested the occurrence of $[HFeO]_2^-$ in highly alkaline conditions [83]. Schwarz and Simon (1963) found iron to electrochemically dissolve as $[FeO]_2{}^{2-}$ in alkaline solution [84]. Flerov and Pavlova confirmed that divalent and trivalent iron hydroxides ($[HFeO]_{2^-}$ and $[FeO]^{2-}$) dissolve in a solution of 6M KOH [85]. Sherstobikova et al. (1969) found the following dissolution/precipitation mechanism to occur [86]:

$$\mathrm{Fe} + [\mathrm{OH}]^- \leftrightharpoons (\mathrm{FeOH})_{\mathrm{ads}} + \mathrm{e}^- \qquad RDS \tag{3.13}$$

$$(\mathrm{FeOH})_{\mathrm{ads}} + [\mathrm{OH}]^- \rightarrow (\mathrm{FeO})_{\mathrm{ads}} + \mathrm{H_2O} + \mathrm{e}^- \tag{3.14}$$

$$(\mathrm{FeO})_{\mathrm{ads}} + [\mathrm{OH}]^- \rightarrow [\mathrm{HFeO_2}]^- \tag{3.15}$$

$$[\mathrm{HFeO_2}]^- + \mathrm{H_20} \rightarrow \mathrm{Fe(OH)_2} + [\mathrm{OH}]^- \tag{3.16}$$

Adsorbed species are indicated with round brackets ( ). While having soluble intermediates involved Fe(II) still is sparingly soluble (Ksp$\approx$1.65 10^{-15}) [17]. This in combination with the high energy of crystallization of Fe causes the tendency to supersaturate near the reaction site, leading to only minute crystal formation of oxidized adsorbed iron(I) hydroxide $(FeOH)_{\mathrm{ads}}$ and iron oxide $(FeO)_{\mathrm{ads}}$ products as a porous gel on the surface of the reactant [16]. This porous gel structure is eloquently illustrated by a SEM study of Öjefors (1976) [48]. The low solubility of $(FeOH)_{\mathrm{ads}}$ is the main parameter that slows crystal growth. Therefore reaction 3.11 is the Rate Determining Step (RDS). During discharge the reaction products are found to precipitate on the surface as a porous gel, blocking the active surface area for electrolyte. Thus, the formed layer, a so-called passivation layer, causes insulation of the active material of the charge carriers, which can lead to a lowering in reactivity and poor charge/discharge rates depending on the accessibility through the passivation layer [8, 16, 56, 57, 68]. In addition the passivating layer of $Fe(OH)_2$ is also electrically insulating. This increases the overpotential of the $Fe/Fe(OH)_2$ reaction by which the hydrogen evolution is believed to be favored, leading to a decrease in efficiency as well. In contrast, the supersaturation is also suggested to have a beneficial effect. The fast crystallization ensures the reformation of a high active surface area ($>100/m^2/g^1$), characterizing the long cycling capability of iron-based electrodes [16]. Shukla (2009) emphasizes that the ionic polarization solely could not fully limit the capacity as the electrolyte is expected to still be able to penetrate the porous gel [56].

The dissolution/precipitation mechanism is confirmed by several other electrochemical studies [31, 32, 48, 76, 87–90] and in particular by Cnobloch et. al (1973) [91]. Nonetheless, solid state processes of the $Fe/Fe(OH)_2$ reaction by equation 3.2 are also found to occur [32, 92]. Thus the overall mechanism of reaction 3.2 could involve a direct solid state and indirect dissolution/precipitation mechanism. The dissolution/precipitation mechanism is heavily dependent of temperature [16] and alkaline concentrations [92]. Among others, the Handbook of Batteries clearly indicates the high temperature dependance of iron electrodes, further elaborated upon in the performance section [16, 49, 93]. Hence, at low alkaline concentrations and/or temperatures the working mechanism of the Fe(0/II) reaction is more of a solid-state type.

WHAT IS KNOWN ABOUT THE IRON(II/III) REDOX PROCESS

More controversy exist concerning the reaction products of iron(III) species that are formed during low discharge. The same as for the Fe(0/II), the $Fe(OH)_2$/FeOOH reaction has a parasitic side-reaction of which the reduction potential of -0.560 V vs SHE is close to the formation of more stable iron(II,III) oxide of -0.660 V vs SHE, following the reaction:

$$3\mathrm{Fe(OH)_2} + 2[\mathrm{OH}]^- + 2\mathrm{H_2O} \underset{charge}{\overset{discharge}{\rightleftharpoons}} \mathrm{Fe_3O_4} + 4\mathrm{H_2O} + 2\mathrm{e}^- \qquad \mathrm{E}^\circ = -0.660\mathrm{V\ vs\ SHE} \tag{3.17}$$

Only at high overpotentials or very low discharges the formation of Fe_3O_4 is expected to occur [12]. The same explanation can be given as for the Fe(0/II) reaction mechanism. The higher kinetic reversibility of β-FeOOH to $Fe(OH)_2$ causes the formation of β-FeOOH by equation 3.3 to be favored. Only at high overpotentials or deep discharges the formation and build-up of Fe_3O_4 can be expected due to its higher irreversibility. This is in line with several studies in which an increase of Fe_3O_4 is found by repeated overdischarge [31, 79, 92, 94]. Conversely, Mössbauer spectroscopy analysis by Geronov et al. (1975) did not encounter this phenomenon [75]. Cyclic voltammetry and X-ray powder diffraction (XRD) literature indicate the formation of Fe_3O_4 [31, 44, 76, 81, 87–89, 91, 94, 95] or even Fe_2O_3 [27, 76, 87–89, 96]. Geronov et al. (1975) suggests the formation of β-FeOOH following reaction 3.3 in a solution of 5M KOH [75], which is in agreement with several other CV and XRD based research [89, 89, 90, 92, 92, 96–99].

β-FeOOH is known for its metastable behavior of spontaneously reforming into more stable species over time. β-FeOOH rearranges into oxidized iron (FeOx) species, which is also suggested by Ravikumar et al. (2015) [44]. The occurrence of metastable compounds in the cycling process in combination with the sensitivity of $Fe(OH)_2$ and FeOOH for air and contaminants but also general measurement limitations in the past could be a reason $Fe(OH)_2$ and FeOOH species to be overlooked by some studies. Under ideal conditions it is assumed that β-FEOOH is the main product of the oxidation of $Fe(OH)_2$. In contrast Zhang (1994) found the formation of FeOOH in the δ formation [46, 76].

(A) β-FeOOH (B) δ-FEOOH

FIGURE 3.11: two of the four known FeOOH isomorphic structures (used from R. Cornell et al., 2003 [9]).

Illustrated in figure 3.11 are the β- and δ-FeOOH structures. δ-FeOOH has a similar structure as the β-NiOOH. β-FeOOH has a tetragonal or monoclinic unit cell in which the anions are arranged as a body centered cubic array bonded together. The overall structure contains actual tunnels per one unit cell in which the anions are missing. Appendix A describes the four known polymorphs of FeOOH in

more detail. It is suggested that prolonged discharge causes anhydrous δ-FEOOH to change to hydrous bernalite ($Fe(OH)_3$), similar to the $Ni(OH_2$ cathode by [56]:

$$\delta - \mathrm{FeOOH} + \mathrm{H_2O} \rightarrow \mathrm{Fe(OH)_3} \tag{3.18}$$

The Fe(III) of the very unstable $Fe(OH)_3$ created by deep discharge spontaneously rearranges with Fe(II) to form the more stable Fe_3O_4 (Fe_3O_4) following another pathway of the Schikorr reactions by [11, 16, 46, 48, 56, 57, 68, 78]:

$$2\mathrm{Fe(OH)_3} + \mathrm{Fe(OH)_2} \rightarrow \mathrm{Fe_3O_4} + 4\mathrm{H_2O} \tag{3.19}$$

Several other pathways exist for the formation of Fe_3O_4 and Fe_2O_3:

$$2\mathrm{Fe^{2+}} + \mathrm{FeOOH} \rightarrow \mathrm{Fe_3O_4} + 2\mathrm{H^+} \tag{3.20}$$

$$2\mathrm{FeOOH} \rightarrow \mathrm{Fe_2O_3} * \mathrm{H_2O} \tag{3.21}$$

FeOOH can react with soluble Fe(II) species to form Fe_3O_4 by equation 3.20 [76] and is also found to spontaneously form the more stable Fe_2O_3 by equation 3.21. The crystal structure of Fe_2O_3 is depicted in figure 3.12a. Fe_2O_3 is even more stable and has a higher irreversibility than Fe_3O_4, that could lead to more non-equilibrium conditions and thus loss of active species within the electrode [92].

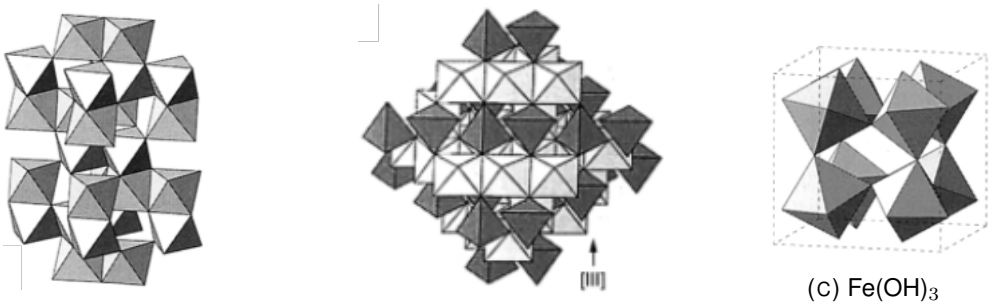

(A) Fe_2O_3 (B) Fe_3O_4 (C) $Fe(OH)_3$

FIGURE 3.12: Structures of various iron oxide species [9]

.

Next to a solid state mechanism, the Fe(II/III) reaction by equation 3.3 is suggested to have a dissolution/precipitation mechanism as well:

$$[\mathrm{HFeO_2}]^- + [\mathrm{OH}]^- \rightleftharpoons [\mathrm{FeO_2}]^- + \mathrm{H_2O} + \mathrm{e}^- \tag{3.22}$$

$$2[\mathrm{FeO}]_2^- + \mathrm{Fe(OH)_2} + 2\mathrm{H_2O} \rightarrow \mathrm{Fe_3O_4} * 4\mathrm{H_2O} \tag{3.23}$$

$$[\mathrm{FeO_2}]^- + \mathrm{H_2O} \rightarrow \beta - \mathrm{FeOOH} + [\mathrm{OH}]^- \tag{3.24}$$

Considering the analysis of Fe(III) species in the electrolyte, ferrates (FeO_2^-) are also believed to take part in the reaction [48, 86–88, 91, 100]. Hence when in contact with the electrode, dissolved Fe(II) species could and are found to oxidize and precipitate following equation 3.22. Again different suggestions are given considering what Fe(III) products form out of the $[FeO]_2^-$ species: Fe_3O_4 or $Fe(OH)_2$ by respectively equation 3.23 or 3.24. The Fe(II/III) reaction is observed to occur more quickly than the Fe(0/II) reaction and seems to be less dependent of temperature and pH [85, 88, 92]. Therefore the Fe(II/III) reaction is suggested to be more of a solid state reaction mechanism.

APPLYING ONLY THE Fe(II/III) REDOX REACTION AS STANDARD

To prevent efficiency losses because of the HER and dense charge capacity losses because of the dissolution/precipitation mechanism at the Fe(0/II) reaction, an obvious alteration to apply is using the Fe(II/III) reaction solely but has never been suggested in scientific literature. It is noteworthy that the nickel-based electrode uses the Ni(II/III) solely. Both $Fe(OH)_2$ and FeOOH species are electrically insulating [33, 97]. At the nickel-based cathode only NiOOH causes electrical insulation. As Fe_3O_4 is electrically conductive, formation of the latter could be an important factor to maintain electric conductivity during discharge. On the other hand, Fe_3O_4 and Fe_2O_3 are less reversible than $Fe(OH)_2$ and FeOOH. To acquire reduction of these species a certain amount of overcharge is necessary but is troubled by the parasitic hydrogen evolution reaction [12]. Although not extensively mentioned in literature, it is expected that (i) the formation of less reversible species by parasitic side-reactions, spontaneous formation and deep discharge in combination with (ii) the electrically insulating properties of the FeOx species and/or (iii) the possibility of passivation due to a dissolution/precipitation mechanism affects the Fe(II/III) redox reaction. Moreover, the Fe(II/III) reaction takes place at low potentials and is only one electron redox process instead of two electrons at the Fe(0/II) reaction causing lower energy densities possible as shown in table 3.2. Therefore the Fe(0/II) redox reaction by equation 3.3 is preferred and literature seems to focus more on the Fe(0/II) reaction.

SUMMARY OF THE REDOX PROCESSES AT THE IRON-BASED ELECTRODE

The above said, having a dissolution/precipitiation mechanism and metastable/stable species into play, it is clear that many side-reactions occur at the iron-based electrode compared to the rather simple $Ni(OH)_2$/NiOOH electrode working mechanism. The overall mechanism could be well described by the definition of green rust formation, which is the formation of Fe(II)OH octahedra with within some Fe(II) can be replaced by Fe(III). To maintain neutrality anions can coincide within the layers. However, the occurrence of green rust species is not mentioned in scientific literature concerning the iron-based electrode. Figure 3.14a shows all suggested species and reaction paths possible at the iron-based electrode, while Figure 3.13b shows an illustration of all possible species and reactions mentioned at the iron electrode. Pourbaix diagrams illustrate the possibility of which species to occur at which pH versus the standard reduction potential. Figure 3.13b shows the Pourbaix diagram for the Fe/H_2O system [10, 11, 97]. Based on theory, the solid lines and bold letters respectively illustrate the area where solids and solutions are prone to occur. The solid or liquid before the dash is the metastable form and behind the dash is the stable form, so metastable/stable. Dashed lines with regular letters indicate the area where reactants in solution can exist, with exception of the dashed lines a and b. Below line a the HER can occur and above line b the oxygen evolution could occur. The region between 0.4 and -1.4 V vs SHE and corresponding pH values >14 are said to be the preferable conditions for alkaline aqueous NiFe systems, which is indicated by the red box in figure 3.13a [11]. The Pourbaix diagram, which is based on theoretical thermodynamics seems to be in line with experimental research

and indicates that the composition of species are heavily dependent of the, and thus can be altered by, electrolyte its pH and temperature. Also additives can be used, such as lithiumhydroxide LiOH and sulfur containing species, explained further in the next additive section below. Figure 3.13 shows an illustration of the possible reaction mechanisms at the iron-based electrode.

To conclude, the reaction mechanisms occurring at the iron-based electrode causes some obvious drawbacks. Issues with the existing system include:

- The necessity to overcharge due to overpotential of the Fe/Fe(OH) reaction resulted by the hydrogen evolution causes (i) low efficiencies (ii) poor energy densities and (iii) hydrogen gas production. The production of gas from the electrolyte leads to the depletion of the electrolyte and as a result the cell can not be sealed. Moreover, the occurrence of the HER causes the electrode to be intrinsically unstable leading to self-discharge.
- Having a dissolution/precipitation mechanism with soluble intermediates involved results in an (i) increased temperature dependent performance and (ii) passivation of the electrode by various FeOx species at high charge density capacities. The passivation ultimately results in even more limited power densities and efficiencies.
- Involved species in the charge/discharge process have the tendency to spontaneously transform into more stable but less reversible species over time, which also lead to a decrease in cycle life, efficiencies and energy densities.

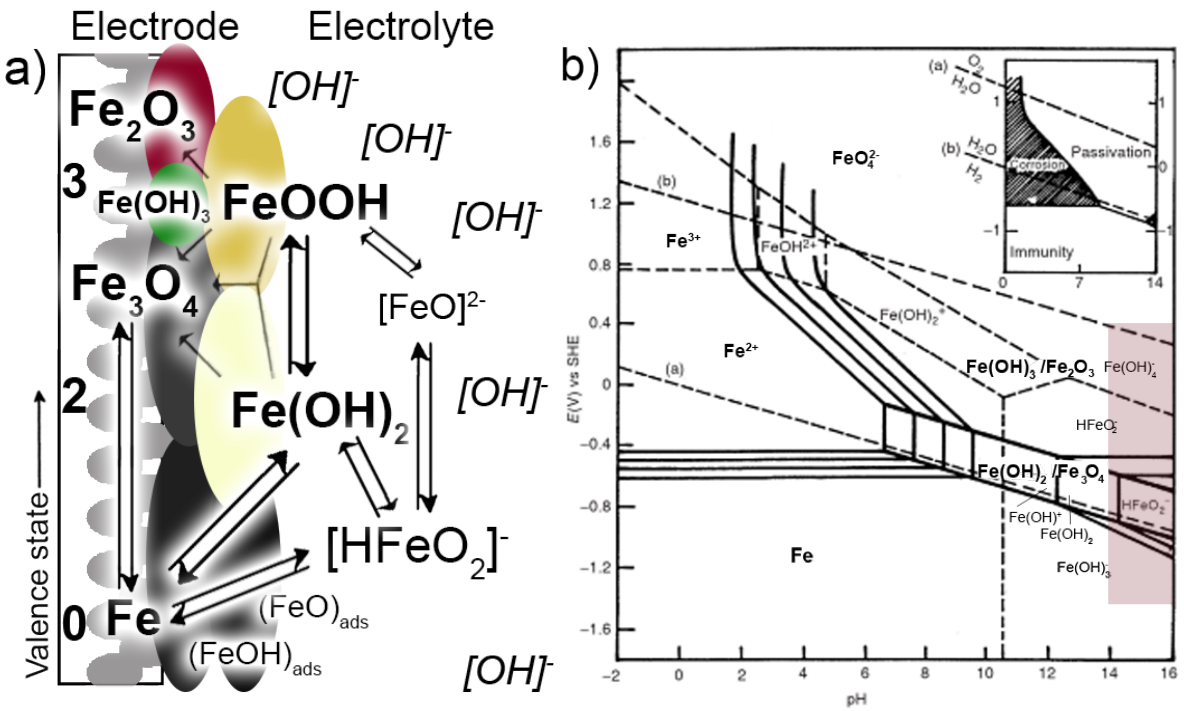

FIGURE 3.13: (a) Illustration of species and reactions occurring at the surface of the iron electrode in alkaline solution and (b) revised potential/pH diagram for the Fe/H_2O system; regions of passivity, corrosion and immunity of iron are shown (Used from Pourbaix, 1966 [10, 11]).

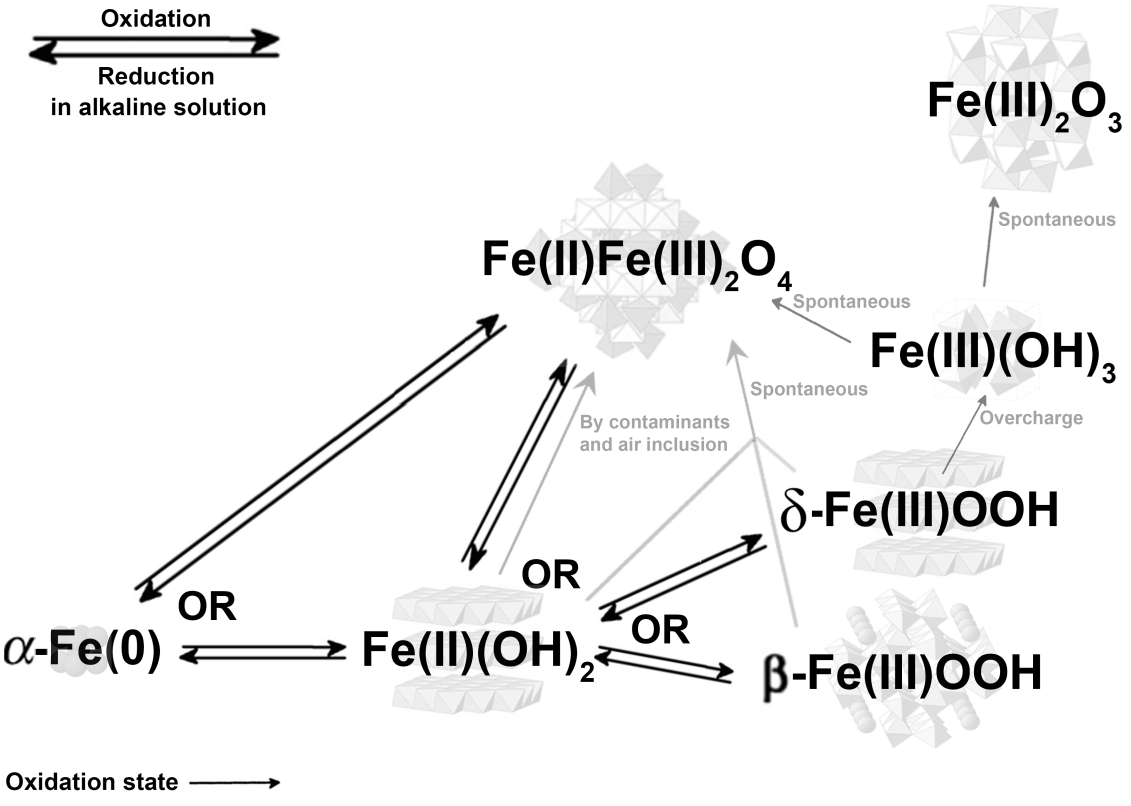

FIGURE 3.14: Reaction mechanisms at the iron-based electrode in alkaline solution illustrating the change in chemical compositions among various phases.

KNOWN PERFORMANCE ENHANCING ADDITIVES FOR THE IRON-BASED ELECTRODE

Several additives are known for their beneficial effect for the iron-based electrode and can be incorporated within the electrode itself or within the electrolyte. Table 3.3 gives an overview of which scientific literature investigated what additive for iron-based electrodes.

TABLE 3.3: Overview of studied additives for the iron-based electrode with their reaction mechanism, standard reduction potential, solubility product and reference [17, 18].

Specie	Reaction mechanism	E° vs SHE	K_{SP}	Studied by
The alkaline iron-based system				
Fe	$Fe + 2[OH]^- \rightleftharpoons Fe(OH)_2 + 2e^-$	-0.877 V		
$Fe(OH)_2$	$Fe(OH)_2 + [OH]^- \rightleftharpoons FeOOH + H_2O + e^-$	-0.560 V	$1.65\ 10^{-15}$	
FeOOH				
Decrease U_{OP} of Fe/Fe(II) reactions & Increase U_{OP} of HER				
FeS	$Fe + [S]^{2-} \rightleftharpoons FeS + 2e^-$	-0.970 V	$1\ 10^{-19}$	[12, 16, 34, 35, 42, 44, 52, 56, 100, 101]
FeSe	$Fe + [Se]^{2-} \rightleftharpoons FeSe + 2e^-$	-1.22 V	$1\ 10^{-26}$	[100, 101]
FeTe	$Fe + [Te]^{2-} \rightleftharpoons FeTe + 2e^-$			
Decrease U_{OP} of Fe/Fe(II) and Fe(II)/Fe(III) reactions				
Superconductive species				[40, 53, 67, 102, 103]
Increase U_{OP} of the HER				
Bi_2O_3	$2Bi + 6[OH]^- \rightleftharpoons Bi_2O_3 + 3H_2O + 6e^-$	-0.460 V	$2.3\ 10^{-11}$	[12, 36, 42, 52, 59]
Bi_2S_3	$2Bi + 3[S]^{2-} \rightleftharpoons Bi_2S_3 + 6e^-$	-0.818 V	$1.6\ 10^{-72}$	[36, 42, 52, 58]
CuO_2	$2Cu + 2[OH]^- \rightleftharpoons Cu_2O + H_2O + 2e^-$	-0.360 V	$1.2\ 10^{-15}$	[104]
Cu_2S	$2Cu + [S^{2-}] \rightleftharpoons Cu_2S + 2e^-$	-0.95 V	$2.5\ 10^{-50}$	
CuS	$Cu + [S^{2-}] \rightleftharpoons CuS + 2e^-$	-0.7 V	$4\ 10^{-38}$	
Organo-sulfur species				[60, 61, 63, 64]
Increase the E° of the Fe/Fe(II) reactions				
$Ni(OH)_2$	$2Ni + 2[OH]^- \rightleftharpoons Ni(OH)_2 + 4e^-$	0.66	$1.6\ 10^{-14}$	[100]
NiOOH			$1\ 10^{-35}$	
$Co(OH)_2$	$Co(OH)_2 + [OH]^- \rightleftharpoons CoOOH + H_2O + e^-$			[100]
Capture H_2 evolved				
CeO_2	$MH_{ads} + [OH]^- \rightleftharpoons 2M + H_2O + e^-$			[55]
$LaNi_5$				[105]

DECREASE THE Fe/Fe(II)- & INCREASE THE H_2/H_2O REACTION OVERPOTENTIALS

Indeed, iron(II) sulfide is suggested to have a dual effect in lowering the overpotential of the Fe/Fe(II) reaction and increasing the overpotential of the HER. Iron-based electrodes with inorganic sulfide species as additives are widely investigated. Yet, their exact working function is still unknown. Therefore appendix D consists of a thorough up to date literature survey of theories concerning the working function of sulfur containing species for iron-based electrodes. In this section solely a summary is given.

FeS is less soluble than $Fe(OH)_2$ as the solubility product of FeS and $Fe(OH)_2$ are 4 10^{-19} and 1.65 10^{-15}, respectively. In addition the Fe/FeS reaction has a standard reduction potential of -0.970 V vs SHE, which is more negative but close to the Fe/$Fe(OH)_2$ reaction of -0.877 V vs SHE [17]. Thereby, during discharge, some of the anionic sulfur species that occur within the electrolyte are suggested to strongly adsorb on the surface of the iron electrode and react to FeS [12, 26–28, 31, 106–108] out of Fe by equation 3.6 or out of $Fe(OH)_2$ by:

$$\mathrm{Fe(OH)_2} + [\mathrm{S}]^{2-} \rightleftharpoons \mathrm{FeS} + 2[\mathrm{OH}]^{-} \tag{3.25}$$

The adsorbed iron(II) sulfide species on the iron electrode surface are suggested to increases the reactivity by:

- The increased disorder in the structure of the FeOx species, as reported by Cerny et al. [31],
- The sustainment of electric conductivity by the incorporation of FeS in the passivating lattice, as suggested by Vijayamohanan et al. [34, 35].
- The increased solubility of FeOx species, which is proposed by several authors [30, 32, 34, 35, 93, 109–111].

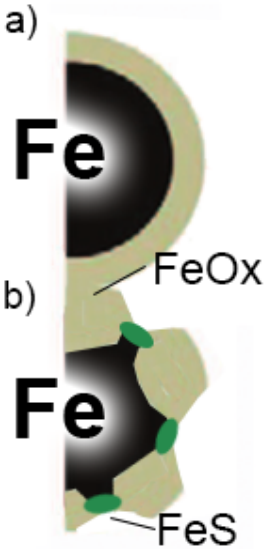

FIGURE 3.15: Illustration of (a) passivating FeOx layer and (b) a possible effect of FeS for the FeOx layer

Ravikumar et al. suggests that the sulfur containing anions in the electrolyte act as a local buffer of pH at the surface of the electrode and cause an increase in the Fe/Fe(II) reactions during discharge [27, 28, 31, 44].

Either way, the presence of iron(II) sulfide added to the iron-based electrode and anionic sulfur species within the electrolyte are both found to prevent the build-up of a passivating layer and generated overpotential by this passivating layer as illustrated in figure 3.15 [12, 16, 27–29, 31, 34–36, 38, 44, 56, 58, 77, 111–113]. A passivating layer helps facilitate the HER. As iron(II) sulfide additives are found to decrease the passivating layer they indirectly increase the overpotential of the HER as well [12, 16, 27–29, 31, 34–36, 38, 44, 56, 58, 59, 77, 111–113]. By increasing the overpotential of the HER and decreasing the overpotential of the Fe/Fe(II) reactions the reversibility of $Fe(OH)_2$ and especially the Fe_3O_4 to Fe is enhanced by which the accumulation of FeOx is prevented [12].

Several authors report that the beneficial effect of anionic sulfur species for the iron electrode as part of a NiFe cell to fade away over subsequent cycles. Sulfur containing anions are suggested to oxidize irreversibly to sulfate, presumably at the cathode, causing a depletion of sulfur containing anions. Manohar et al. (2015) found that when having high concentrations of FeS incorporated in the electrode as starting material leads to long-term stability. The high concentration as precursor material acts as a reservoir, providing a sustained release of anionic sulfur species in the electrolyte over a long period of time as illustrated in figure 3.16.

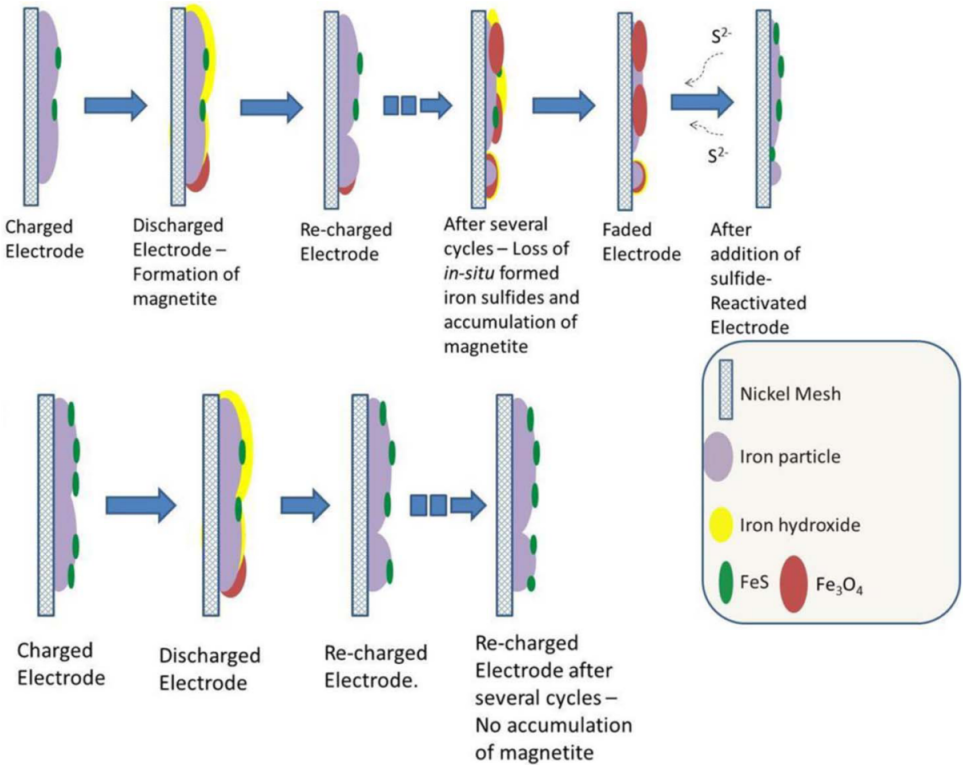

FIGURE 3.16: Illustration of the charge/discharge behavior of a carbonyl iron electrode with (a) Bi_2S_3 additives and (b) FeS + Bi_2O_3 additives (Used from Manohar et al., 2015) [12].

Comparably, selenium and tellurium containing anions could have a similar beneficial effect for iron-based electrodes as sulfur containing anions [107, 114]. Cerny et al. (1993) indicates comparable effects of selenium(IV) dioxide (SeO_2) as sulfur containing anions and assumes a similar adsorption mechanism of iron(II) selenide (FeSe) as FeS [101]. FeSe has lower solubility than FeS, having a K_{SP} of approximately 10^{-26} and the standard reduction potential of the Fe/FeSe reaction is -1.22 V vs SHE, which is more negative as well [17, 115]. This suggests a higher irreversibility of the formed FeSe on the electrode surface. Selenium and tellurium containing compounds as additives for the iron-based electrode are not further reported in scientific literature.

SPECIES THAT DECREASE THE OVERPOTENTIAL OF THE Fe/FE(II) REACTIONS BY SUPERCONDUCTIVITY

Sustaining electrical conductivity during the discharge can be problematic due to the formation of electrically insulating FeOx. A high electric conductivity of the electrode can lead to lowering the overpotential of the oxidation of iron, causing the prevention of rapid passivation of the Fe electrode surface and HER. In addition, conductivity can also enhance the utilization of the active material. Highly conductive (superconductive) materials and methods to attain superconductivity have been investigated, such as nano-structures [103], grafting- [53, 67, 102] and coating methods [40].

SPECIES THAT INCREASE THE OVERPOTENTIAL OF THE HYDROGEN EVOLUTION

Several species are known for their high overpotential for the hydrogen evolution to occur, such as lead, cadmium, indium, mercury, bismuth and copper containing species [100]. Solely bismuth and copper are considered non-toxic and thus suited for an eco-friendly iron-based electrode.

As bismuth containing species bismuth(II) oxide and bismuth(II) sulfide have a more positive standard electrode potential compared to reaction Fe/Fe(OH)$_2$, elemental bismuth is formed more readily than elemental iron during the reductive charging. The presence of bismuth or bismuth containing species increase the overpotential of the HER. The high hydrogen overpotential on bismuth is due to its weak electrosorption of surface bonded hydrogen intermediates [42, 58, 59]. In addition, as elemental bismuth and bismuth containing species are electrically conductive, it is suggested that they decrease the passivation of the iron-based electrode, supporting higher discharge rates. Belasubramanian et al. (1993) was the first to incorporate bismuth(III) sulfide (Bi_2S_3) [36] after which Manohar et al. (2013) applied Bi_2O_3 into the iron-based electrode [58].

Copper and copper containing additives for the iron electrode also increase the overpotential of the hydrogen evolution. Unfortunately only Paruthimal Kalaignan et al. (1996) studied metallic copper as additive to improve charge retention and cycle life of iron-based electrodes. He suggests that inorganic copper containing species increase the hardness strength, electric conductivity and favor a uniform pore size distribution. The solubility of Cu in alkaline solution is relatively high compared to iron, having a K_{SP} of approximately 1.2 10^{-3} [17]. Paruthimal Kalaignan et al. (1996) identified ionic copper species by CV as discharge reaction products. The higher solubility of copper is problematic as it favors self-discharge by enhancing the dissolution of iron species. In contrast, dicopper(I) sulfide and copper(II) sulfide have standard reduction potentials of 0.95 V and 0.7 V vs SHE and have very low solubility with a K_{SP} of approximately 2.5 10^{50} and 4 10^{38}, respectively [17]. In line with the theory of Cerny et al. and manohar et al., copper containing metal sulfides could attain an even higher irreversibility at the iron-based electrode during charge/discharge as iron(II) sulfides, looking to their standard electrode potential and solubility.

SPECIES THAT MODIFY THE HYDROPHOBICITY OF THE ELECTRODE SURFACE

Organo-sulfur species are well known for their tendency to form self-assembled monolayers on gold, copper and other metal surfaces [116]. Yang (2011) shows that the HER can be strongly influenced by alkanethiols as additive in the electrolyte. [64]. The HER is highly influenced by the chain length. The longer the chain the more the hydrogen evolution is suppressed. However too long chains cause total exclusion of the iron-based electrode from the electrolyte leading to limiting reactivity. Malkhandi together with Manohar et al. (2011) reported a coulombic efficiency of 90% over multiple cycles by using alkalnethiols as additives for an iron-based electrode [61, 63]. Unfortunately little is mentioned concerning long-term stability. In a subsequent study the stability of organo-sulfur additives is questioned by Yang et al. (2014) [60]. In this way sulfur containing species are used mainly as a ligature. It has not been questioned by the authors if the organo-sulfur species still have the beneficial effects for the iron-based electrode as with inorganic-sulfur species.

SPECIES THAT SHIFT THE POTENTIAL OF THE OXIDATION OF IRON TO MORE POSITIVE POTENTIALS

The standard reduction potential of the Fe/Fe(OH)$_2$ reaction can be lowered by mixing the iron containing compounds with compounds that have a more positive standard reduction potential. Even active material of the counter electrode (Ni(OH)$_2$) is known as additive for the iron-based electrode but also Co(OH)$_2$ can be applied [100].

SPECIES THAT CAPTURE GAS EVOLUTION

In order to attain sealed NiFe cells, species can be applied that capture possible H_2 gas production at

the iron-based electrode. This can be done by using additives or rather catalysts that can recombine with the gas evolved. Intermetallic compounds are known to be able to store large quantities of H_2. Hence, it is expected that H_2 gas produced upon charge is adsorbed by these intermetallic compounds. During subsequent discharge the adsorbed hydrogen can recombine with O_2 to form H_2O and replenish in the electrolyte. Hariprakash et al. (2005) investigated platinum/Cerium(IV) oxide for within the electrolyte that resulted in the first starved and sealed NiFe cell [55]. Rangel Cárdenas recently investigated the use of $LaNi_5$ as additive for an iron(II) sulfide electrode for E_STONE Batteries [105]. In practice the addition of $LaNi_5$ even increased the efficiency of the cell, presumably by increasing electric conductivity, taking part of the redox reaction and/or decreasing the overpotential caused by hydrogen gas bubbles.

SPECIES THAT FAVOR REVERSIBILITY
Some additives tend to favor the reversibility. As already explained in the previous additive section, spacing agents, such as $Ni(OH)_2$ and $Co(OH)_2$, maintain reactivity and homogeneity of the solid mass [100]. Recently, Manohar et al. (2015) found to sustain the beneficial effect of sulfur containing additives to maintain more reversible species of iron as already discussed before [12]. A recent study by Kwon et al. (2005) suggests that addition of ionic silicate species could also inhibit the spontaneous formation of FeOOH to Fe2O3 but is not yet investigated by an electrochemical study [117]. LiOH and NaOH additives within the electrolyte also seem to increase the reversibility of the NiFe system as a whole. These are further discussed in the electrolyte section.

THE IRON(II) SULFIDE ELECTRODE

So far, iron(II) sulfide as starting material for an electrode has solely been studied by E_STONE Batteries and Shangguan et al. versus a nickel-based electrode in alkaline electrolyte and has not been applied commercially. Based on the characterization study of Shangguan et al. the charge/discharge behavior of the FeS electrode is considered to be similar to the iron-based electrode [67]. No possible other species are mentioned than already given in the employed materials, iron-based electrode section.

Iron(II) sulfide has a hexagonal crystal structure

is an inorganic compound containing transition metal iron in +2 oxidation state and sulfide ion 1:1 ratio. It is pyrophoric in nature. It adopts a hexagonal crystal structure. It belongs to the category of inorganic sulfide compounds. It is also known as troilite, iron sulfide, ferrous sulfide, black iron sulfide and protosulphuret of iron.

SEPARATOR

The function of the separator is to physically separate the electrodes while allowing ionic charge carriers to penetrate through the separator. An alternative is to apply a salt bridge between the two half cells but in most cases this limits the current density of the total cell. Main criteria of the material of the separator is the chemical stability and wettability for permeability over the lifetime of the cell. Standard applied separators for alkaline aqueous cells are made of polyolefin nonwoven separators. Polypropylene and polyethylene based separators are hydrophobic and must be treated to enhance its wettability before being used as separator. [8].

ELECTROLYTE

To maintain a good reactivity between the electrode and electrolyte it is advantageous to use a solid/liquid interface as the reactions cause volume changes of the electrodes and electrolyte. Most nickel-based systems use an alkaline aqueous potassium hydroxide salt environment to transport charge carriers, which the electrodes use to reduce or oxidize.

OPTIMAL CONCENTRATION AND VOLUME OF THE ELECTROLYTE

The rate of the oxidation and reduction reactions depend on the ionic conductivity of the electrolyte and the possibility of hydrogen evolution. Following the Nernst equation the hydrogen evolution is less prone to occur at the surface of the electrode with increasing $[OH^-]/[H_2O]$ ratio, by which the discharge capacity and stability of the iron-based electrode is found to increase [47, 50, 103, 118, 119]. Nonetheless, too high alkaline concentrations increases the dissolution of iron, which is suggested to reduce the high current density rate performance and discharge capacity [47, 103]. The increase in discharge capacity and decrease of the oxygen evolution by an increase of the $[OH^-]/[H_2O]$ ratio also accounts for the nickel-based counterelectrode. A high $[OH^-]/[H_2O]$ ratio of the electrolyte is also known to favor swelling of the nickel-based electrode, leading to a reduced cycle life. Too high salt concentrations also lead to high viscosities and resistance limitations in diffusion and convection of the electrolyte, resulting in a lowering of the ionic conductivity. Several electrochemical studies indicate an optimal salt concentration of 5-6M of the electrolyte for the performance of the NiFe system [47, 89, 119]. The electrolyte concentration can also be altered because of the performance requirements, such as the reaction rate, temperature and cycle life [8].

There is little scientific research found concerning the effect of difference in electrolyte volumes on the performance of the cell. Nonetheless, when having a sealed cell design the electrolyte quantity is said to be a key parameter for the electrochemical performance [8]. Low electrolyte quantities can cause an increased ionic resistance due to dry-out of the electrodes. On the other hand, high electrolyte volumes lead to high distances between the electrodes that can result in high ionic conductivities and differences in internal pressure due to the possible hydrogen- and oxygen evolution. A proposed optimal volume of electrolyte is in the range of 1.5 $10^{2.5}$ mL/Ah [8].

FOULING OF THE ELECTROLYTE

Contact of the electrolyte with air can cause carbonate (CO_3^{2-}) fouling. Atmospheric carbondioxide (CO_2) can react with KOH, Fe or FeOx species to form potassiumcarbonates (KCO_3) and ironcarbonates ($FeCO_3$), respectively in the solution by a dissolution/precipitation mechanism. This is suggested to infer with the Fe(0/II) redox reaction [56, 120], most certain for a FeO_2 cell [51, 62] but also studies exist that indicate no limiting effect of $[CO_3]^{2-}$ fouling for a NiFe cell in aqueous solution [50, 94].

THE EFFECT OF THE CATION IN THE ELECTROLYTE ON THE ELECTROCHEMICAL BEHAVIOR

Additions of LiOH are already known since the discovery of the alkaline NiFe cell [121]. For the iron-based electrode it has been found that pure LiOH/-NaOH electrolytes or addition of small proportions of LiOH/NaOH into the electrolyte makes the redox reaction more reversible, resulting in a longer cycle life [16, 29, 96, 119] and/or higher discharge capacities [93, 103, 118]. Some studies found that these beneficial effects occur specifically for the Fe(II/III) redox

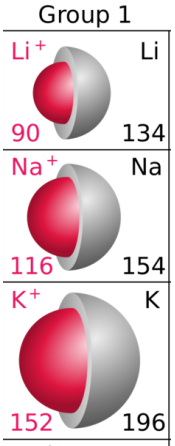

reaction mechanism [29, 31, 94, 107]. In contrast, Lei et al. reported better stability of iron-based electrodes in pure KOH solutions [103]. For the nickel-based electrode it has been found that the addition of LiOH increases the discharge capacity, decreases the swelling of the positive active material and improves the high current density and temperature performance. In turn it has detrimental effects on the low temperature and discharge rate performance due to lower ionic conductivity [8]. Different theories exist concerning the working mechanism and effect of LiOH additives for the iron-based electrode:

- Increased reactivity of the electrodes due to the smaller ionic radius of the cation [26, 56, 75, 93].
- Smaller ionic radius of the cation causes the hydrogen evolution to be less prone to occur [8].
- Formation of a more porous passivating oxide layer [103].
- Change in reaction kinetics [29, 103].
- Enhancement of solubility of iron species [16, 103].

As shown in figure 3.17 the Na^+- and Li^+ cations have a smaller ionic radius than the K^+ cation, whereby the ionic penetration capability through the electrode/electrolyte passivating oxide lattice is increased, allowing bigger film growth. This is suggested to lead to higher discharge capacities and possible discharge current densities [26, 56, 75, 93]. It is also suggested that the smaller the cation the bigger the interaction is between the electrolyte and the cation [8]. This causes the electrolyte to become less prone to oxidation and reduction by which the oxidation overpotential of the HER and OER is increased. In contrast, addition of LiOH is suggested to increase the HER and decrease the ionic resistivity of the electrolyte without explanation or mentioning where this is based on [56]. Lei et al. (2015) suggests that Li^+ cations favor the formation of a more porous $Fe(OH)_2$ layer and thereby enables faster $[OH]^-$ diffusion across the electrode/electrolyte interface. They also suggest that Li^+ cations prevent the formation of Fe_3O_4 as Li+ cations incorporate in the oxide lattice. In line, it is suggested Li^+ to be reduced to form $Li_xFe_yO_z$ intercalation-compound intermediates, that are reduced more easily than Fe_3O_4. By cyclic voltammetric experiments, Poa et al. (1985) found another reaction mechanism for the Fe(II/III) redox reaction [29]. The occurrence of another reaction mechanism leads to the suggestion that the Li^+ cation to change kinetic parameters, such as exchange current densities and transfer coëfficients [56, 103]. In contrast, LiOH is found to significantly enhance the dissolution of iron species, reducing the high current density rate performance and discharge capacity [16, 103]. In addition it is suggested that Li^+ additions in the electrolyte prevent CO_3^{2-} fouling as lithiumcarbonate (Li_2CO_3) is less soluble than KCO_3 [16]. Moreover, for the NiFe system it is believed that addition of LiOH into the electrolyte leads to the deposition of metallic nickel onto the iron-based electrode, thereby blocking active surface area, resulting in a lowering of reactivity [103].

3.5 DESIGN, COMPOSITION & PRODUCTION TECHNIQUES FOR THE ELECTRODE & TOTAL CELL

Different electrode production techniques and cell constructions exist for alkaline aqueous systems. These influence both the overpotentials of the half reactions as the electronic conductivity and reactivity can be altered but also the occurrence of parasitic unwanted reactions. Unfortunately, little scientific literature exists discussing such *design parameters* [42, 43, 65, 93, 95, 101, 122–124]. In practice, commercial NiFe cells reach energy densities of 40-60 Wh/kg, while the theoretical energy density is 337 Wh/kg. This relatively high difference can be explained by the use of solely the weight of the electrodes. Energy density losses that are not accounted for are (i) the electrolyte, (ii) weight of the current collector, (iii) additives, (iv) added active material for life duration, and (v) casing parts [46].

COMPOSITION OF THE ELECTRODE

An ideal electrode structure maintains a high reactivity at the electrode/electrolyte interface over a long cycling lifetime, which does not lead to conduction limitations of the electrons to the current collector. Nano-porous structures within the electrode cause a high active surface area of the active material, by which all of the active species is in contact with the electrolyte leading to a high reactivity. A microporous structure prevents diffusion or migration limitations of the charge carriers that are necessary for the reaction to occur. Within the electrode a high electronic conductivity prevents limitations in the transfer of electrons from the electrochemical reaction to the current collector or vice versa. A high electronic conductivity does not go hand in hand with a porous structure. To preserve mechanical integrity of the electrodes, changes of the active material should be minimal. Most electrode designs only contain active material in contact with a current collector but in some electrode designs binding- and conductive additives are added to increase cohesion and conductivity, respectively.

THE ACTIVE MATERIAL

Excluding sintered plate designs, it is preferred to have small particles of active material uniformly dispersed over the current collector. The small particles have a high active surface area, while a uniform dispersion increases the electronic conductivity and prevents rapid passivation [56]. It is suggested to have an optimum in particles size in the submicron range. Decreasing the particles size increases the active surface area but on the other hand too small particles are expected to decrease the reactivity by the total dissolution of the particles. Different grinding and mixing methods can be applied to attain small particles and a uniform mixture, respectively. Moreover, a recent study by Li and Shangguan et al (2015) indicates that a pre heat treatment of the particles can cause a crystal grain refinement that improves the physical and electrochemical performance of FeOx material in charging efficiency, capability and cycling stability [125].

THE CURRENT COLLECTOR

As depicted in figure 3.18, the current collector is usually a metallic nickel mesh or foam. Metallic nickel is preferred over other metals such as iron because of its higher durability in alkaline solutions.

BINDER ADDITIVE

To adhese the active material to the current collector a polymer binder can be necessary to be applied,

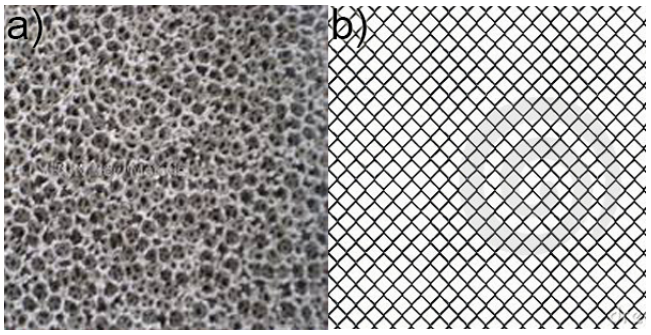

FIGURE 3.18: Typical metallic nickel current collectors: (a) foam- and (b) mesh type

depending on the production technique. The polymer binder is selected for its thermochemical resistance and adhesive properties. Most thermochemical resistant polymer binders have the disadvantage to be electronically insulating and hydrophobic. Kitamura et al. (2012) showed differing results for iron-based electrodes due to different binders applied [124]. PE and PTFE as binder resulted in the highest discharge capacities in a solution of 6M KOH electrolyte.

CONDUCTIVE ADDITIVE

The active material can have insulating intermediates involved during the charge/discharge process, such as $Fe(OH)_2$. Due to insulating intermediates and/or the insulating property of the polymer applied it can be necessary to blend the active material with conductive nanoparticles, such as amorphous conductive black carbon (Super P) or graphite to increase the electronic conductivity. In my previous work I applied amorphous carbon and graphite for phase inversion iron-based electrodes [126]. For phase inversion produced iron-based electrodes, the highest discharge capacities were achieved by using Super P as conductive additive.

PRODUCTION TECHNIQUES FOR THE ELECTRODES

Commercially applied electrode designs are: pocket-plate-, sintered-, and pasted electrodes. A new electrode design has been investigated by E-STONE Batteries based on a phase inversion production technique [126]. Figure 3.19 shows the volume distribution of the different electrode designs.

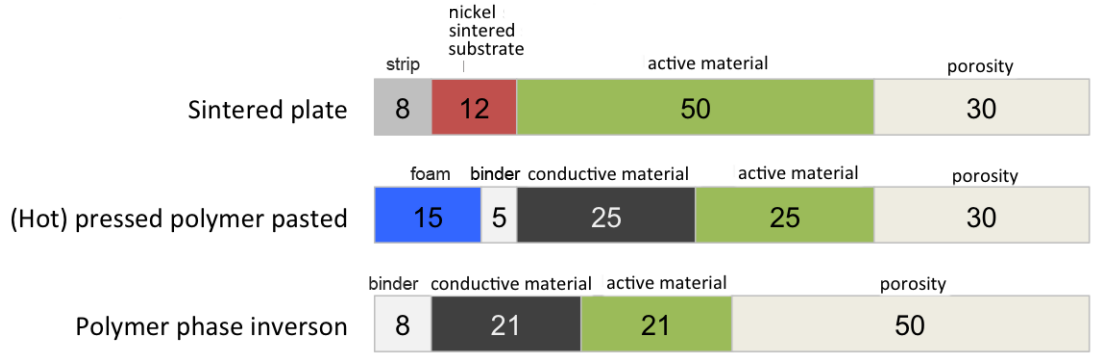

FIGURE 3.19: Volume distribution of different electrode designs (Updated from P. Bernard et al., 2015 [8]).

THE POCKET PLATE TECHNIQUE

Back in 1897-1903 the first electrode design was based on the pocket-plate technology as shown in figure 3.20 [100]. Preshaped perforated nickel plated steel sheets are filled with palletized active material particles, which is blended with conductive additive, mostly graphite. the particles are then pressed and hold together as pockets with folded strips along the edges. The nickel pockets both act as holder of the small particles and current collector [8]. The occurrence of the current collector at the electrode/electrolyte interface is believed to increase the overpotential of the hydrogen evolution. On the other hand the nickel-based pockets also cause a general increase in overpotential due to necessity of diffusion through the perforated steel and pressed palletized active material. Therefore, this design is only suitable for low-current density applications [100]. The pocket plate technology is still widely applied, presumably due to its robust design.

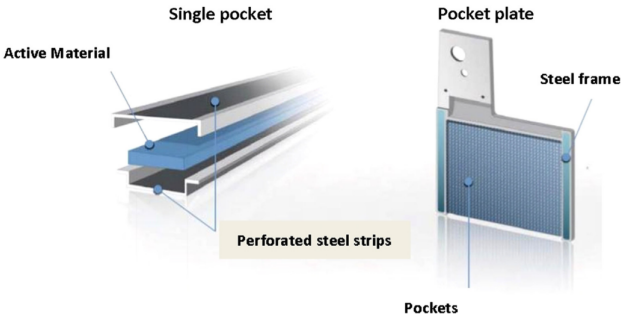

FIGURE 3.20: Pocket plate design (used from P. Bernard et al., 2015 [8]).

THE SINTERED PLATE TECHNIQUE

Sintering is a thermal deposition process in which loose active particles are transformed into a coherent porous body by heating just below the melting point in a reducing atmosphere. The active material can be sintered on a conducting mesh to act as a current collector and blended with pore formers and binders. Sintered electrodes are famous for their porosity leading to a large surface-area and high electrical conductivity within the electrode. The high electric conductivity is due to the crystal binding between the active material in combination with a high mechanical strength. Unfortunately, these type of electrodes have a relatively high inactive/active weight ratio and involve high production costs [8, 100]. Subsequent to the pocket plate technology, sintered electrodes have been the dominant technology as they allow higher charge/discharge rates than the pocket plate technology [8].

THE (PRESSED) POLYMER PASTED FOAM TECHNIQUE

Polymer pasted foams are interesting due to their low-cost production method and allow higher volumetric energy densities than the designs discussed above. The active particles are pasted onto a metal substrate that acts as current collector using a polymer binder. As the polymer negatively influences the electric conductivity of the electrode, conductive additives are necessary additives to maintain conductivity. The pasting occurs by a thermal or evaporation mechanism in which the polymer fluidizes and precipitates onto the substrate, ideally holding the active and conductive material onto the substrate. During the pasting the substrate containing the active material can be pressed to decrease the thickness of the electrode and attain a more rigid structure.

THE POLYMER PHASE INVERSION TECHNIQUE

A new low-cost production method has been investigated by E_STONE Batteries in my previous work to create highly porous structures and thin electrodes in order to attain a very high reactive surface

area [126]. This technique is based on a polymeric solidifying structure that can be created by phase inversion, activated by a demixing process without applying heat nor pressure and without the necessity to use a foam nor plate. In contrast to the polymer binder used for polymer pasted foams, caution needs to be taken for the polymer used. The polymer needs to be solvable, which goes hand in hand with less thermochemical resistance. Though this technique looks promising, it needs more investigation.

CELL DESIGN

As shown in figure 3.21, aqueous cells are available in winded cylindrical- or rectangular parallelepiped cells. The cells can be stacked in series or parallel (bipolar), depending on the necessary energy capacity. To deal with the depletion of the electrolyte, non-sealed valve regulated cells exist to refill the electrolyte [8]. Cells can be sealed when no build-up of gas occurs within the cell (100% coulombic efficiency) or hydrogen and oxygen adsorbing additives are applied.

CYLINCRICAL CELLS

The electrodes can be coiled together with a separator in a jelly roll. The roll is then inserted in a cylindrical nickel plated steel can with the top cover welded to the positive electrode and the negative electrode connected to the can. The electrolyte can be poured into the can by which the electrolyte equals the volume of the porous electrode and separator. The top is cramped by which it can be ripped of by internal overpressure due to over charge/discharge.

RECTANGULAR PARALELLPIPED CELLS

For the bigger cells rectangular designs in parallelepiped cases exist. Therefore the electrode needs to be cutted in a rectangular shape. In between the electrodes a separator is placed. For rectangular parallelepiped cells an excess amount of electrolyte is added and sealed with a safety vent, which makes it also possible to refill the cell.

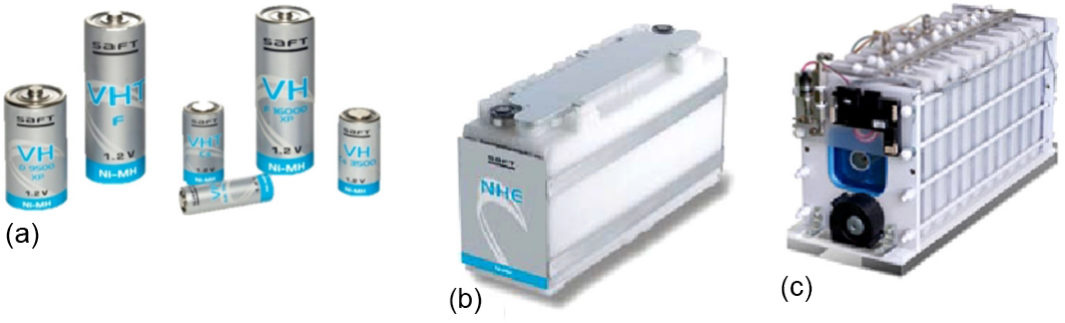

FIGURE 3.21: (a) Cylindrical-, (b) rectangular parallelpiped- and (c) bipolar alkaline cells (used from P. Bernard et al., 2015 [8]).

3.6 ELECTROCHEMICAL ACTIVATION OF THE NiFe CELL

For all types of electrochemistry in the first series of charge/discharge cycles an increase in discharge capacity occurs until a comparatively stable discharge capacity is attained [8]. For iron-based electrodes this can take up to 20-50 cycles and is known as *formation* or *activation* cycles. Other battery chemistries, such as lead-acid, have the necessity of just one formation cycle. Activation of the electrodes is a critical step during manufacturing of a cell before it can be used. Therefore activation cycles do affect the final cost of the battery. The stable discharge capacity at the end of the activation indicates the possible utilizable amount of active material within the electrode. For an iron-based electrode this involves the increase in reactivity between the electrode and the electrolyte leading to the formation of FeOx species during oxidation and following redeposition to metallic iron by reduction. Figure 3.22 shows typical activation cycles of an FeS hot pressed electrode. During the charge an electron flux into the cell causes reduction of the iron-based active material by which the voltage increases up to its nominal capacity. Subsequently, an electron flux can be attained out of the cell during discharge by the oxidation of the active material leading to the discharge capacity. Vijayamohanan et al. (1990)

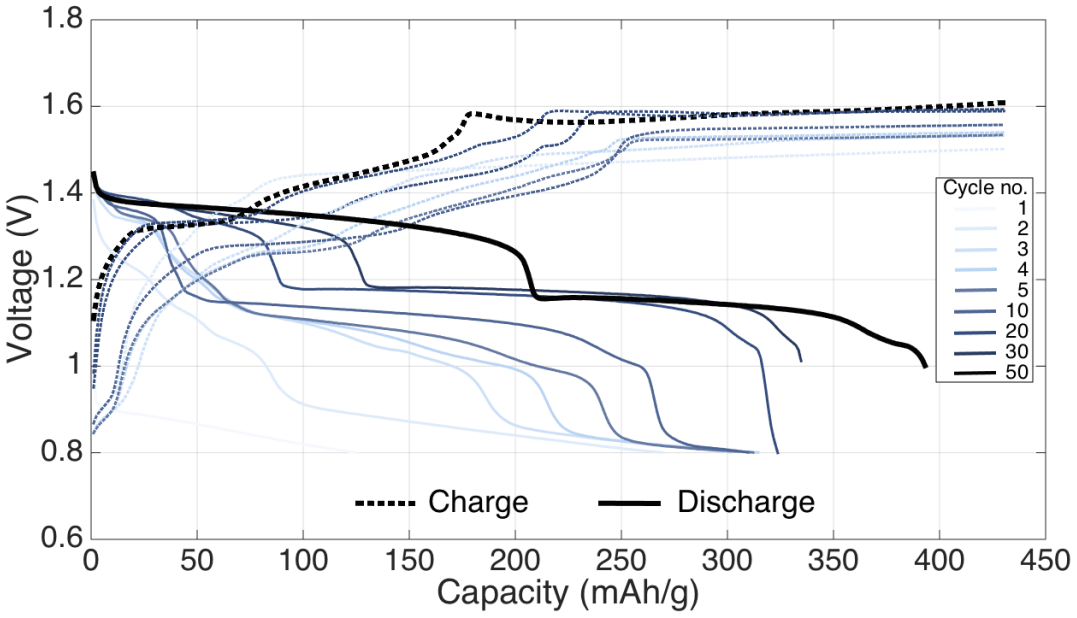

FIGURE 3.22: Typical formation cycles of an FeS hot pressed electrode.

attributes changes in morphology and conductivity as a result of the activation cycles of iron-based electrodes [54]. It can also involve an increase in reactivity due to a decrease in surface tension or increase in wettability between the electrode and the electrolyte. For example Manohar et al. (2012) ascribes the slow formation on the poor wettability of the electrode. As it takes several cycles to penetrate the pores. The poor wettability is suggested to be due to the use of a hydrophobic polymerbinder [13] but can also be due to the hydrophobicity of the conductive additive.

The discharge products of an iron-based electrode are relatively insoluble. Hence the iron-based electrode is expected not to have a shape change as encountered with zinc electrodes. Nonetheless, as the iron based species are still sparingly soluble this causes the dissolution/precipitation mechanism to occur, which leads to an increase in roughness of the surface and thus an increase in electrochemically

active surface area as shown in figure 3.23 [13, 16]. In addition it is suggested by doing so activation cycles are expected to remove any soluble impurities and thereby to purify the electrode [**?**]. What also can be altered by the activation cycles is the crystallite grain, which is also called *inoculation*.

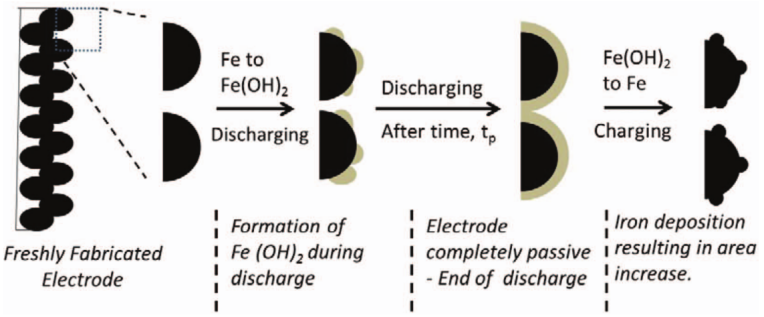

FIGURE 3.23: activation and creation of high active surface area of the iron-based electrode (used from Manohar et al., 2015 [13])

The number of activation cycles depends on the properties of the starting material: Its solubility, active surface area and if it is in an oxidized or reduced state. Manohar et al. (2012) says that the metallic reduced state of a metal takes more activation cycles than an oxidized precursor material. He also ascribes the length of activation to the method of production-e.g. pocket plate, sintered or polymer-bound (hot)-pressed- and electrode or electrolyte additives [13, 54, 93, 122, 123, 126]. Manohar et al. (2012) found that porous electrodes or by applying a wetting agent to the electrolyte, an accelerated activation can be achieved [13].

Both Vijayamohanan et al. (1990) and Manohar et al. (2012) mention a beneficial effect of sulfur containing anionic species for the activation of an electrode. The former attributes this to the increased electrical conductivitiy by FeS in the passivating oxide layer when added to the electrode active material [54]. This suggests that the passivation of the electrode restricts the discharge capacity in every cycle during formation [13]. As already discussed in the additives section of the iron-based electrode, the addition of sulfur containing anionic species can prevent the build-up of the passivating layer and are suggested to accelerate the activation process.

CHAPTER 4

PERFORMANCE

4.1 INTRODUCTION

In this section current performance parameters and most recent performance enhancements are discussed of NiFe based batteries for the application of daily stationary energy storage. The main important parameters are the efficiency, lifetime, power capacity, self-discharge, robustness and maintenance requirements. Most losses in performance are caused by limitations of the iron based electrode. Therefore most performance-related research is focused on the performance of the iron electrode but equals the performance of the overall NiFe cell.

4.2 GENERAL CHARGE/DISCHARGE BEHAVIOR

THE WELL STUDIED NiFe CELL

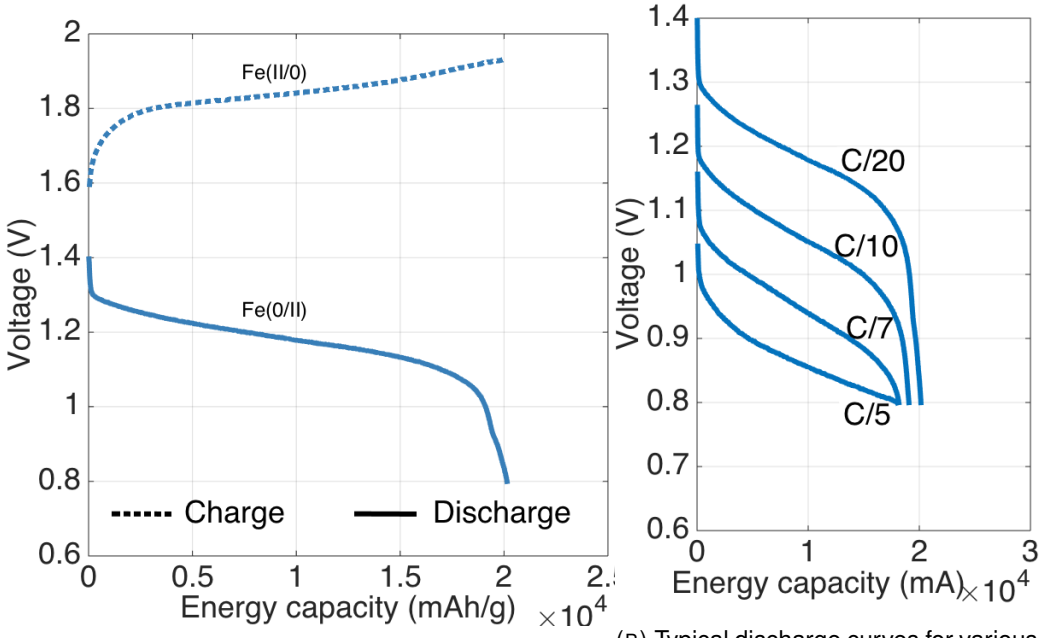

(A) Typical charge/discharge curves with which reaction at which plateau at 25 °C.

(B) Typical discharge curves for various c-rates at 25 °C.

FIGURE 4.1: charge-discharge curves of a commercial NiFe cell.

Typical charge/discharge curves of a commercial CHANGHONG NiFe battery are shown in figure 4.1a and for different C-rates in figure 4.1b at 25 °C. The open circuit potential is 1.4 V, the nominal voltage is 1.2 V and the maximum voltage that can be applied is 1.7-1.8 V. During discharge of a NiFe cell a flattening in discharge capacity with decreasing voltage can be found, a so-called discharge plateau, around 1.2 V and 0.85 V at C/20 and C/5 rate, respectively. In commercial cells the nickel-based electrode is rate limiting. Therefore the discharge capacity against the voltage shows the charge/discharge behavior of the nickel-based electrode resulting in one plateau ascribed to the biphasic reaction between nickel hydroxide and nickel oxyhydroxide. Compared to other nickel-based systems the NiFe cell shows a high internal resistance, as by increasing the C-rate the potential shifts significantly to more negative potentials. Therefore the NiFe battery is only suited for 5-10 h rates of discharge.

THE NiFeS CELL

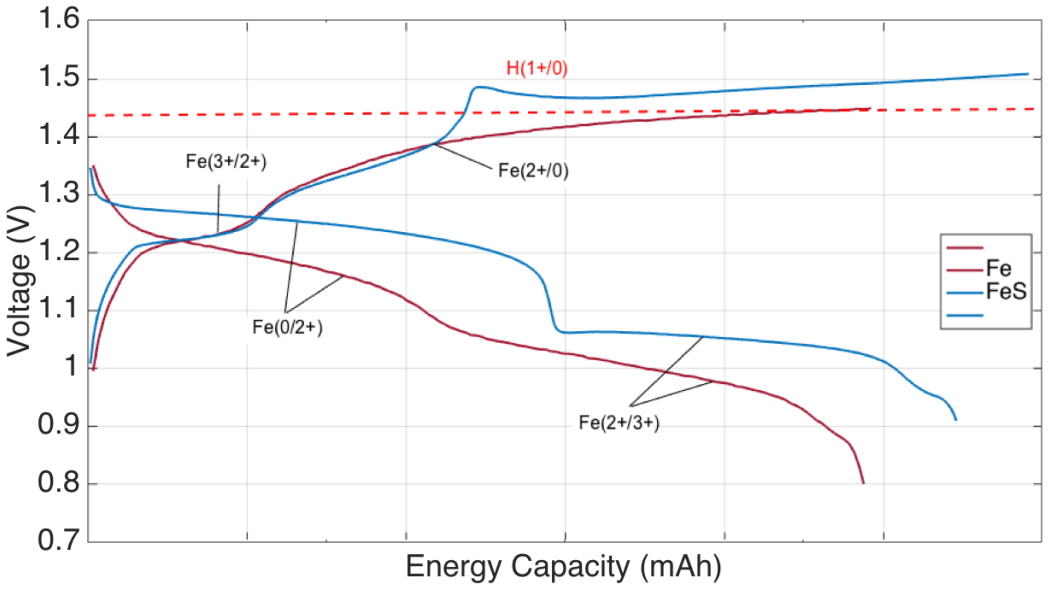

FIGURE 4.2: Typical charge-discharge curves for a NiFe and NiFeS cell in which the Fe and FeS electrodes are limiting.

Figure 4.2 shows charge/discharge curves for a NiFe cell in red and a NiFeS cell in blue in which the Fe and FeS electrodes are rate limiting. In contrast to figure 4.1a, two distinct plateau's can be found for both electrodes. For the iron electrode, from more positive potentials and decreasing, the first plateau accounts for the oxidation of Fe(0) to Fe(II) species between 1.3-1.08 V. The second plateau accounts for the oxidation of Fe(II) to Fe(III) at 1.08-0.85 V. Then, during charge, from a low potential and increasing, the first plateau accounts for the reduction of Fe(III) to Fe(II) species between 1.22-1.25 V. At potentials more positive than 1.3 V, the subsequent plateau accounts for the reduction of Fe(II) to metallic Fe and/or the hydrogen evolution. For the FeS electrode the plateau's occur at the same potentials, except that during charge a third plateau can be found subsequent to the second plateau.

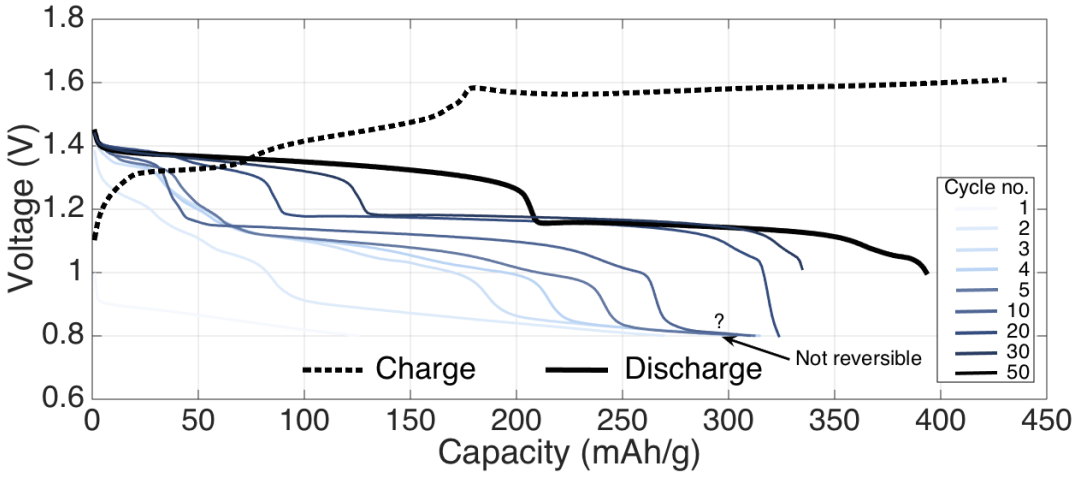

FIGURE 4.3: Typical activation cycles for a hot pressed FeS electrode.

Figure 4.3 depicts the activation cycles of the FeS electrode. An irreversible reaction at 0.9-0.8 V is observed during the initial cycles. The occurrence of this reaction plateau leads to a high discharge capacity during the first number of cycles and causes the activation of the other reactions to be accelerated.

4.3 PERFORMANCE OF IRON-BASED ELECTRODES

In table 4.1 the performance parameters of iron-based electrodes are given that are recently published in comparison to a commercial electrode and electrodes manufactured by E_STONE Batteries. The performance parameters that are compared are the overall- and coulombic efficiency, the discharge capacity, the number of cycles and the self-discharge at C/5 rate. Figure 4.4 illustrates the discharge capacities of these electrodes at different C-rates. For these different C-rates little is mentioned concerning the stability over subsequent cycling, solely for a rate of C/5. Caution must be taken with comparing discharge capacities for different c-rates as the c-rate depends on the nominal capacity, which can be chosen arbitrarily.

In 2012 Rajan et al. (2014) published results of sintered iron electrode containing carbon grafted Fe_3O_4 (Fe_3O_4/C) as starting material and having carbonyl iron and Bi_2O_3 as main additives. The Fe_3O_4/C electrode (A) achieved a discharge capacity of 400 mAh/g at C/5 rate with a coulombic efficiency of 80%, reported for 100 subsequent cycles. The discharge capacity remains stable also at higher C-rates, presumably as sintering is used as production technique. Unfortunately little is mentioned concerning self-discharge and long-term stability. In a series of articles Manohar et al. (2012-2015) investigated different compositions with carbonyl iron as starting material. Using Bi_2O_3 as additive (B.2), resulted in a coulombic efficiency of 96% and appeared to be stable over a number of 300 cycles. The addition of FeS and Bi_2O_3 to the carbonyl iron electrode (B.3) ultimately led to stable cycling over 1200 cycles with a 92% coulombic efficiency. Nothing is mentioned concerning self-discharge. In comparison to other electrolyte compositions, it is remarkable that Manohar et al. used pure KOH without the addition of LiOH. By 2015 Shangguan et al. (2015) introduced iron(II) sulfide as starting material for an electrode (C.1) [67]. By applying carbon grafting of the material and addition of Bi_2O_3 (C.3), a coulombic efficiency of 90% has been achieved over a series of 200 cycles. They demonstrated specific capacities of 230 mAh/g at high C-rates of up to 4, introducing the suitability for high power applications. In another study Shangguan et al. showed the effect of annealing Fe_3O_4 (C.4) on the performance of an electrode [125] . The annealing material resulted in a discharge capacity of 604 mAh/g, which is 66% of the theoretical energy density of iron, and a coulombic efficiency of 84% over 100 cycles. In 2012 Wang et al. introduced a graphene coated FeO electrode (D) with a coulombic efficiency of 100%, a discharge capacity of 125 mAh/g for 800 cycles and a stable discharge capacity at high C-rates up to 10C [102]. Wang et al. achieved these results by using a nickel-based counterelectrode with carbonnanotubes. This suggests that nickel cathodes could also affect cycling performance at high c-rates. In 2012 T. van Dijk showed coulombic efficiencies of 100% of a cold pressed pure FeS electrode (E.1) stable over 150 cycles by only cycling on the Fe(II/III) plateau [45]. Though the discharge capacity is 120 mAh/g very high efficiencies were met by the prevention of attaining potentials at which the hydrogen evolution takes place. Unfortunately after multiple efforts the Fe(II/III) reaction could not have been stabilized. By the end of 2015, efforts for writing this thesis resulted in a hot-pressed electrode having FeS as starting material

(E.2) with a discharge capactiy of 396 mAh/g and a coulombic and overall efficiency of 92% and 77%, respectively, stable for a series of 120 cycles. The self-discharge has been found to be 5% at a 100% SoC. Appendix [**?**] describes the experiment in more detail.

Based on research by Manohar et al. and E_STONE batteries commercial pocket plated Fe_3O_4 electrodes already achieve coulombic efficiencies of 96% for 4000 cycles, with discharge capacities of 380 mAh/g and a 0% self-discharge.

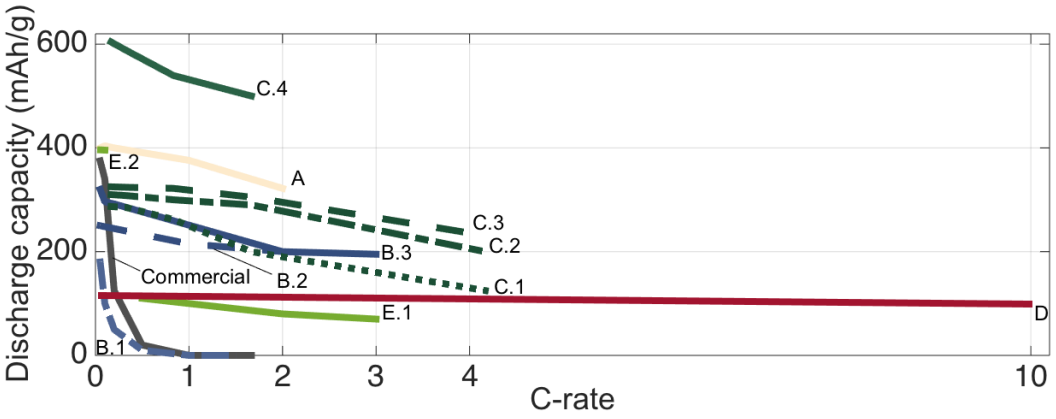

FIGURE 4.4: Discharge capacities of iron-based electrodes as a function of the c-rate.

TABLE 4.1: Performance characteristics of iron-based electrodes at C/5 rate.

Label	Active material	Particle size	Production technique & design	Composition electrode & electrolyte	Efficiency		Discharge capacity	Cycles	Self-discharge	Author
		(μm)		(wt%) & (M)	(c%)	(%)	(mAh/g)	(no.)	(%/day)	
Comm-ercial	Fe_3O_4	1-3	pressed on Ni pocket plate	Fe_3O_4:Graphite= 80-90:10-20% & ~4.5M KOH 0.5M LiOH	96	55	380	-	≈ 0	CHANGHONG [59]
A	Fe_3O_4/C	5-10	pressed at 675kg/cm^3 & sintered at 350C on Ni grid	Fe_3O_4/C:c-α-Fe[a]: PTFE[b]:Carbon[c]: Bi_2O_3: $NiSO_4$*$7H_2O$= 72.5:10:6:10:1:0.5% & 6M KOH 0.4M LiOH	80	-	400	100	-	Rajan et al. (2014) [44, 52, 53]
	c-α-Fe[d]	0.5-3	hotpressed at 5kg/cm^3 & 140°C on Ni grid	c-α-Fe:PE:K_2CO_3: Bi_2O_3:Bi_2S_3:FeS=						Manohar et al. (2012-2015) [12, 58, 59]
B.1				81:9:10:0:0:0%	90	-	180	30	-	
B.2				71:9:10:10:0:0%	96	-	290	300	-	
B.3				67:9:10:0:10:5% & 5.3M KOH	92	-	250	1200	-	
	FeS/C[e]	5-15	Dried at 80°C & pressed at 10MPa on Ni foam	FeS:FeS/C:PTFE[f]: Carbon:Bi_2O_3=						Shangguan et al. (2015) [67, 125]
C.1				85:0:5:10:0%	80	-	287	200	-	
C.2				0:85:5:10:0%	86	-	310	200	-	
C.3				0:82:5:10:3% & 6M KOH 0.5M LiOH	90	-	325	200	-	
C.4	Fe_3O_4	0.2	Heated to 700°C, dried at 80°C & pressed at 10MPa on Ni foam	Fe_3O_4:PTFE:Graphite= 87:3:10% & 6M KOH	84	-	604	100	-	
D	FeO/ graphene	-	dried on Ni foam at 80°C, heated at 550°C and pressed to 0.5 mm	FeO:glucose:PTFE= 100:20:5% & 1M KOH	100	-	125	800	-	Wang et al. (2012) [102]
E.1	FeS[g]	-	Pressed at ?	FeS= 100% & 6M KOH	100	82	120	150	5	T van Dijk (2012) [45]
E.2	FeS[e]	-	Hotpressed at ? on Ni foam	FeS:PE:Carbon= 85:5:10 & % 6M KOH 0.5M LiOH	92	77	396	120	5	Appendix **??**

[a] Carbonyl iron
[b] in H_2O solution
[c] Carbon black Super P
[d] Carbonyl iron SM grade BASF
[e] Analytical grade iron(II) sulfide Alfa Aesar
[f] in H_2O solution
[g] Technical grade iron(II) sulfide BASF

4.3.1 EFFICIENCY & C-RATE PERFORMANCE

COULOMBIC EFFICIENCY

For the application of stationary energy storage it has been suggested it is necessary to be able to charge/discharge up to 5C rates. A commercial cell attains a coulombic efficiency of 96% but shows a decrease to near zero discharge capacities at C-rates higher than C/5. Research by Manohar et al. (B) and Shangguan et al. (C) exemplary indicates the effect of additives on the cycling behavior.

In a series of articles Manohar et al. (2012-2015) investigated different compositions with carbonyl iron as starting material. Already surprisingly high coulombic efficiencies of 90% were reached for a high-purity carbonyl iron electrode (B.1) but shows a high instability as just 30 cycles were met and near zero discharge capacities at C-rates higher than C/5, similar to a commercial pocket plated cell. The former is suggested to be caused by the formation of irreversible FeOx species and the latter is found to be a result of the occurrence of the passivation layer. Efforts to prevent the formation of the passivation layer resulted in a carbonyl iron electrode with Bi_2O_3 additives (B.2), which showed less loss of discharge capacity at higher C-rates, an increase in coulombic efficiency up to 96% and appeared to be stable over a number of 300 cycles. The addition of FeS and Bi_2O_3 to the carbonyl iron electrode (B.3) ultimately led to stable cycling over 1200 cycles with a 92% coulombic efficiency.

Shangguan et al. showed a coulombic efficiency of 80% for a FeS electrode (C.1). By grafting the FeS with carbon (C.2) a 86% coulombic efficiency has been reached. By adding 3wt% Bi_2O_3 (C.3) a 90% coulombic efficiency has been attained. The sulfur containing specie as starting material of all iron(II) sulfide based electrodes (C.1-C.3) resulted in a less decrease in discharge capacities at C-rates between C/5-4.2C in comparison to the pure carbonyl iron-based electrode by manohar et al. (B.1).

OVERALL EFFICIENCY

Due to the design of the pocket plated electrodes commercial NiFe cells possess a high loss of overall efficiency up to 55%. By using a pasted electrode design and FeS as starting material, E_STONE Batteries shows that the overall efficiency can be increased to 82% at C/5 rate. No other research exist concerning the overall energy efficiency of iron-based electrodes.

4.3.2 LIFETIME PERFORMANCE

In primary literature the commercial NiFe system is reported to have a long cycle life of 4000 cycles, which represents 20-60 years and to be very robust for over-charge/discharge and elevated temperature operation [8, 16, 57]. Actual scientific literature to support this is scarce. B.3 and D reach 1200 and 800 cycles, respectively. This indicates that using different starting material roughly the same order of cycle life can be obtained similar to the NiFe system. In general a photovoltaic cell has a lifetime of 15 years. Thus reaching in the order of 1000 cycles can be considered as a minimal criteria for a stationary energy storage system.

4.3.3 SELF-DISCHARGE PERFORMANCE

The self-discharge of the commercial CHANGHONG NiFe cell has been found to be near 0% per day. Primary literature mentions the self-discharge of NiFe cells to be 0.6-1.0% per day. Studies that investigate sulfur containing additives for iron-based electrodes mention little concerning the self-discharge. The hot-pressed FeS based electrodes that are produced by E_STONE Batteries show a self-discharge of 4.5% per day at 100% state of charge by which the potential decreases up to 1.4 V. This is roughly five times the amount of a commercial NiFe battery and suggests sulfur containing additives within the electrode increase the self-discharge of the iron-based electrode significantly.

Self-discharge occurs due to unstable forms of iron alloys and/or hydrogen evolution on the surface of the iron electrode. As the Hydrogen evolution occurs mainly at the more positive potentials within the voltage range, it is plausible that at lower state of charges less self-discharge could occur at the FeS electrode. Therefore a more elaborate self-discharge study is necessary at different states of charges.

4.3.4 ROBUSTNESS, SAFETY & MAINTENANCE OF THE NiFeS CELL

ROBUSTNESS FOR OVER-CHARGE/DISCHARGE

The NiFe cell is known for its robustness to withstand over-charge/discharge. The Hydrogen evolution and Oxygen evolution causes the battery to be resistant again over(dis)charge. The addition of sulfur containing additives is not expected to influence the robustness for over-charge/discharge of the cell.

TEMPERATURE PERFORMANCE

As for all battery systems, low temperatures causes the charge and discharge reactions to be kinetically reduced and the resistance and viscosity of the electrolyte to increase. Both lead to a decrease in capacity. For the NiFe system also the solubility of reaction intermediates decreases, contributing to the decrease in capacity. Too high temperatures exceeding 50 °C must be avoided as well as the high solubility of the iron species can adversely affect the nickel-based electrode by incorporating iron species in the crystal lattice. The effect of temperature on the performance of the FeS electrode compared to commercial iron-based electrodes is not yet investigated and is still necessary.

SAFETY & MAINTENANCE

By using iron(II) sulfide as starting material the iron-based electrode can be charged and discharged at higher C-rates with higher coulombic efficiencies. Thereby the production of hydrogen gas and depletion of the electrolyte is significantly reduced and lowers the frequency of neccessary refilling of the electrolyte when a NiFe cell is used at C-rate higher than C/5 or possible explosion hazards of the cell due to hydrogen gas build-up. $LaNi_5$ additives can be applied to further eliminate electrolyte depletion and path the way for sealed NiFeS cells.

CHAPTER 5

DISCUSSION & RECOMMENDATIONS

CHAPTER 6

CONCLUSION

Therefore the main question of this research will be:

Does the NiFeS battery have sufficient potential to be an interesting competitor as stationary short-term energy storage system?

The short term SESS market is defined as $<$ 5C charge rates. the C-rate is a measure for the current charge or discharge rate. Hence, a 5C rate stands for charging a battery in 12 minutes. Critical technical performance parameters of the FeS anode will be investigated, which are depicted in the following sub-questions:

What are currently the best obtainable stable capacity, efficiency, cycle life and to what extend is self-discharge a limiting parameter and what are the causes under standard cycling conditions?

To investigate whether sulfur containing additives are actual effective additives is validated by the sub-question:

Are bismuth, sulphur and sulphides necessary additives to the cell to effectively delimit the Hydrogen Evolution Reaction, passivation of the iron and by doing so, respectively decrease the self-discharge and capacity loss?

To appoint also the possibility to introduce the NiFeS battery for high performance applications is validated by the sub-question:

Has NiFeS also the potential to be an alternative for high performance applications?

The high performance market is defined as $>$5C charge rates. Based on the identified technical performance parameters the economic potential of the NiFeS battery as short-term SESS will be investigated following the sub-question:

What are the minima of criteria an FeS based battery needs to meet to be an interesting alternative?

If the nickel cathode is limiting in costs, or abundance and if there are alternatives is validated by the sub-question:

Is the toxicity and abundance of nickel limiting and are there alternatives as cathode?

Assuming a large-scale transition to a renewable energy economy in which storage systems are a prerequisite.

As the effect of FeS as starting material the effect still disappears... metal containing sulfide specie that has lower solubility and is less prone to electrochemically react such as Cu2S.

It is suggested that the application of organosulfur additives is advantageous instead of Bi_2S_3 additives in terms of costs and recycling [60].

The downfall with most superconductive materials are the expenses.

Regarding the reaction happening at the iron electrode the 0/2 reaction is thermodynamically limitated as there are dissolved intermediates involved. This leads to low c-rates and for the iron electrode to maintain stable no full dissolution of the species hsould occur.

Commercial NiFe batteries only use the Fe(0-2+) reaction of the iron electrode. Thereby the battery has a low coulombic efficiency due to a parasitic side reaction, the hydrogen evolution, leading to low discharge capacities and depletion of the aqueous electrolyte. Shangguan et al. (2015) and research by E-Stone Batteries shows that by using FeS as starting material the parasitic side reaction can be reduced. In addition also the Fe(2+/3+) gets more reversible. E-Stone Batteries have shown a stability so far of 100 cycles with a discharge capacity of 400 mAh/g using FeS with 10wt% conductive additive. Shangguan et al (2015) showed 200 subsequent cycles of a stable discharge capacity of 325 mAh/g using carbon grafted FeS with 10wt% conductive additive and 3wt% Bi_2O_3 additive. For E-Stone Batteries the discharge capacity of the FeS based electrode decreased as a result of a degradation of the Fe(2+/3+) reaction. If this occurred for Shangguan et al. (2015) is not known. Thomas van dijk (2012) showed a single cell, using pure FeS as starting material and only the Fe(2+/3+) reaction, being stable or 150 cycles. The use of only Fe(2+/3+) reaction leads to a 100% coulombic efficiency but to lower discharge capacities of around 120 mAh/g. Unfortunately, after an appreciable amount of effort this has not been reproducible so far.

A possible explanation of the Fe(2+/3+) reaction not being reversible when the Fe(0/2+) reaction is used, is the parasitic formation of Fe_3O_4 by both the Fe(0/2+)- and Fe(2+/3+) reaction. This iron oxide involves Fe(2+) and Fe(3+) cations in the structure. To fully reduce this material the Fe(0/2+) reaction is necessary. The addition of sulfur containing species could help as the addition of sulphur containing species in the electrode or electrolyte is suggested to decrease the hydrogen evolution and thereby increases the reduction of Fe_3O_4 to metallic iron, leading to a higher reversibility of the iron electrode [12] and is also shown by in-situ research by [44]. However, research by Manohar et al. (2015) and E-Stone Batteries show that the beneficial effect of sulfur containing species as additives for the iron electrode, disappears after subsequent cycling.

For the FeS as precursor material to be an interesting material, the stability should be enhanced to at least 1000 cycles. Manohar et al. (2015) already showed that the use FeS and Bi_2O_3 additive

for a carbonyl iron electrode resulted in a stability of 1200 cycles with a discharge capacity of 250 mAh/g. It is suggested that the low solubility of FeS leads to a constant source of sulfide anions in the electrolyte over a long time period. E-Stone batteries uses FeS as main starting material. therefore higher concentrations of sulfides are applicable. Hence, similar performances should be possible to be attained. Moreover, enhancement methods, such as attaining superconductivity and annealing methods of the FeS particles or use additives to decrease the hydrogen evolution, have not been explored thus far.

It could be interesting to find other ways to attain a constant sulfide concentration in the electrolyte, such as titration methods find ways to prevent depletion of the sulfide species. Caution must be taken for too high concentrations of sulfide cations as the beneficial effect then disappears.

APPENDIX A

THE IRON OXIDES

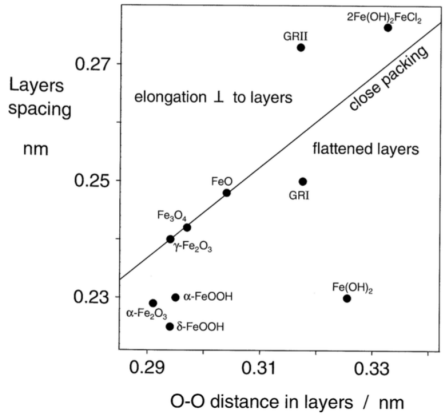

FIGURE A.1: inter-layer space versus the intra-layer space for ironoxide structures GRI and GRII: Green rust I and II [9].

In total sixteen different FeOx species exist: oxides, hydroxides and oxide-hydroxides. In general, FeOx have slabs of Fe(2+) or Fe(3+) mostly layered as $Fe(O,OH)_6$ octahedra but in some cases FeO_4 tetrahedra. Figure A.1 shows the inter-layer space versus the intra-layer space for ironoxide structures. The closer both spaces are located, the more stable and crystalline the polymorph crystal is. Anions can participate in the structure. Hence, traces of electrolyte could intercalate in the structure-e.g. K^+ Na^+ and Li^+ [9]. The structures of FeOx species are briefly explained below. Figures A.3 and A.4 illustrate respectively the four different polymorphs of Fe(3+)OOH and the different oxide structures. For more information concerning FeOx structures I would like to recommend you to read 'The Iron Oxides: Structure, Properties, Reactions, Occurences and Uses' by Cornell and Schwertmann (2003) [9]:

FeOH

HFeO - ferrihydrite (HFeO) exists as nano-crystals and transforms by aging into more stable iron oxides. HFeO is an important intermediate. The composition depends on the amount of OH^- and H_2O involved. *Fe(OH)*$_2$ - Irondihydroxide ($Fe(OH)_2$) does not exist in nature as mineral as it is readily oxidized. It can be formed by dehydration in alkali. It has a similar crystal structure as β-$Ni(OH)_2$, as shown in figure 3.8. But then the slabs are layered FeO_6 octahedra. No polymorph exists. When it oxidizes it is said to develop into green rusts and by further oxidation it turns into black Fe_3O_4 [9]. *Fe(OH)*$_3 * nH_2O$ - bernalite ($Fe(OH)_3 * nH_2O$) has a cubic structure and consists out of four corner sharing octahedra per unit cell.
green rusts - Green rusts are a group of blueish-green Fe(2+)-Fe(3+) hydroxy compounds that are formed under anoxic conditions mostly during the corrosion of steel. They consist of sheets of hexagonal closed packed $Fe(2+)(OH)_6$ octahedra in which some of the Fe(2+) is replaced by Fe(3+). The Fe(3+) creates a positive layer which is balanced by the incorporation of anions. Green rust I contains Cl^- impurities while Green rust II contain SO_4^{2-} impurities. Other anions can also be involved such as halogenides, carbonates, perchlorates, nitrates, oxalates and selenates.

FEOOH

α*-FeOOH* - The most thermodynamically stable FeOOH is goethite (α-FeOOH). Therefore it is often the end product or intermediate during a transformation but is not mentioned in Fe related electrochemical studies. It has a diaspore structure, based on a hexagonal close packed lattice. Within OH^- ions are hydrogen bonded to O^{2-}. It forms in acid aqueous media by precipitation of soluble Fe(3+) species by hydrolysis or by the oxidation of green rusts in neutral aqueous conditions.
β*-FeOOH* - The identified structure during discharge at the Fe electrode following mössbauer by Geronov

et al. (1975) is akaganéite (β-FeOOH) [75]. β-FeOOH has a tetragonal or monoclinic unit cell in which the anions are arranged as a body centered cubic array bonded together. The overall structure contains actual tunnels per one unit cell in which the anions are missing. These tunnels are stabilized having anionic impurities involved. Therefore it is mainly found in Cl^- or F^- rich acidic solution. This mineral occurs rarely in nature. Geronov et al (1975) suggests that he found β-FeOOH electrochemical formation in alkaline environment.

$Fe_{16}O_{16}(OH)_y(SO_4)_z*H_2O$ - The recently discovered schwertmannite ($Fe_{16}O_{16}(OH)_y(SO_4)_z*H_2O$) has the same basic structure as β-FeOOH but contains S^{2-} instead of Cl^-. This polymorph occurs in nature as an oxidation product of FeS in acidic environment. Unlike the other FeOOH polymorphs β-FeOOH and $Fe_{16}O_{16}(OH)_y(SO_4)_z*H_20$ have body centered cubic packing of anions. The recent discovery of this mineral and the occurrence in sulphidic environments suggests that the product of the oxidation of $Fe(OH)_2$ is rather $Fe_{16}O_{16}(OH)_y(SO_4)_z*nH_2O$ than β-FeOOH.

γ-FeOOH - Lepidodocrocite (γ-FeOOH) is an oxidation product of Fe(2+) solutions via a green rust intermediate as well. Direct precipitation from Fe(3+) can also take place. It has a layered plate cubic close packed crystal shape.

δ-FeOOH - δ-FeOOH is isostructural with $Fe(OH)_2$. It is formed by rapid oxidation. It has a hexagonal closed packed unit cell with sheets of edge sharing octahedra. δ-FeOOH is poorly crystalline and is rarely found in nature.

FeO

α-Fe_2O_3 - hematite (α-Fe_2O_3) is the oldest known FeOx and widespread in rocks and soils. It is extremely stable and often the last in a sequence of transformations.

Fe_3O_4 - magnetite (Fe_3O_4) contains both Fe(2+) and Fe(3+). It has an inverse spine structure. and is also very stable.

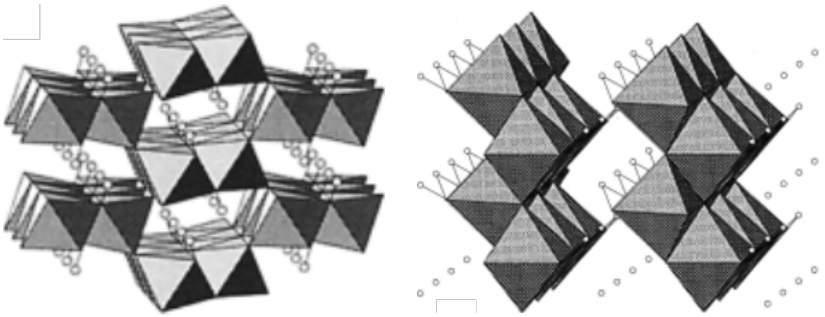

(A) α-FeOOH (B) γ-FeOOH

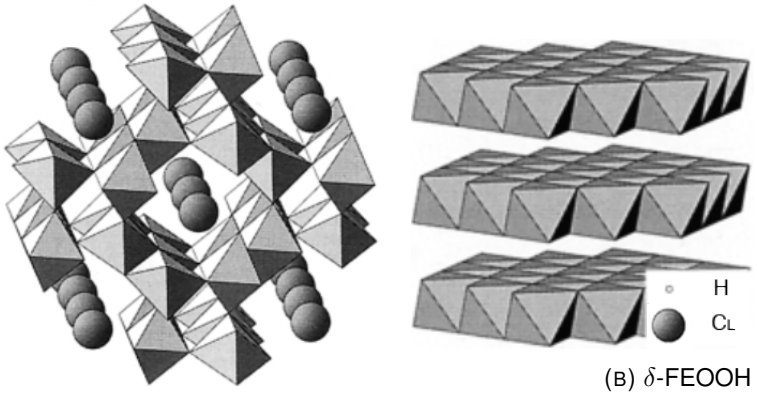

(A) β-FeOOH (B) δ-FEOOH

FIGURE A.3: two of the four FeOOH isomorphic structures possible [9].

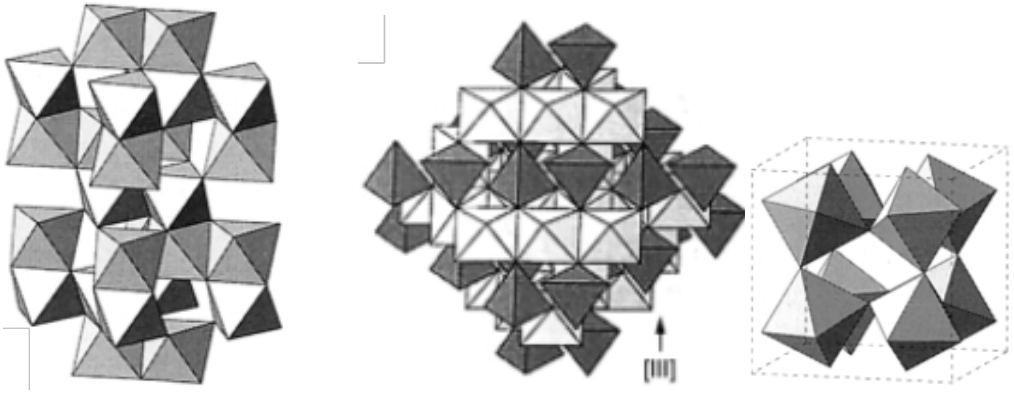

(A) Fe_2O_3 (B) Fe_3O_4 (C) $Fe(OH)_3$

FIGURE A.4: Fe oxide structures [9].

APPENDIX B

GENERAL PROPERTIES OF THE IRONOXIDES, IRONSULFIDES & NICKELOXIDES

TABLE B.1: General properties of the iron oxides [9]

Mineral name			Cell dimensions nm	Formula units, per unit cell, Z g cm^{-3}	Density	Octahedral occupancy	Colour	Hardness	Type of magnetism	Néel (Curie) temperature (K)	Standard free formation energy ΔG_f	Solubility product (pFe+3pOH)
Iron	*Fe*	orthorhombic										
Ironhydroxide	*Fe(OH)*$_2$	monoclinic										
goethite	α-*FeOOH*	orthorhombic	*a=0.9956* *b=0.30215* *c=0.4608*	4	4.26	$1/2$	yellow-brown	5-$51/2$	antiferromag.	400	-488.6	40-44
Akagénite	β-*FeOOH*	monoclinic	*a=1.0546* *b=0.3031* *c=1.0483* $\beta = 90.63^{\circ}$	8	-	$1/2$	yellow-brown	-	antiferromag.	290	n.k.	34.9[1]
Schwertmannite	$Fe_{16}O_{16}(OH)_y(SO_4)_z * nH_2O$	tetragonal	*a=0.1065* *c=0.3604*	2	≈3.8	$1/2$	orange-brown	-	antiferromag.	-	-	-
Lepidodocrocite	γ-*FeOOH*	orthorhombic	*a=0.307* *b=1.253* *c=0.388*	4	4.09	$1/2$	orange	5	antiferromag.	77	-477.7	$\tilde{4}2$
Feroxyhyte	δ'-*FeOOH*	hexagonal	*a=0.293* *c=0.456*	2	4.20	$1/2$	red-brown	-	ferrimag.	440-460	n.k.	n.k.
Ferrihydrite	*HFeO*	hexagonal	*a=0.2955* *c=0.937*	4 4	3.96 3.96	$2/3$	red-brown	-	speromag.	25-115[2]	-699	38.0-39.5
Bernalite	*Fe(OH)*$_3$	bernalite	*a=0.7544* *b=0.7560*	8	3.32	$1/2$	dark green					
Hematite	*Fe2O3*	cubic or tetragonal	*a=0.50536* *c=1.37489*	6	5.26	$2/3$	red	$61/2$	weakly ferromag. or antiferromag.	956[3]	-742.7	42.2-43.3
Magnetite	*Fe3O4*	cubic	*a=0.8396* *c=0.7558*	8	5.18	-	black	$51/2$	ferrimag.	850[3]	-1012.6	35.7[4]
Ironsulphide	FeS											
Pyrite	*FeS2*											
Nickelhydroxide	*Ni(OH)2*											
Pyrite	*NiOOH*											

APPENDIX C

FORMATION & TRANSFORMATION PATHWAYS

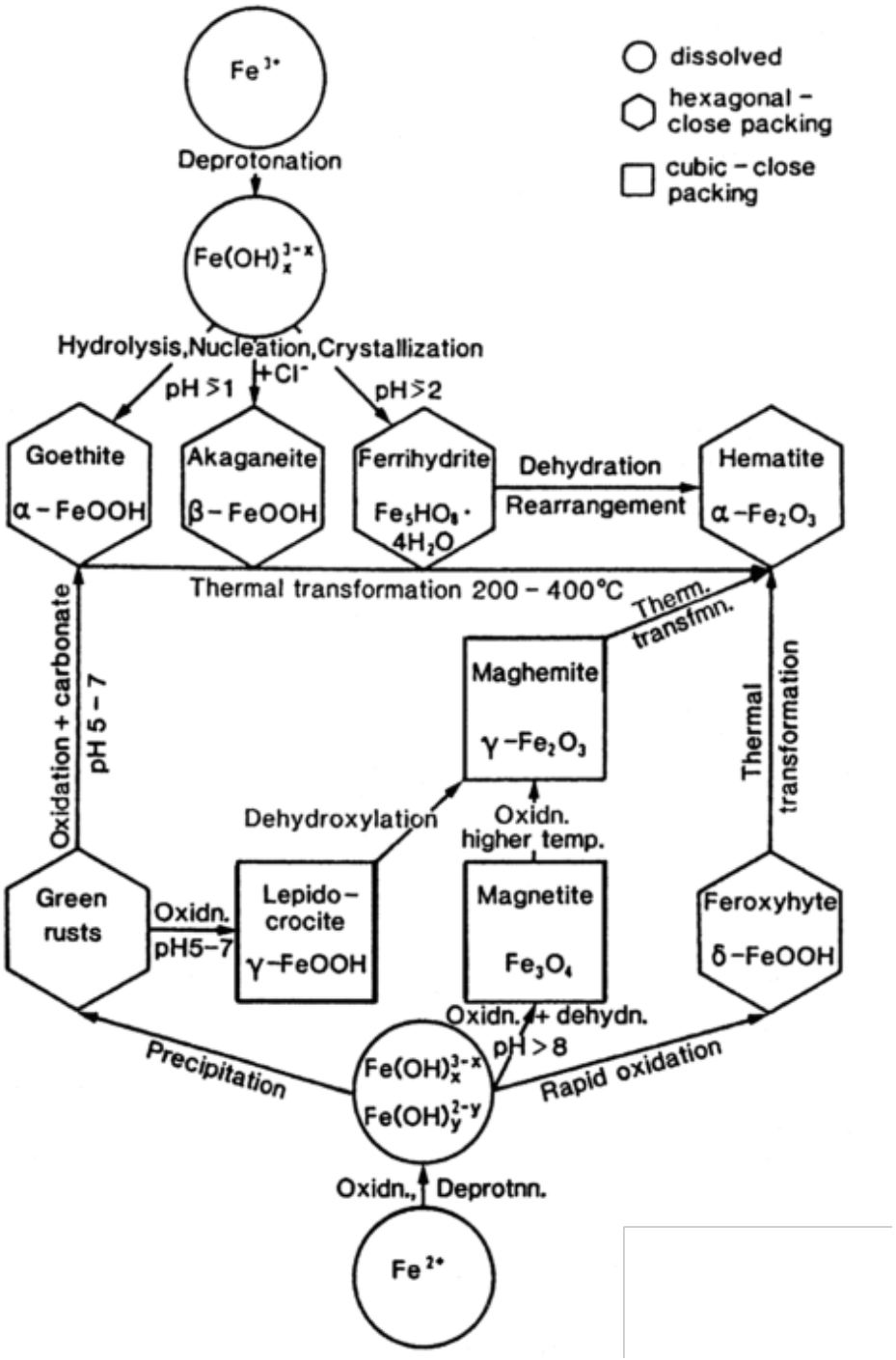

FIGURE C.1: Schematic representation of major formation and transformation pathways of common iron oxides [9].

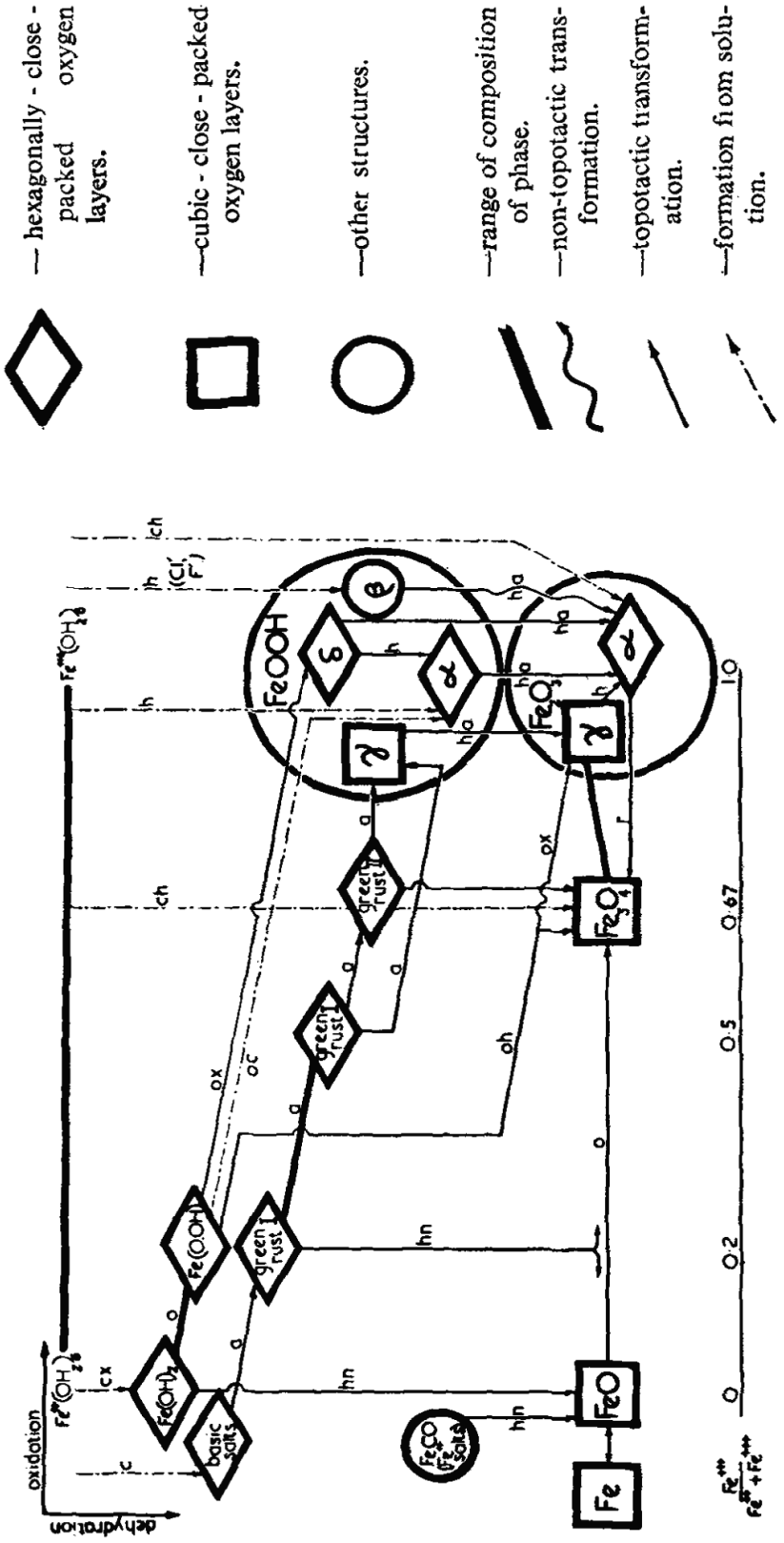

FIGURE C.2: Structural transformations in the iron oxide/hydroxide system. a: on exposure to air; c: in alkali; h: on heating; n: in nitrogen; o:on oxidation; r: on reduction; x: in excess. [14].

APPENDIX D

THE WORKING FUNCTION OF ANIONIC SULPHUR SPECIES FOR THE IRON-BASED ELECTRODE

PROPOSED WORKING PRINCIPLE OF ANIONIC SULPHUR SPECIES FOR THE IRON-BASED ELECTRODE

In the beginning of the twentieth century it was already known from the steel industry that corrosion of steel can be initiated by inclusions of sulfur complexes in metal [19]. Corrosion is initiated by the formation of so called pits [1]. As shown in figure D.1, sulfide dianions (S^{2-}) and bisulfide ions (HS^{-}) only occur in alkaline to neutral solutions. They belong to a group of anions with a high electric polarization (dipole character), resulting in strong contact adsorption on certain metal surfaces. In strongly acidic solutions this leads to the inhibition of corrosion by the formation of a passivating layer. In weakly acidic, neutral and alkaline solutions it results into a catalytic effect, leading to a reduction in activation energy for the redox reaction between the metal and the base, resulting in a strong increase in metal corrosion [19]. The catalytic effects of different anions can be classified, depending on its contact absorption based on the Hofmeister iyotropic series, which are depicted in table D.1.

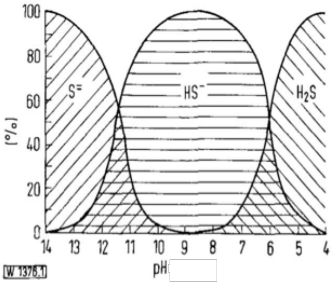

FIGURE D.1: anionic sulfur concentration by pH [15].

TABLE D.1: anion contact absorption classification [19]

Weak contact absorption	Strong contact absorption
$F^{-} > ClO^{-}_{4} > SO^{2-}_{4} > CO^{2-}_{3} > PO^{3-}_{4} > CrO^{2-}_{4} > OH^{-} >$	$Cl^{-} > NO^{-}_{3} > Br^{-} > HS^{-} > I^{-} > SCN^{-} > S^{2-}$
Low molar polarization	High molar polarization
Low adsorbability	High adsorbability
High overpotential	Low overpotential
Weakly peptizing	Strongly peptizing
Passivating Low corrosivity	Activating High corrosivity

The effect of small proportions of anionic sulphur species for the iron-based electrode are possibly known since the early stages of the development of the NiFe battery. In 1974 Öjefors et al. showed that 1 g/l potassiumsulfide (K_2S) or hydrazinesulfate within the electrolyte both decrease the HER and increase the discharge capacity at a pH>12 [47]. In 1984 Micka and Zabransky indicated that addition of 0.02 M sodium(I) sulfide (Na_2S) within the electrolyte has a similar effect in increasing the discharge capacity as doping the Fe electrode with 0.02 w% transition metal(II) sulfides, such as FeS, NiS, CuS, HgS [77]. In scientific literature, the working function of sulfur containing additives is considered to be (also summarized by Vijayamohanan and Shukla et al.,1990 [34, 35]):

- Increasing the solubility of iron complexes.
- Incorporation within the oxide layer of the electrode surface.
- Modification of the electrode texture and morphology, increasing electronic conductivity and reactivity

[1] pitting corrosion is a form of extremely localized corrosion. it can be described as a dissolution or attack of an (passivating) oxide-covered metal in environments that contain specific aggressive species such as chlorides. During the initiation stage the passive film of the metal is broken down and causes an extremely localized corrosive micro-environment to be created within a so-called pit. The pH tends to be lowered significantly by the liberating hydroxides, which favors further corrosion within the pit as a result of the chemical pitting reaction mechanisms. At higher concentrations of the aggressive species a propagation stage can follow by which the pit goes even deeper into the metal. Next to chlorides also thiosulfate ($S_2O^{2-}_3$), fluorides and iodides can initiate pitting. In particular $S_2O^{2-}_3$ are aggressive reactants and are formed by partial oxidation of pyrite (FeS_2) or partial reduction of sulfate (SO^{2-}_4). Pitting corrosion is of concern for many industries.

- Modification of the pH electrolyte.
- Modification of electrode kinetics.

INCREASING SOLUBILITY OF IRON COMPOUNDS

From 1961 and onwards several authors found increased dissolution of Fe compounds by the addition of small proportions of sulfur containing species [15, 30, 32, 108, 110**?**]. As the Fe(0/2+) reaction is considered to be a dissolution/precipitation mechanism, it can be inferred that the addition of anionic sulphur species enhance this reaction. In turn, high concentrations of anionic sulfur species lead to a lower concentration of dissolved Fe species [27, 32].

INCORPORATION OF ANIONIC SULPHUR SPECIES WITHIN THE OXIDE LAYER Bolmer (1965) indicated that the diffusion of H_2S on the iron electrode surface decreases the HER [113]. Based on this finding he suggests that the $[S^{2-}]$ in solution decrease the build-up of a passivating oxide layer. This is in agreement with the findings of Berger and Haschka (1986) [30] Hampson et al. (1973) studied the oxidation of iron in strong alkaline solutions by Faradaic impedance and potential step techniques using 10 M^{-4} M Na_2S additives in 4*25M KOH(?). They found that the rate determining film growth process is modified by the presence of $[S^{2-}]$ in solution. They suggest S^{2-} is incorporated into the non-stochiometric layer adjacent to the Fe and thereby exchange reactions are higher [26]. In 1978, CV measurements of Shoesmith et al. in low molarity NaOH and NaSH solutions also confirmed that $[HS^-]$ added to the electrolyte inhibit the oxide growth [27]. They suggest anionic sulphur species attack the oxide layer in a similar method as Cl^- by the formation of pits following reaction 3.6. They also suggest the formation of elemental sulphur (S) initiates the pitting by acting as a source of protons. The protons locally increase the $[HS^-]/[OH^-]$ concentration ratio. The formation of elemental S probably has anionic polysulfides (S^n_{2-}) intermediates involved. Subsequently, Shoesmith et al. describes the mechanism as a competitive adsorption mechanism [106]:

$$8[\mathrm{HS}]^- \rightarrow \mathrm{S}_8 + 8[\mathrm{H}]^+ + 16\mathrm{e}^- \tag{D.1}$$

$$(\mathrm{OH})^-_{\mathrm{ads}} + [\mathrm{SH}]^- \leftrightarrow (\mathrm{SH})^-_{\mathrm{ads}} + [\mathrm{OH}]^- \tag{D.2}$$

At a low $[HS^-]/[OH^-]$ concentration ratio the elemental sulphur repassivates the electrode by blocking the faults and pores in the oxide. In turn an excess of bisulfide ions ($[HS^-]/[OH^-] \gtrapprox 4$) is suggested to lead to a similar propagation stage of a pitting attack by which the metal gets penetrated and dissolved. Within the pit the creation of protons increases the $[HS^-]/[OH^-]$ ratio even further leading to an increase in adsorption of $[HS^-]$. When the equilibrium is sufficiently displaced the charge discharge of the iron-based electrode will involve $[HS^-]$ instead of $[OH^-]$ species having the following intermediate steps:

$$\mathrm{Fe} + [\mathrm{SH}]^- \leftrightarrow (\mathrm{FeSH})^-_{\mathrm{ads}} \tag{D.3}$$

$$(\mathrm{FeSH})^-_{\mathrm{ads}} \leftrightarrow (\mathrm{FeSH})^+_{\mathrm{ads}} + 2\mathrm{e}^- \tag{D.4}$$

$$\mathrm{x}(\mathrm{FeSH})^+_{\mathrm{ads}} \leftrightarrow \mathrm{FeS}_{1-\mathrm{x}} + \mathrm{x}[\mathrm{SH}]^- + (1-\mathrm{x})\mathrm{H}^+ \tag{D.5}$$

The above is based on the analogy of the hydroxide system. Further oxidation yields colloidal thioferrite ($NaFeS_2$) by:

$$\mathrm{Fe}^{3+} + 2[\mathrm{SH}]^- + [\mathrm{Na}]^+ \rightarrow \mathrm{NaFeS}_2 + 2[\mathrm{H}]^+ \tag{D.6}$$

The pitting corrosion is suggested to lead to a spreading of local dense FeS centres on the electrode by a nucleation and growth process. $NaFeS_2$ and S_{2-}^{n} are identified by UV-visible spectroscopy. S_n^{2-} are suggested to increase the FeS growth by catalyzing the [HS^-] oxidation. They also found that stirring of the electrolyte shows a big decrease in corrosion of the oxide layer and presumethis is due to a flux of bisulfide ions away from the pits. Electrochemical, SEM and X-Ray analysis of Salvarezza et al. (1982) partly support the theory suggested by Shoesmith et al. (1978) [28]. They did not find evidence of the sulfur deposition. Together with the fact that anionic sulphur species are rapidly oxidized by O_2, they find the deposition of sulphur on the surface of the electrode suggested by Shoesmith et al. (1978) unlikely. They suggest that the deposition of sulphur on the electrode following equation D.3, must not be seen as the initiation of the pitting mechanism. Salvarezza et al. propose a direct competitive adsorption mechanism following D.4.

MODIFICATION OF THE ELECTRODE TEXTURE AND MORPHOLOGY

In 1986, Vera et al. found enhancement of penetration or dissolution of the oxide film by sulfur containing additives unlikely [111]. By applying potentiodynamic experiments she concluded that addition of anionic sulphur species on a passive surface layer of an iron electrode results into a competitive ion adsorption mechanism, followed by possible flaws in the oxide film. Subsequently, the dissolution of Fe follows but could be compensated by the electro-oxidation of the metal. Cerny et al. (1989) [31] takes in doubt both the formation of soluble Fe complexes suggested by Berger et al. 1986 [30] or the pitting attack by shoesmith et al [27, 106]. He suggests that most obvious S^{2-} ions are strongly and adsorbed as FeS in the iron-electrolyte interface, which is still in agreement with Shoesmith et al. and others [26, 27, 106–108]. In contrast, they mention that anionic sulphur species do not increase solubility of the iron species as the solubility of FeS $(4 * 10^{-19})$ is lower than that of $Fe(OH)_2$ [17]. Cerny et al. suggest that the adsorbed FeS cause disorder in the structure of the $Fe(OH)_2$, which in turn enhances diffusion of ions and further growth of the film, which is in line with several other authors [34, 37, 40] Cerny et al. also found that FeS is irreversibly adsorbed onto iron, as the discharge capacity, nor the CV did not change after replacing the electrolyte containing Na_2S for pure KOH solution. From an electrochemical point of view, FeS is more stable than $Fe(OH)_2$ regarding the E_0 of Fe/FeS is equal to -0.970 V compared with -0.877 V for $Fe/Fe(OH)_2$. Furthermore, Vijayamohanan et al. (1990) suggests the possibility of grain refinement of Fe particles [34]. The irreversible adsorption of anionic sulfur species on the iron-based electrode is taken in doubt by Vijayamohanan et al. (1990). They found that the observed increased performance of the iron-based electrode tend to be lost during repetitive deep discharge, which Poa et al. (1985) already observed [29, 35]. They suggest this is due to the electrooxidation of anionic sulfur species at the cathode to irreversible gaseous species. Hegazy et al. (2001) suggests the following electrooxidation pathways of anionic sulfur species:

$$3[SH^-] \rightarrow S_3^{2-} + 3[H^+] + 4e^- \qquad E_0 = -0.097 \text{VvsSHE} \quad \text{(D.7)}$$

$$[SH^-] \rightarrow S + [H^+] + 2e^- \qquad E_0 = -0.065 \text{VvsSHE} \quad \text{(D.8)}$$

$$2[SH^-] + 3H_2O \rightarrow S_2O_3 + 6H^+ + 8e^- \qquad E_0 = 0.200 \text{VvsSHE} \quad \text{(D.9)}$$

INCREASE IN ELECTRODE CONDUCTIVITY

Vijayamohanan et al. (1990) mentions that the incorporation of FeS species also increases the electronic conductivity at the interface of the iron electrode, as FeS is more electrically conductive than most FeOx species [34, 35].

MODIFICATION OF pH ELECTROLYTE

Shoesmith et al. and Vera et al. already mentioned localized increase in acidity during pitting causes further growth of FeS species following equations D.3, D.4 and D.5 [27, 111]. They also found that stirring decreases the pitting, presumably by a reduction of local acidity. Ravikumar et al. (2015) suggest that the local increase of protons in the vicinity of the iron-based electrode during discharge favors the formation of FeS over FeOx species [44]. Based on

theoretical thermodynamic stable species they assume that the following reactions are possible:

$$[\mathrm{HS}]^- \leftrightarrow [\mathrm{S}]^{2-} + [\mathrm{H}]^+ \qquad \mathrm{pH} \approx 14 \tag{D.10}$$

$$\mathrm{FeS} + \mathrm{H_2O} + [\mathrm{H}]^+ + 2\mathrm{e}^- \leftrightarrow [\mathrm{HS}]^- + (\mathrm{Fe} - \mathrm{H_2O})_{\mathrm{ads}} \tag{D.11}$$

$$\mathrm{FeS} + \mathrm{H_2O} \leftrightarrow (\mathrm{FeO})_{\mathrm{ads}} + [\mathrm{HS}]^- + [\mathrm{H}]^+ \tag{D.12}$$

Equations D.11 and D.12 act as a source of [HS^-] and thereby sustain the pH in the pores of the electrode over a longer time period-similar to the pitting mechanism-. Thereby the formation of $Fe(OH)_2$ increases by:

$$[\mathrm{HFeO}^{2-}] + \mathrm{HS}^- \rightarrow \mathrm{Fe(OH)_2} + [\mathrm{S}^{2-}] \tag{D.13}$$

MODIFICATION OF ELECTRODE KINETICS - As already mentioned in the Material section of this thesis both the Fe(0)/$Fe(OH)_2$ and $Fe(OH)_2$/FeOOH reactions have side-reactions, leading to the formation of the more stable Fe_3O_4. In addition, more stable FeOx species form spontaneously out of the species $Fe(OH)_2$ and FeOOH. Caldas et al. (1998) reported that sulfide di-anions incorporated within the passive layer results in promotion of the Fe/$Fe(OH)_2$ reaction but does not increase the $Fe(OH)_2$/Fe_3O_4 reaction [37]. Both Manohar (2015) and Ravikumar (2015) suggest that the addition of anionic sulphur species increases the reduction of Fe_3O_4 to α-Fe, presumably by increasing the overpotential of the hydrogen evolution and decreasing the overpotential of the FeOx/Fe reaction.

BENEFICIAL EFFECTS OF SULPHUR CONTAINING ANIONS FOR THE IRON-BASED ELECTRODE

The aforementioned porposed working principles of sulfur containing anions for iron-based electrodes are found to have the following beneficial effects for the Fe electrode.

- Decrease the overpotential of the Fe/FeOx reactions.
- Increase the overpotential of the HER.
- Decrease the self-discharge.

DECREASE THE OVERPOTENTIAL OF THE Fe/FeOX REACTIONS
The decrease in the electrically insulating passivation layer and buffering effect of the anionic sulphur species are said to retard the passivation of the iron electrode [34, 37, 77]. This results in an increase in anodic current density and (dis)charge capacity.

SUPPRESSION OF THE HYDROGEN EVOLUTION The passivation layer decreases the reactivity of the electrochemically active species, yet still contain some electronic conductivity. This is suggested to favor the HER by decreasing the overpotential of the Fe(0-2+) and Fe(0/3+) reaction and increasing the overpotential of the HER. As sulfur containing anionic species are suggested to decrease the passivation layer they suppress the HER as well. Different polarization studies recognize this effect [12, 27–29, 31, 34–36, 38, 44, 58, 59, 77, 111, 112, 112, 113, 113]. This results in an increase in anodic current density and charge/discharge capacity as well.

DECREASE THE SELF-DISCHARGE
Having sulfur containing species involved, the surface of the iron-based electrode in an alkaline environment still

creates a passivating layer. This in combination with an increase of the overpotential and decrease of the overpotential of the Fe/FeOx reactions suggests an increase in self-discharge as well [47, 93]. Souza et al. (2004) found 1wt% additions of FeS and lead(II) sulfide incorporated in the electrode retard self-discharge [39]. Nevertheless the the self-discharge still remains at least 30% over 6 days, while the commercial NiFe battery only has 0.6-1.0% per day.

However, the beneficial effects disappear after deep discharge or a series of discharges. Sulfur containing anions are suggested to oxidate irreversibly to sulfate, presumably at the cathode. This leads to a depletion of sulfur containing anions. Manohar et al. (2015) found that when having high concentrations of FeS (5-10 wt%) incorporated in the electrode leads to long-term stability. They were able to reach 1200 cycles with a discharge capacity of 0.24 Ah $g^{-}1$. The low solubility of FeS and lower standard reduction potential of FeS/Fe compared to the standard reduction potential of $Fe(OH)_2$/Fe is suggested to lead to a reservoir, providing a sustained release of anionic sulfur species in the electrolyte over a long period of time. However, they do not mention the stability at higher c-rates

Bibliography

[1] IEA. TECHNOLOGY ROADMAP. In SpringerReference, page 64. Springer-Verlag, Berlin/Heidelberg, 2014. doi: 10.1007/SpringerReference_7300. URL http://www.springerreference.com/index/doi/10.1007/SpringerReference{_}7300https://www.iea.org/publications/freepublications/publication/TechnologyRoadmapEnergystorage.pdf.

[2] IPCC. Renewable energy sources and climate change mitigation: special report of the Intergovernmental Panel on Climate Change. Technical Report 11, International Panel on Climate Change, 2012. URL http://srren.ipcc-wg3.de/report/IPCC{_}SRREN{_}Full{_}Report.pdf.

[3] Tesla Motors. Tesla Powerwall, 2015. URL http://www.teslamotors.com/powerwall.

[4] Matthias Leuthold. Energy Storage Technologies Battery Storage for Grid Stabilization. page 39, Berlin, 2014.

[5] Anissa Dehamna, Alex Eller, and Peter Asmus. Executive Summary : Energy Storage for Renewables Integration. Technical report, Navigant Research, 2015.

[6] Tjark Thien, Tobias Blank, Benedikt Lunz, and Dirk Uwe Sauer. Life Cycle Cost Calculation and Comparison for Different Reference Cases and Market Segments. Elsevier B.V., 2015. ISBN 9780444626165. doi: 10.1016/B978-0-444-62616-5.00021-8. URL http://linkinghub.elsevier.com/retrieve/pii/B9780444626165000218.

[7] Edison Storage Battery Company. The edison Alkaline storage battery. 1924.

[8] Patrick Bernard and Michael Lippert. Nickel-Cadmium and Nickel-Metal Hydride Battery Energy Storage. Elsevier B.V., 2015. ISBN 9780444626165. doi: 10.1016/B978-0-444-62616-5.00014-0. URL http://dx.doi.org/10.1016/B978-0-444-62616-5.00014-0.

[9] R. M. Cornell and U. Schwertmann. The Iron Oxides. Wiley-VCH Verlag GmbH & Co. KGaA, Weinheim, FRG, jul 2003. ISBN 3527302743. doi: 10.1002/3527602097. URL http://doi.wiley.com/10.1002/3527602097.

[10] Marcel Pourbaix. Atlas of Electrochemical Equilibria in Aqueous Solutions. National Association of Corrosion Engineers, 1974, Michigan, 1966. ISBN 0915567989. URL http://www.bcin.ca/Interface/openbcin.cgi?submit=submit{&}Chinkey=78430.

[11] Dennis W Barnum. Potential-pH diagrams. Journal of Chemical Education, 59(10):809, oct 1982. ISSN 0021-9584. doi: 10.1021/ed059p809. URL http://pubs.acs.org/doi/abs/10.1021/ed059p809.

[12] Aswin K Manohar, Chenguang Yang, and S R Narayanan. The Role of Sulfide Additives in Achieving Long Cycle Life Rechargeable Iron Electrodes in Alkaline Batteries. Journal of The Electrochemical Society, 162

(9):A1864–A1872, 2015. ISSN 0013-4651. doi: 10.1149/2.0741509jes. URL http://jes.ecsdl.org/content/162/9/A1864.abstract.

[13] a. K. Manohar, C. Yang, S. Malkhandi, B. Yang, G. K. Surya Prakash, and S. R. Narayanan. Understanding the Factors Affecting the Formation of Carbonyl Iron Electrodes in Rechargeable Alkaline Iron Batteries. Journal of the Electrochemical Society, 159(12):A2148–A2155, 2012. ISSN 0013-4651. doi: 10.1149/2.021301jes.

[14] J D Bernal, D R Dasgupta, and A L Mackay. The oxides and hydroxides of iron and their structural interrelationships. Clay Minerals, 4(21):15–30, 1959. ISSN 0009-8558. doi: 10.1180/claymin.1959.004.21.02.

[15] H. Kaesche. Elektrochemische Untersuchungen über die Korrosion des Eisens in sulfidhaltigen Lösungen. Materials and Corrosion, 21(3):185–195, mar 1970. ISSN 09475117. doi: 10.1002/maco.19700210305. URL http://doi.wiley.com/10.1002/maco.19700210305.

[16] David Linden and Thomas B Reddy. Handbook of Batteries. McGraw-Hill, New York, 3rd editio edition, 2001. ISBN 0071359788. doi: 10.1016/0378-7753(86)80059-3.

[17] WENDEL M. LATIMER. The Oxidation States of the Elements and Their Potentials in Aqueous Solutions. Soil Science, 48(4):349, oct 1939. ISSN 0038-075X. doi: 10.1097/00010694-193910000-00009. URL http://hdl.handle.net/2027/uc1.b4074350http://pubs.acs.org/doi/abs/10.1021/ed017p350.3http://content.wkhealth.com/linkback/openurl?sid=WKPTLP:landingpage{&}an=00010694-193910000-00009.

[18] George C. Stone. NOTE ON THE SOLUBILITY OF BISMUTH SULPHIDE IN ALKALINE SULPHIDES. Journal of the American Chemical Society, 18(12):1091–1091, dec 1896. ISSN 0002-7863. doi: 10.1021/ja02098a012. URL http://pubs.acs.org/doi/abs/10.1021/ja02098a012.

[19] G. Wranglen. Pitting and sulphide inclusions in steel. Corrosion Science, 14(5):331–349, jan 1974. ISSN 0010938X. doi: 10.1016/S0010-938X(74)80047-8. URL http://linkinghub.elsevier.com/retrieve/pii/S0010938X74800478.

[20] D Larcher and J-m Tarascon. Towards greener and more sustainable batteries for electrical energy storage. Nature Publishing Group, 7(January), 2014. ISSN 1755-4330. doi: 10.1038/nchem.2085.

[21] REN21. Renewables 2015: Global status report. page 31, 2015. URL http://www.ren21.net/wp-content/uploads/2015/07/REN12-GSR2015{_}Onlinebook{_}low1.pdf.

[22] F. M. Mulder. Implications of diurnal and seasonal variations in renewable energy generation for large scale energy storage. Journal of Renewable and Sustainable Energy, 6(3):033105, 2014. ISSN 1941-7012. doi: 10.1063/1.4874845. URL http://scitation.aip.org/content/aip/journal/jrse/6/3/10.1063/1.4874845.

[23] Haisheng Chen, Thang Ngoc Cong, Wei Yang, Chunqing Tan, Yongliang Li, and Yulong Ding. Progress in electrical energy storage system: A critical review. Progress in Natural Science, 19(3):291–312, mar 2009. ISSN 10020071. doi: 10.1016/j.pnsc.2008.07.014. URL http://www.sciencedirect.com/science/article/pii/S100200710800381X.

[24] ETA. Coal financial trends. Technical report, Energy Transition Advisors, 2014.

[25] Anthony Price. The Exploitation of Renewable Sources of Energy for Power Generation. Elsevier B.V., 2015. ISBN 9780444626165. doi: 10.1016/B978-0-444-62616-5.00001-2. URL http://dx.doi.org/10.1016/B978-0-444-62616-5.00001-2.

[26] N.a. Hampson, R.J. Latham, A. Marshall, and R.D. Giles. Some aspects of the electrochemical behaviour of the iron electrode in alkaline solutions. Electrochimica Acta, 19(7):397–401, 1974. ISSN 00134686. doi: 10.1016/0013-4686(74)87015-5. URL http://linkinghub.elsevier.com/retrieve/pii/0013468674870155.

[27] D.W. Shoesmith, P Taylor, M.G. Bailey, and B Ikeda. Electrochemical behaviour of iron in alkaline sulphide solutions. Electrochimica Acta, 23(9):903–916, sep 1978. ISSN 00134686. doi: 10.1016/0013-4686(78)87014-5. URL http://linkinghub.elsevier.com/retrieve/pii/0013468678870145.

[28] RC Salvarezza, HA Videla, and A.J. Arvía. The electrodissolution and passivation of mild steel in alkaline sulphide solutions. Corrosion Science, 22(9):815–829, jan 1982. ISSN 0010938X. doi: 10.1016/0010-938X(82)90078-6. URL http://www.sciencedirect.com/science/article/pii/0010938X82900786http://linkinghub.elsevier.com/retrieve/pii/0010938X82900786.

[29] D.S. Poa, J.F. Miller, and N.P. Yao. Effects of additives and temperature on iron electrode behavior in KOH electrolytes. [Addition of K/sub 2/S, LiOH or FeO to KOH]. Technical report, apr 1985. URL http://www.osti.gov/scitech/biblio/5533634.

[30] G. Berger and F. Haschka. proceedings? Power sources 11, 11(16), 1986.

[31] J. Černý and K Micka. Voltammetric study of an iron electrode in alkaline electrolytes. Journal of Power Sources, 25(2):111–122, feb 1989. ISSN 03787753. doi: 10.1016/0378-7753(89)85003-7. URL http://linkinghub.elsevier.com/retrieve/pii/0378775389850037.

[32] C. Chanson. A Ring-Disk Study of Electrochemical Behavior of Iron in Strong Alkaline Medium: Influence of Additive Sulfide Ions. Journal of The Electrochemical Society, 136(12):3690, 1989. ISSN 00134651. doi: 10.1149/1.2096531. URL http://jes.ecsdl.org/cgi/doi/10.1149/1.2096531.

[33] K Vijayamohanan, A.K. Shukla, and S Sathyanarayana. Open-circuit potential—time transients of alkaline porous iron electrodes at various states-of-charge. Electrochimica Acta, 36(2):369–380, jan 1991. ISSN 00134686. doi: 10.1016/0013-4686(91)85264-8. URL http://linkinghub.elsevier.com/retrieve/pii/0013468691852648.

[34] K. Vijayamohanan, A.K. Shukla, S. Sathyanarayana, and K Vijayamohamn. Role of sulphide additives on the performance of alkaline iron electrodes. Journal of Electroanalytical Chemistry, 289:55–68, 1990. ISSN 00220728. doi: 10.1016/0022-0728(90)87206-Y. URL http://www.sciencedirect.com/science/article/pii/002207289087206Y.

[35] K. Vijayamohanan, A.K. Shukla, and S. Sathyanarayana. Kinetics of electrode reactions occurring on porous iron electrodes in alkaline media. Journal of Electroanalytical Chemistry and Interfacial Electrochemistry, 295(1-2):59–70, nov 1990. ISSN 00220728. doi: 10.1016/0022-0728(90)85005-P. URL http://linkinghub.elsevier.com/retrieve/pii/002207289085005P.

[36] T.S. Balasubramanian and A.K. Shukla. Effect of metal-sulfide additives on charge/discharge reactions of the alkaline iron electrode. Journal of Power Sources, 41(1-2):99–105, 1993. ISSN 03787753. doi: 10.1016/0378-7753(93)85008-C.

[37] C.a. Caldas, M.C. Lopes, and I.a. Carlos. The role of FeS and (NH4)2CO3 additives on the pressed type Fe electrode. Journal of Power Sources, 74(1):108–112, 1998. ISSN 03787753. doi: 10.1016/S0378-7753(98)00039-1.

[38] H. S. Hegazy, E. A. Ashour, and B. G. Ateya. Effect of benzotriazole on the corrosion of alpha brass in sulfide polluted salt water. Journal of Applied Electrochemistry, 31(11):1261–1265, 2001. ISSN 0021891X. doi: 10.1023/A:1012740323483.

[39] C.a.C. Souza, I.a. Carlos, M. Lopes, G.a. Finazzi, and M.R.H. de Almeida. Self-discharge of Fe–Ni alkaline batteries. Journal of Power Sources, 132(1-2):288–290, may 2004. ISSN 03787753. doi: 10.1016/j.jpowsour.2003.12.043. URL http://linkinghub.elsevier.com/retrieve/pii/S0378775304000552.

[40] Bui Thi Hang and Doan Ha Thang. Effect of additives on the electrochemical properties of Fe2O3/C nanocomposite for Fe/air battery anode. Journal of Electroanalytical Chemistry, 762:59–65, 2016. ISSN 15726657. doi: 10.1016/j.jelechem.2015.12.012. URL http://linkinghub.elsevier.com/retrieve/pii/S1572665715302344.

[41] S. M. Abd El Haleem and E. E. Abd El Aal. Electrochemical behaviour of iron in alkaline sulphide solutions. Corrosion Engineering, Science and Technology, 43(2):173–178, jun 2008. ISSN 1478-422X. doi: 10.1179/174327807X234769. URL http://www.maneyonline.com/doi/abs/10.1179/174327807X234769.

[42] Jorge Omar Gil Posada and Peter J. Hall. Multivariate investigation of parameters in the development and improvement of NiFe cells. Journal of Power Sources, 262:263–269, sep 2014. ISSN 03787753. doi: 10.1016/j.jpowsour.2014.03.145. URL http://linkinghub.elsevier.com/retrieve/pii/S0378775314004789.

[43] Jorge Omar Gil Posada and Peter J. Hall. The Effect of Electrolyte Additives on the Performance of Iron Based Anodes for NiFe Cells. Journal of The Electrochemical Society, 162(10):A2036–A2043, 2015. ISSN 0013-4651. doi: 10.1149/2.0451510jes. URL http://jes.ecsdl.org/lookup/doi/10.1149/2.0451510jes.

[44] M. K. Ravikumar, a. Sundar Rajan, S. Sampath, K. R. Priolkar, and a. K. Shukla. In Situ Crystallographic Probing on Ameliorating Effect of Sulfide Additives and Carbon Grafting in Iron Electrodes. Journal of The Electrochemical Society, 162(12):A2339–A2350, 2015. ISSN 0013-4651. doi: 10.1149/2.0721512jes. URL http://jes.ecsdl.org/lookup/doi/10.1149/2.0721512jes.

[45] Thomas van Dijk. A new Nickel Iron-Sulphide battery. Thesis, TU Delft, 2012.

[46] A.K. Shukla and B. Hariprakash. Nickel – Iron. Elsevier, 2009.

[47] Lars Öjefors. Self-discharge of the alkaline iron electrode. Electrochimica Acta, 21(4):263–266, apr 1976. ISSN 00134686. doi: 10.1016/0013-4686(76)80016-3. URL http://linkinghub.elsevier.com/retrieve/pii/0013468676800163.

[48] Lars Ojefors. SEM Studies of Discharge Products from Alkaline Iron Electrodes. Journal of The Electrochemical Society, 123(11):1691, 1976. ISSN 00134651. doi: 10.1149/1.2132669. URL http://jes.ecsdl.org/cgi/doi/10.1149/1.2132669.

[49] Lars Ojefors. Temperature Dependence of Iron and Cadmium Alkaline Electrodes. Journal of The Electrochemical Society, 123(8):1139, 1976. ISSN 00134651. doi: 10.1149/1.2133023. URL http://jes.ecsdl.org/cgi/doi/10.1149/1.2133023.

[50] Bo Andersson and Lars Ojefors. Slow Potentiodynamic Studies of Porous Alkaline Iron Electrodes. Journal of The Electrochemical Society, 123(6):824, 1976. ISSN 00134651. doi: 10.1149/1.2132940. URL http://jes.ecsdl.org/cgi/doi/10.1149/1.2132940.

[51] Lars Öjefors and Lars Carlsson. An iron—air vehicle battery. Journal of Power Sources, 2(3):287–296, feb 1978. ISSN 03787753. doi: 10.1016/0378-7753(78)85019-8. URL http://linkinghub.elsevier.com/retrieve/pii/0378775378850198.

[52] A Sundar Rajan, M K Ravikumar, K R Priolkar, S Sampath, A K Shukla, and Open Access. Carbonyl-Iron Electrodes for Rechargeable-Iron. pages 2–9, 2014. doi: 10.1515/eetech-2014-0002.

[53] Aravamuthan Sundar Rajan, Srinivasan Sampath, and Ashok Kumar Shukla. An in situ carbon-grafted alkaline iron electrode for iron-based accumulators. Energy & Environmental Science, 7(3):1110–1116, 2014. ISSN 1754-5692. doi: 10.1039/c3ee42783h. URL http://dx.doi.org/10.1039/C3EE42783H.

[54] K. Vijayamohanan, A. K. Shukla, and S. Sathyanarayana. Formation mechanism of porous alkaline iron electrodes. Journal of Power Sources, 32(4):329–339, 1990. ISSN 03787753. doi: 10.1016/0378-7753(90)87002-9.

[55] B. Hariprakash, S. K. Martha, M. S. Hegde, and a. K. Shukla. A sealed, starved-electrolyte nickel-iron battery. Journal of Applied Electrochemistry, 35(1):27–32, jan 2005. ISSN 0021-891X. doi: 10.1007/s10800-004-2052-y. URL http://www.springerlink.com/openurl.asp?id=doi:10.1007/s10800-004-2052-y.

[56] A.K. Shukla and B. Hariprakash. SECONDARY BATTERIES – NICKEL SYSTEMS — Electrodes: Iron. In Encyclopedia of Electrochemical Power Sources, pages 418–423. Elsevier, 2009. doi: 10.1016/B978-044452745-5.00163-5. URL http://linkinghub.elsevier.com/retrieve/pii/B9780444527455001635.

[57] A Shukla. Nickel-based rechargeable batteries. Journal of Power Sources, 100(1-2):125–148, nov 2001. ISSN 03787753. doi: 10.1016/S0378-7753(01)00890-4. URL http://linkinghub.elsevier.com/retrieve/pii/S0378775301008904.

[58] a. K. Manohar, C. Yang, S. Malkhandi, G. K. S. Prakash, and S. R. Narayanan. Enhancing the Performance of the Rechargeable Iron Electrode in Alkaline Batteries with Bismuth Oxide and Iron Sulfide Additives. Journal of the Electrochemical Society, 160(11):A2078–A2084, oct 2013. ISSN 0013-4651. doi: 10.1149/2.066311jes. URL http://jes.ecsdl.org/cgi/doi/10.1149/2.066311jes.

[59] a. K. Manohar, S. Malkhandi, B. Yang, C. Yang, G. K. Surya Prakash, and S. R. Narayanan. A High-Performance Rechargeable Iron Electrode for Large-Scale Battery-Based Energy Storage. Journal of the Electrochemical Society, 159(8):A1209–A1214, jul 2012. ISSN 0013-4651. doi: 10.1149/2.034208jes. URL http://jes.ecsdl.org/cgi/doi/10.1149/2.034208jes.

[60] Bo Yang, Souradip Malkhandi, Aswin K. Manohar, G. K. Surya Prakash, and S. R. Narayanan. Organo-sulfur molecules enable iron-based battery electrodes to meet the challenges of large-scale electrical energy storage. Energy & Environmental Science, 7(8):2753, jul 2014. ISSN 1754-5692. doi: 10.1039/C4EE01454E. URL http://xlink.rsc.org/?DOI=C4EE01454E.

[61] Souradip Malkhandi, Bo Yang, Aswin K Manohar, G K Surya Prakash, and S R Narayanan. Self-Assembled Monolayers of n Alkanethiols Suppress Hydrogen Evolution and Increase the E ffi ciency of Rechargeable Iron Battery Electrodes. (1), 2013.

[62] S. R. Narayanan, G. K Surya Prakash, A. Manohar, Bo Yang, S. Malkhandi, and Andrew Kindler. Materials challenges and technical approaches for realizing inexpensive and robust iron-air batteries for large-scale energy storage. Solid State Ionics, 216:105–109, 2012. ISSN 01672738. doi: 10.1016/j.ssi.2011.12.002.

[63] S. Malkhandi, B. Yang, A. Manohar, G. K. S. Prakash, and S. R. Naranayan. Organo-Sulfur Additives for Suppressing Hydrogen Evolution in Iron-Air Battery. In Journal of Chemical Information and Modeling, volume 53, pages 1689–1699, 2011. ISBN 9788578110796. doi: 10.1017/CBO9781107415324.004.

[64] B. Yang, S. Malkhandi, A. K. Manohar, G. K. S. Prakash, and S. R. Naranayan. Effect of Chain Length of Linear Alkanethiols on the Inhibition of Electrode Processes on Iron in Alkaline Medium. 2011. ISBN 9788578110796. doi: 10.1017/CBO9781107415324.004.

[65] Jorge Omar Gil Posada and Peter J. Hall. Post-hoc comparisons among iron electrode formulations based on bismuth, bismuth sulphide, iron sulphide, and potassium sulphide under strong alkaline conditions. Journal of Power Sources, 268:810–815, dec 2014. ISSN 03787753. doi: 10.1016/j.jpowsour.2014.06.126. URL http://linkinghub.elsevier.com/retrieve/pii/S0378775314009902.

[66] Jorge Omar, Gil Posada, @bullet Peter, and J Hall. Towards the development of safe and commercially viable nickel– iron batteries: improvements to Coulombic efficiency at high iron sulphide electrode formulations. Journal of Applied Electrochemistry, pages 451–458, 2016. ISSN 0021-891X. doi: 10.1007/s10800-015-0911-3.

[67] Enbo Shangguan, Fei Li, Jing Li, Zhaorong Chang, Quanmin Li, Xiao-Zi Yuan, and Haijiang Wang. FeS/C composite as high-performance anode material for alkaline nickel–iron rechargeable batteries. Journal of Power Sources, 291:29–39, 2015. ISSN 03787753. doi: 10.1016/j.jpowsour.2015.05.019. URL http://linkinghub.elsevier.com/retrieve/pii/S0378775315008903.

[68] K. Vijayamohanan, T.S. Balasubramanian, and A.K. Shukla. Rechargeable alkaline iron electrodes. Journal of Power Sources, 34(3):269–285, apr 1991. ISSN 03787753. doi: 10.1016/0378-7753(91)80093-D. URL http://linkinghub.elsevier.com/retrieve/pii/037877539180093D.

[69] S. L. Medway, C. A. Lucas, A. Kowal, R. J. Nichols, and D. Johnson. In situ studies of the oxidation of nickel electrodes in alkaline solution. Journal of Electroanalytical Chemistry, 587(1):172–181, 2006. ISSN 00220728. doi: 10.1016/j.jelechem.2005.11.013.

[70] Bui Thi Hang, Tomonori Watanabe, Minato Egashira, Izumi Watanabe, Shigeto Okada, and Jun Ichi Yamaki. The effect of additives on the electrochemical properties of Fe/C composite for Fe/air battery anode. Journal of Power Sources, 155(2):461–469, 2006. ISSN 03787753. doi: 10.1016/j.jpowsour.2005.04.010. URL http://linkinghub.elsevier.com/retrieve/pii/S0378775305006397.

[71] A. Van der Ven, D. Morgan, Y. S. Meng, and G. Ceder. Phase Stability of Nickel Hydroxides and Oxyhydroxides. Journal of The Electrochemical Society, 153(2):A210, 2006. ISSN 00134651. doi: 10.1149/1.2138572. URL http://jes.ecsdl.org/cgi/doi/10.1149/1.2138572.

[72] Antonio Motori, Franco Sandrolini, and Giovanni Davolio. Electrical properties of nickel hydroxide for alkaline cell systems. Journal of Power Sources, 48(3):361–370, 1994. ISSN 0378-7753. doi: http://dx.doi.org/10.1016/0378-7753(94)80032-4. URL http://www.sciencedirect.com/science/article/pii/0378775394800324.

[73] Z. Mao, A. Visintin, S. Srinivasan, A. J. Appleby, and H. S. Lim. Microcalorimetric study of the self-discharge of the NiOOH/Ni(OH)2 electrode in a hydrogen environment. Journal of Applied Electrochemistry, 22(5):409–414, may 1992. ISSN 0021-891X. doi: 10.1007/BF01077541. URL http://link.springer.com/10.1007/BF01077541.

[74] S. Licht. Energetic Iron(VI) Chemistry: The Super-Iron Battery. Science, 285(5430):1039–1042, aug 1999. ISSN 00368075. doi: 10.1126/science.285.5430.1039. URL http://www.sciencemag.org/cgi/doi/10.1126/science.285.5430.1039.

[75] Y. Geronov, T. Tomov, and S. Georgiev. Mössbauer spectroscopy investigation of the iron electrode during cycling in alkaline solution. Journal of Applied Electrochemistry, 5:351–358, 1975. ISSN 0021891X. doi: 10.1007/BF00608799.

[76] Haiyan Zhang. Rotating Ring-Disk Electrode and Spectroelectrochemical Studies on the Oxidation of Iron in Alkaline Solutions. Journal of The Electrochemical Society, 141(3):718, 1994. ISSN 00134651. doi: 10.1149/1.2054798. URL http://jes.ecsdl.org/cgi/doi/10.1149/1.2054798.

[77] K Micka and Z. Zábranský. Study of iron oxide electrodes in an alkaline electrolyte. Journal of Power Sources, 19(4):315–323, apr 1987. ISSN 03787753. doi: 10.1016/0378-7753(87)87007-6. URL http://linkinghub.elsevier.com/retrieve/pii/0378775387870076.

[78] Gerhard Schikorr. Über Eisen(II)-hydroxyde und ein ferromagnetisches Eisen(III)-hydroxyde. Zeitschrift für anorganische und allgemeine Chemie, 212(1):33–39, may 1933. ISSN 0863-1786. doi: 10.1002/zaac.19332120105. URL http://doi.wiley.com/10.1002/zaac.19332120105.

[79] A. Dibrov, S. M. Chervyak-Voronich, T. V. Grigoreva, and G. M. Kozlova. No Title. Electrochemica acta, 16 (786), 1980.

[80] V. J. Linnenbom. The Reaction between Iron and Water in the Absence of Oxygen. Journal of The Electrochemical Society, 105(6):322, 1958. ISSN 00134651. doi: 10.1149/1.2428838. URL http://jes.ecsdl.org/cgi/doi/10.1149/1.3071303http://jes.ecsdl.org/cgi/doi/10.1149/1.2428838.

[81] Alvin J. Salkind, C. J. Venuto, and S. Uno Falk. The Reaction at the Iron Alkaline Electrode. Journal of The Electrochemical Society, 111(5):493, 1964. ISSN 00134651. doi: 10.1149/1.2426166. URL SALKINDhttp://jes.ecsdl.org/cgi/doi/10.1149/1.2426166.

[82] Lee Blaney. Magnetite (Fe3O4): Properties, Synthesis, and Applications. Technical report, 2007. URL http://preserve.lehigh.edu/cas-lehighreview-vol-15/5.

[83] B. Schrager. Polarographic studies with the dropping mercury cathode- part I- the amphoterity of ferrous hydroxide. Collection of the Czechoslovak Chemical Communications, 1:275–281, 1929.

[84] Wolfram Schwarz and Wolfgang Simon. Untersuchungen zum elektrochemischen Verhalten des Eisens in Alkalilösungen. Berichte der Bunsengesellschaft für physikalische Chemie, 67(1):108–117, jan 1963. ISSN 00059021. doi: 10.1002/bbpc.19630670120. URL http://doi.wiley.com/10.1002/bbpc.19630670120.

[85] V. N. Flerov and L. I. Pavlova. No Title. Electrochemica acta, 3(621), 1967.

[86] N. Sherstobikova, D. I. Leikis, and B. N. Kabanov. No Title. ibid, 5(461), 1969. URL MISSINGPAPER.

[87] D Geana, A A El Miligy, and W J Lorenz. Electrochemical behaviour of iron in alkaline sulphate solutions. Journal of Applied Electrochemistry, 4(4):337–345, 1974. ISSN 0021-891X. doi: 10.1007/BF00608976. URL http://dx.doi.org/10.1007/BF00608976.

[88] R.D. Armstrong and I Baurhoo. The dissolution of iron in concentrated alkali. Journal of Electroanalytical Chemistry and Interfacial Electrochemistry, 40(2):325–338, dec 1972. ISSN 00220728. doi: 10.1016/S0022-0728(72)80377-2. URL http://linkinghub.elsevier.com/retrieve/pii/S0022072872803772.

[89] V. S. Muralidharan and M. Veerashanmugamani. Electrochemical behaviour of pure iron in concentrated sodium hydroxide solutions at different temperatures: a triangular potential sweep voltammetric study. Journal of Applied Electrochemistry, 15(5):675–683, 1985. ISSN 0021891X. doi: 10.1007/BF00620563.

[90] Laurence D. Burke and Michael E.G. Lyons. The formation and stability of hydrous oxide films on iron under potential cycling conditions in aqueous solution at high pH. Journal of Electroanalytical Chemistry and Interfacial Electrochemistry, 198(2):347–368, feb 1986. ISSN 00220728. doi: 10.1016/0022-0728(86)90010-0. URL http://linkinghub.elsevier.com/retrieve/pii/0022072886900100.

[91] Herbert Cnobloch, Dieter Gröppel, Waldemar Nippe, and Ferdinand von Sturm. Eisen-Elektroden für Metall/Luft-Zellen. Chemie Ingenieur Technik - CIT, 45(4):203–206, feb 1973. ISSN 0009-286X. doi: 10.1002/cite.330450415. URL http://doi.wiley.com/10.1002/cite.330450415.

[92] R.S. Schrebler Guzmán, J.R. Vilche, and A.J. Arvía. The potentiodynamic behaviour of iron in alkaline solutions. Electrochimica Acta, 24(4):395–403, 1979. ISSN 00134686. doi: 10.1016/0013-4686(79)87026-7. URL http://www.sciencedirect.com/science/article/pii/0013468679870267.

[93] P.R. Vassie and A.C.C. Tseung. High performance, rechargeable sintered iron electrodes—I: The effect of preparative methods and additives on the structure and performance of sintered iron electrodes. Electrochimica Acta, 21(4):299–302, apr 1976. ISSN 00134686. doi: 10.1016/0013-4686(76)80023-0. URL http://linkinghub.elsevier.com/retrieve/pii/0013468676800230.

[94] H Graham Silver and Elfriede Lekas. The Products of the Anodic Oxidation of an Iron Electrode in Alkaline Solution. Journal of The Electrochemical Society, 117(1):5, 1970. ISSN 00134651. doi: 10.1149/1.2407439. URL http://jes.ecsdl.org/cgi/doi/10.1149/1.2407439.

[95] C S Tong. A Study of the Iron Electrode Structure of Ni-Fe Cell. Journal of The Electrochemical Society, 129 (6):1173, 1982. ISSN 00134651. doi: 10.1149/1.2124082. URL http://jes.ecsdl.org/cgi/doi/10.1149/1.2124082.

[96] Digby D. Macdonald and D. Owen. The Electrochemistry of Iron in 1M Lithium Hydroxide Solution at 22 and 200C. Journal of The Electrochemical Society, 120(3):317–324, 1973. ISSN 00134651. doi: 10.1149/1.2403446. URL http://jes.ecsdl.org/content/120/3/317.full.pdf.

[97] B Kabanov, R Burstein, and A Frumkin. Kinetics of Electrode Processes. Zeitschrift für Physikalische Chemie, 1:259–269, 1947. ISSN 0942-9352. doi: 10.1524/zpch.1972.80.1_2.110a.

[98] G. S. Alexandrova, I. A. Shoshina, T. V. Subbotina, V. M. Fantgof, and A. L. Rotinyan. No Title. Zh. Prikl. Khim, 56(1540), 1983. URL MISSINGPAPER.

[99] E. B. Eronko, A. V. Bogdanov, I. A. Shoshina, T. K. Teplinskaya, and A. L. Rotinyan. No Title. Zh. Prikl. Khim., 59(1011), 1986.

[100] C Chakkaravarthy, P. Periasamy, S. Jegannathan, and K.I. Vasu. The nickel/iron battery. Journal of Power Sources, 35(1):21–35, jun 1991. ISSN 03787753. doi: 10.1016/0378-7753(91)80002-F. URL http://linkinghub.elsevier.com/retrieve/pii/037877539180002F.

[101] J. Černý, J. Jindra, and K. Micka. Comparative study of porous iron electrodes. Journal of Power Sources, 45 (3):267–279, jul 1993. ISSN 03787753. doi: 10.1016/0378-7753(93)80016-I. URL http://linkinghub.elsevier.com/retrieve/pii/037877539380016I.

[102] Hailiang Wang, Yongye Liang, Ming Gong, Yanguang Li, Wesley Chang, Tyler Mefford, Jigang Zhou, Jian Wang, Tom Regier, Fei Wei, and Hongjie Dai. An ultrafast nickel–iron battery from strongly coupled inorganic nanoparticle/nanocarbon hybrid materials. Nature Communications, 3(May):917, jun 2012. ISSN 2041-1723. doi: 10.1038/ncomms1921. URL http://www.nature.com/doifinder/10.1038/ncomms1921.

[103] Danni Lei, Dong-Chan Lee, Alexandre Magasinski, Enbo Zhao, Daniel Steingart, and Gleb Yushin. Performance Enhancement and Side Reactions in Rechargeable Nickel–Iron Batteries with Nanostructured Electrodes. ACS Applied Materials & Interfaces, 8(3):2088–2096, 2016. ISSN 1944-8244. doi: 10.1021/acsami.5b10547. URL http://pubs.acs.org/doi/abs/10.1021/acsami.5b10547.

[104] G. Paruthimal Kalaignan and V. S. Muralidharan. Iron-copper electrodes for alkaline batteries. Bulletin of Electrochemistry, 12(3-4):213–217, 1996.

[105] Angie L Rangel Cárdenas. Overcoming the detrimental effects of the Hydrogen Evolution Reaction (HER) on Ni-Fe(S) batteries. PhD thesis, Delft University of Technology, 2015.

[106] Peter Taylor and David W Shoesmith. The nature of green alkaline iron sulfide solutions and the preparation of sodium iron(III) sulfide, NaFeS2. Canadian Journal of Chemistry, 56(22):2797–2802, 1978. doi: 10.1139/v78-462. URL http://dx.doi.org/10.1139/v78-462.

[107] T. K. Teplinskaya, N. N. Fedorova, and S. A. Rozentsveig. No Title. Zh. Fiz. Khim., 38(2176), 1964.

[108] S. A. Rozentsveig and Z. V. Shcherbakova. Effect of sulfur on the iron electrode in alkaline solution. Zhurnal Fizicheskoi, 35(11):2547–2552, 1961. URL https://scholar.google.nl/scholar?q=EFFECT+OF+SULFUR+ON+THE+IRON+ELECTRODE+IN+ALKALINE+SOLUTION{&}btnG={&}hl=nl{&}as{_}sdt=0,5{#}0.

[109] T. I. K. Kochetova, Teplinskaya T., and K. M. Novakovskii. Influence of concentration of sodiumsulfide in alkali on anodic activity of a smooth iron electrode. Soviet electrochemistry, 12.5:725–728, 1976.

[110] R. Bonnaterre, R. Doisnean, M. C. Petit, J. P. Servinon, and J. Thomson. MISSING PAPER. Power sources, 7:1, 1978.

[111] J. Vera, S. Kapusta, and N. Hackerman. Localized Corrosion of Iron in Alkaline Sulfide Solutions. Journal of The Electrochemical Society, 133(3):461–461, 1986. ISSN 00134651. doi: 10.1149/1.2108602. URL http://jes.ecsdl.org/cgi/doi/10.1149/1.2108602.

[112] Desmond Tromans. Anodic Polarization Behavior of Mild Steel in Hot Alkaline Sulfide Solutions. Journal of The Electrochemical Society, 127(6):1253, 1980. ISSN 00134651. doi: 10.1149/1.2129865. URL http://jes.ecsdl.org/content/127/6/1253.shorthttp://jes.ecsdl.org/cgi/doi/10.1149/1.2129865.

[113] P.W Bolmer. Polarization of Iron in H2S-NaHS Buffers. Corrosion, 21(3):69–75, mar 1965. ISSN 0010-9312. doi: 10.5006/0010-9312-21.3.69. URL http://corrosionjournal.org/doi/abs/10.5006/0010-9312-21.3.69?journalCode=corr.

[114] E. N. Lescheva and T. K. Teplinskaya. No Title. Khimicheskie Istochniki Toka, 59(59):48, 1986.

[115] David Rickard. The solubility of FeS. Geochimica et Cosmochimica Acta, 70(23):5779–5789, dec 2006. ISSN 00167037. doi: 10.1016/j.gca.2006.02.029. URL http://linkinghub.elsevier.com/retrieve/pii/S0016703706001992.

[116] J. Christopher Love, Lara A. Estroff, Jennah K. Kriebel, Ralph G. Nuzzo, and George M. Whitesides. Self-Assembled Monolayers of Thiolates on Methals as a Form of Nanotechnology, volume 105. 2005. ISBN 2172440809. doi: 10.1021/cr0300789.

[117] Sang-Koo KWON, Ken'ichi KIMIJIMA, Kiyoshi KANIE, Atsushi MURAMATSU, Shigeru SUZUKI, Eiichiro MATSUBARA, and Yoshio WASEDA. Inhibition of Conversion Process from Fe(OH)3 to .BETA.-FeOOH and .ALPHA.-Fe2O3 by the Addition of Silicate Ions. ISIJ International, 45(1):77–81, 2005. ISSN 0915-1559. doi: 10.2355/isijinternational.45.77. URL http://joi.jlc.jst.go.jp/JST.JSTAGE/isijinternational/45.77?from=CrossRef.

[118] Stanley Hills. Beneficial Effect of Lithiated Electrolyte on Iron Battery Electrodes. Journal of The Electrochemical Society, 112(10):1048, 1965. ISSN 00134651. doi: 10.1149/1.2423340. URL http://jes.ecsdl.org/cgi/doi/10.1149/1.2423340.

[119] V. M. Fantgof Lishanskii and L. M. V. M. Fantgof and L. M. Lishanskii, Elektrokhimiya, 18 (1982) 647 - Google Scholar. URL https://scholar-google-nl.proxy.library.uu.nl/scholar?hl=nl{&}q=V.+M.+Fantgof+and+L.+M.+Lishanskii{%}2C+Elektrokhimiya{%}2C+18+{%}281982{%}29+647{&}btnG={&}lr=.

[120] M Jayalakshmi and V S Muralidharan. Passivation of iron in alkaline carbonate solutions. Journal of Power Sources, 35(2):131–142, 1991. ISSN 03787753. doi: 10.1016/0378-7753(91)80030-2. URL http://www.sciencedirect.com/science/article/B6TH1-43MF1M8-FG/2/9740282d1f7e442755e4ef8bf82d294b.

[121] T. A. Edison. Electrolyte for alkaline storage batteries, 1908.

[122] W. A. Bryant. The structure and performance of sintered iron electrodes. Electrochimica Acta, 24(10):1057–1060, 1979. ISSN 00134686. doi: 10.1016/0013-4686(79)85001-X.

[123] K. Vijayamohanan, , A. K. Shukla, and S. Sathyanarayana. Statistical Optimization of Iron Electrodes for Alkaline Storage Batteries. Indian Journal of Technology, 24(7):430–434, 1986.

[124] Hiroki Kitamura, Liwei Zhao, Bui Thi Hang, Shigeto Okada, and Jun-ichi Yamaki. Effect of binder materials on cycling performance of Fe2O3 electrodes in alkaline solution. Journal of Power Sources, 208:391–396, jun 2012. ISSN 03787753. doi: 10.1016/j.jpowsour.2012.02.051. URL http://dx.doi.org/10.1016/j.jpowsour.2012.02.051http://linkinghub.elsevier.com/retrieve/pii/S0378775312004119.

[125] Fei Li, Enbo Shangguan, Jing Li, Lijin Li, Jing Yang, Zhaorong Chang, Quanmin Li, Xiao-Zi Yuan, and Haijiang Wang. Influence of annealing temperature on the structure and electrochemical performance of the Fe3O4 anode material for alkaline secondary batteries. Electrochimica Acta, 178:34–44, 2015. ISSN 00134686. doi: 10.1016/j.electacta.2015.07.106. URL http://linkinghub.elsevier.com/retrieve/pii/S001346861530181X.

[126] L N Sturkenboom. Feasibility of Phase Immersion Precipitation for the Application of Electrode Production : A Literature & Parameter study . PhD thesis, University Utrecht, 2015.